

Identification of host dependency factors for ZIKV infection using proteomic techniques.

by

Kathleen Korkor Marie Glover

A Thesis Submitted to the Faculty of Graduate Studies of
The University of Manitoba
in Partial Fulfillment of the Requirements of the Degree of

Doctor of Philosophy

Department of Medical Microbiology and Infectious Diseases,
University of Manitoba
Winnipeg.

Copyright © 2021 by Kathleen KM Glover.

ABSTRACT

Newly re-emerging viruses are major sources of concern around the world, especially when no treatment options are available during an outbreak. ZIKV is a neurotropic virus that causes congenital abnormalities in babies when they are infected in utero. Some studies have reported that these congenital abnormalities result from ZIKV attacking neural progenitor cells within the brain that differentiate into neurons, oligodendrocytes, and astrocytes. Each of these glial cells plays an important role in fetal brain development. Newborns infected with ZIKV suffer from microcephaly and delayed neurodevelopment, but the underlying causes at the proteomic level are largely unknown. In addition to congenital defects caused by ZIKV, infected patients have been documented to suffer gastrointestinal problems such as diarrhea, nausea, vomiting, and abdominal discomfort, among other things. My PhD thesis for the first time identified host proteins, which we predicted to be linked in the development of; 1) neurosensory alterations that have been reported to occur in babies born to ZIKV infected pregnant mothers and 2) gastrointestinal complications reported in ZIKV infected patients.

Invitro proteomic analysis of ZIKV-induced changes was performed in Vero and Caco-2 cells, which are known to be permissive to ZIKV infection. Tandem mass tag mass spectrometry-based proteomic and the SOMAScan were used in monitoring these cells infected with ZIKV. Thousands of host proteins were identified to be dysregulated across selected multiple time point post ZIKV infection. Many protein candidates were linked to neurodevelopmental processes, including the development of the auditory and visual/retinal system as well as gastrointestinal complications as predicted after bioinformatics analysis by IPA. The role of these dysregulated neurodevelopmental associated, as well as gastrointestinal related host proteins for ZIKV propagation, needs to be validated to gain more understanding of ZIKV biology as well as determine the potential of these proteomic candidates for future ZIKV therapeutic modality development. In conclusion, my PhD project was the first to identify temporal neurodevelopmental and gastrointestinal proteomic responses in ZIKV-infected cells.

ACKNOWLEDGEMENT.

There is a saying that “A journey of a thousand miles begins with one step” which for me began when I started my PhD training in the Coombs Lab. Successful completion of my PhD research was only possible because of the excellent supervision and support I received from my supervisor, Dr. Kevin Marshall Coombs. I would like to thank him immensely for his patience, constant support, motivation, and direction I received during my training. I learnt a lot and gained lots of research skills that would be useful in my future profession. I would next like to express my immense gratitude to my committee members Dr. Thomas Klonisch, Dr. Blake Ball, Dr. Lorrie Kirshenbaum and Dr. David Safronetz for their motivation, thought-provoking input, suggestions, during all the yearly committee meeting I had during my PhD training. The collaborative direction and motivation from the committee member contributed to the completion of my thesis for which I am very grateful.

Very grateful to present and past members of the Coombs lab for their research support, critics as well as input made to this thesis during our Research in Progress meetings. Working in the Coombs lab was very exciting due to the great team spirit that exist within the Coombs Lab members which created a very conducive research environment for my PhD training. Members of the Manitoba Centre for Proteomics and Systems Biology (MCPSB) where the Coombs Lab is located contributed in various ways especially during the Institute’s Research in Progress meetings which created a wonderful platform to receive more insights and inputs regarding my PhD thesis. I am most grateful to Dr. John Wilkins, the former Director of the MCPSB for always making his doors open to discuss any research related questions I had during my training.

I would like to express my immense gratitude to the Canadian Institutes of Health Research (CIHR) and the Children’s Hospital Research Institute of Manitoba (CHRIM) for providing funding and the Canadian Foundation for Innovation (CFI) for providing infrastructure funds for the SOMAScan equipment used in generating the data for my PhD thesis.

Members of the Department of Medical Microbiology and Infectious Diseases played a great role during my training especially during our research seminar presentations where I additionally received research suggestions from both faculty as well as graduate students within our department. I am most grateful to our Head of Department Dr. Keith Fowke for all the support

provided to graduate students in our department which made my PhD training very smooth. I am also tremendously grateful to the department's graduate program coordinator Ms. Angela Nelson for her many wonderful supports and concern throughout my studies.

Finally, I would like to express my heartfelt gratitude to my mentors Dr. Arzu Ozturk Aptekmann and Mr. Abdulrahman Hammond for being great mentors any graduate student could wish for. Their unbiased critics and feedback, always ready to grant mentorship support and guidance at some time very short notices made a huge difference.

DEDICATION.

I dedicate my PhD thesis to my late lovely, caring, and motivating Father Mr. Stephen Tetteh Glover who I loved so dearly. I know he is smiling down me very proud of my accomplishment.

I would also like to dedicate my thesis to my mom Mrs. Kathleen Asmah Glover and my siblings, Dr. Harry Benjamin Korli Glover, Dr. Stephen Tetteh Glover and Mrs. Winifred Dedo Tetteh for all their emotional support. I could not have come this far without their love, care, and continuous concern during every step of my PhD training.

Table of Contents

ABSTRACT	ii
DEDICATION.....	v
Table of Contents	vi
LIST OF TABLES.	viii
LIST OF FIGURES.	viii
ABBREVIATIONS.....	ix
Copy Right Permission for Publications used in thesis.	xiii
Chapter: 1.....	1
1.1 Introduction.....	1
1.1.1 Historical background of ZIKV.....	1
1.1.2 ZIKV Structure and proteins.....	2
1.1.3 ZIKV Structural Proteins	3
1.1.4 ZIKV Nonstructural Proteins.....	3
1.1.5 Epidemiology and Pathogenesis of Zika infection.....	4
1.1.6 Clinical manifestation of ZIKV infection.....	6
1.1.7 Diagnosis of ZIKV infection.....	7
1.1.8 Prevention (Antiviral and Vaccine development against ZIKV).....	8
1.1.9 Proteomics	10
1.1.9a SOMAScan Proteomic Analysis.....	10
1.1.9b Tandem Mass Tagging Mass Spectrometry.....	12
1.2 Hypothesis and Aim of Study.....	13
1.3 Specific Objectives.	13
1.4 Significance of study.	14
Chapter 2: Materials and Methods	14
2.1 Cells and Viruses.....	14
2.1.i Cells.....	14
2.1.ii Virus:	14
2.2 Infection	14
2.3 Protein Quantification	15
2.4. Immunofluorescent Staining.....	15
2.5. Cell Viability.....	15

2.6. Immunoblotting.....	16
2.7. SOMAScan Analyses.	16
2.8 Tandem Mass Tagging (TMT) Mass Spectrometry (MS) Analyses	16
2.9 Peptide and Protein Identification and Quantification.	18
2.10 Statistical and Bioinformatics Analysis.....	18
Chapter 3: Results.....	20
3.1 Vero Cell Proteomic Changes Induced by ZIKV Infection.....	20
3.1.i Contributory Role.....	20
3.1.ii Kinetics of Virus-Induced Cytopathology and Virus Replication.	20
3.1.iii ZIKV Induction of Proteomic Dysregulation.....	22
3.1.v Bioinformatic and Pathway Analyses Highlight Multiple Cellular Processes and Pathways Affected by ZIKV Infection.	28
3.2. ZIKV disrupts proteins involved in the neurosensory system	35
3.2.i Contributory Role.....	35
3.2. ii. ZIKV causes specific temporal changes in the cellular proteome.	35
3.2.iii ZIKV infection dysregulates a wide variety of bio-functions and pathways.	41
3.2. iv. ZIKV alters protein interaction networks linked to developmental processes.....	45
3.3. ZIKV Infection Induces DNA Damage Response and Alters the Proteome of Gastrointestinal Cells	52
3.3.i. Contributory Role.....	52
3.3. ii. ZIKV Virus Induces Cytopathology in Caco-2 with Increased Viral Titer.....	52
3.3.iii ZIKV Induces Proteomics Dysregulation of Caco-2 Host Proteins.....	55
3.3.iv ZIKV Infection Results in Numerous Diseases and Alters Biofunctions.	64
3.3.v Proteomic Prediction of ZIKV Activation of DNA Damage Response	65
Chapter 4: Discussion and Conclusion.....	61
4.1. Discussion.	69
4.1.i. Vero Cell Proteomic Changes Induced by ZIKV Infection.....	72
4.1. ii. ZIKV disrupts proteins involved in the neurosensory system in Vero cells	76
4.1.iii ZIKV Induces DNA Damage Response (DDR) and Alters the Proteome of Gastrointestinal Cells.....	80
References.....	89
Appendix: Supporting Information	117
Figure S1A: PCA of > 1300 SOMAScan protein for 3 biological replicates after 12, 24 and 48hr ZIKV of infection	116
Figure S1B: Heatmap of fold-changes showing the most dysregulated of host proteins across all 3 time	

points after ZIKV infection. Blue indicates downregulated while red indicated up regulated.	117
Figure S1C: GO analysis of using fold changes dysregulated host proteins.	119
Figure S2: Protein-protein interaction network of ZIKV- induced differentially dysregulated Vero cell proteins at 48hpi.	120
Table S1. IPA-predicted dysregulated bio-functions, activation state and specific molecules associated with each biofunction.	123
Table S2: Comparative list of commonly and differentially dysregulated host proteins after ZIKV infection identified in Vero, Caco-2 and U251 cells.	124

LIST OF TABLES.

Table 1: Numbers of significantly dysregulated ZIKV-infected Vero proteins.	24
Table 2: Vero cell proteins significantly affected by ZIKV infection.	27
Table 3: Numbers of ZIKV-induced significantly dysregulated proteins.	37
Table 4: Vero cell proteins dysregulated ≥ 2.0 -fold by ZIKV infection.	39
Table 5: Numbers of significantly dysregulated ZIKV-infected CaCo-2 proteins.	56
Table 6: List of significantly dysregulated Caco-2 proteins after ZIKV infection.	57

LIST OF FIGURES.

Figure 1: The Zika virus genome.	2
Figure 2: Transmission cycle of ZIKV(72).	5
Figure 3: Omics methods to study virus-induced cellular perturbations.	10
Figure 4: General steps of the SOMAScan Assay. (109)	11

Figure 5: TMT Labeling Protocol. by Bio Render, J u l y 2020, retrieved from https://app.biorender.com/biorender-templates/t-5f4963c5b59c7a00ad18b5fd-tmt-labeling-protocol Copyright 2021 by Bio Render.\.....	12
Figure 6: Kinetics of virus induced cytopathology and virus replication in Vero cells.....	21
Figure 7: Characteristics of dysregulated proteins.....	24
Figure 8: Validation of protein dysregulation.....	28
Figure 9: GO determined by Panther classifications and IPA generated top networks of dysregulated Vero cell proteins.	32
Figure 10: IPA-predicted activation and inhibition of various signaling pathways.	33
Figure 11: Mass spectrometry proteomic analysis of ZIKV-infected Vero cells.	39
Figure 12: Proteomic prediction of top affected biofunctions, canonical pathways, and upstream molecules in Vero cells after ZIKV infection.	45
Figure 13: Effect of ZIKV infection on protein-protein interaction network of developmental abnormalities.	48
Figure 14: Proteomic prediction of ZIKV-induced changes in the neurosensory system.	51
Figure 15: ZIKV growth kinetics in Caco-2 cells and proteomic validation.....	54
Figure 16: ZIKV dysregulated Caco-2 proteins and predicted signaling pathway.....	60
Figure 17: Proteomic prediction by IPA of Disease and function affected by ZIKV infection....	63
Figure 18: Interactions between network molecules and DNA damage checkpoint pathways	65
Figure 19: Summary of future directions:.....	85

ABBREVIATIONS

ZIKV- Zika virus.

BSA- Bovine serum albumin.

DMEM- Dulbecco's modified Eagle's medium

EMEM- Eagle's Minimum Essential Medium

FBS- Fetal bovine serum.

GO- Gene ontology.

KD-Knockdown.

MOI- Multiplicity of Infection.

mRNA - Messenger RNA.

PBS- Phosphate buffered saline.

PFU Plaque-forming unit.

RT-PCR- Reverse Transcription Polymerase Chain Reaction.

SDS-PAGE Sodium dodecyl polyacrylamide sulphate gel electrophoresis.

siRNA- Small interfering RNA.

COVID-19- coronavirus disease of 2019.

PANTHER- Protein Analysis Through Evolutionary Relationships.

Ingenuity Pathway Analysis -IPA.

Principal component analysis- PCA.

μL – microliter.

μg- microgram.

RFU -Relative fluorescent units.

WHO- World Health Organization.

Publications earned during PhD training.

1. **Kathleen K. M. Glover**, Danica M. Sutherland, Terence S. Dermody and Kevin Coombs. (2021). A single point mutation, Asn16→Lys, dictates the temperature-sensitivity of the reovirus tsG453 mutant. *Viruses*. 12(771): 13. <http://dx.doi.org/10.3390/v12070771>.

First Listed Author

Contribution Percentage: 41-50.

Description of Contribution Role: Generated all mutation reported for temperature sensitive (ts)phenotypes of the mutant Reovirus used in this study by site directed mutagenesis of the affected reovirus gene segment, generated and validated ts mutant Reovirus virus generated by reverse genetics, analysis of mutant virus sequence after Sanger sequencing for identification of generated mutations by reverse genetics and contributed to writing up of the manuscript.

2. Mahamud-ur Rashid, Ali Zahedi-Amiri, **Kathleen K. M. Glover**, Ang Gao, John Wilkins, and Kevin M. Coombs. (2020). ZIKV Dysregulates Human Sertoli Cell Proteins Involved in Spermatogenesis and Blood-Testes Tight Junctions. *Journal of Human Reproduction*. PLOS Neglected Tropical Diseases.

Co-Author

Contribution Percentage: 31-40.

Description of Contribution Role: Prior to the proteomic analysis, I assisted in the execution of all experiments that led to this publication, including the generation of Zika viral stock for cell infection, optimization of Sertoli cell ZIKV infection conditions, determination of viral titers production by plaque assay, and manuscript review before submission for publication.

3. **Kathleen Glover**, Kevin M Coombs. (2020). ZIKV (ZIKV) infection induces DNA damage response and alters the proteome of gastrointestinal cells. *Viruses*.

First Listed Author

Contribution Percentage: 51-60.

Description of Contribution Role: Designed and Performed research experiment such as determination of optimal conditions for ZIKV infection of Caco-2 cells prior to proteomic analysis and contributed to writing up manuscript.

4. **Kathleen K.M. Glover**, Ali Zahedi-Amiri, Ying Lao, Victor Spicer, Thomas Klonisch and Kevin M. Coombs. (2020). Zika infection disrupts proteins involved in the neurosensory system. *Frontiers Cell and Developmental Biology*. 20-30.

Co-share First Author

Contribution Percentage: 41-50

Description of Contribution Role: Designed and performed all research experiment such as optimizing conditions for ZIKV infection of Vero cells, generation of peptides prior to TMT, MS,

contributed to bioinformatic analysis of proteomic data generated and contributed to writing up manuscript up the entire manuscript and addressing reviewers' comment after manuscript submission.

5. Affan A. Sher, **Kathleen K. M. Glover**, and Kevin M. Coombs. (2019). ZIKV Infection Disrupts Astrocytic Proteins Involved in Synapse Control and Axon Guidance. *Frontiers in Microbiology*. 10(596):1-20.

Co-Author.

Contribution Percentage: 31-40

Description of Contribution Role: Provided mentorship guidance during designing research experiment for this publication and assisted also in experimental set-up, in results interpretation, and editing the manuscript and contributed to addressing reviewers comment after manuscript submission.

6. Parvaneh, M., Sudharsana, R. A., Javad A., Shahrzad, R., Aryana, S., Hadis, M., Mohammad, H., **Glover, K K. M.**, Sher, A. A., Coombs, K.M. and Ghavami, S. (2018). The roles of apoptosis, autophagy and unfolded protein response in arbovirus, influenza virus and HIV infections. *Virulence*.1-126. <http://dx.doi.org/10.1080/21505594.1605803>.

Co-Author

Contribution Percentage: 21-30

Description of Contribution Role: Contributed to writing the virology section of this Review publication and reviewed the entire manuscript before and after submission and reviewing the manuscript.

7, **Glover KKM**, Gao A, Zahedi-Amiri A, Coombs KM. (2018). Vero cell Proteomic Changes Induced by ZIKV Infection. *Proteomics*. 19(4): 1-16.

<http://dx.doi.org/https://doi.org/10.1002/pmic.201800309>

First Listed Author

Contribution Percentage: 61-70

Description of Contribution Role: Designed and performed all research experiment such as optimizing conditions for ZIKV infection of Vero cells prior to SOMAScan proteomic analysis, bioinformatic analysis of proteomic data generated and contributed to writing up manuscript up the entire manuscript and addressing reviewers' comment after manuscript submission.

8. **Kathleen KM Glover** and Kevin M Coombs. (2017). ZIKV infection: a review of available techniques towards early detection. *Journal of Molecular Biochemistry*. 6: 26-32.

Co-Author

Contribution Percentage: 61-70.

Description of Contribution Role: Contributed to writing up the entire manuscript, formatted the manuscript based on journal's manuscript submission guidelines and reviewed the entire before submission of manuscript.

Submitted and Working Manuscript

1, **Glover K**, Rashid M, and Coombs KM (2021) ' Proteomics, a promising tool towards development of COVID-19 therapeutic modalities. K Jayanna (eds.), COVID-19: Many Facets and Dimensions, Ramaiah Groups, Bengaluru, pp 267-92.

2, **Kathleen K.M. Glover**, Affan A Sher, Mahamud-ur Rashid, and Kevin M. Coombs. Chloride Intracellular Channel Protein 1 (CLIC 1) upregulation modulates ZIKV replication.

Copy Right Permission for Publications used in thesis.

1) **Kathleen K.M. Glover**, Ali Zahedi-Amiri, Ying Lao, Victor Spicer, Thomas Klonisch and Kevin M. Coombs. (2020). Zika infection disrupts proteins involved in the neurosensory system. Frontiers Cell and Developmental Biology. 20-30.

Dear Glover,

Thank you for your email.

Under the Frontiers Terms and Conditions, authors retain the copyright to their work. Furthermore, all Frontiers articles are Open Access and distributed under the terms of the Creative Commons Attribution License (CC-BY 3,0), which permits the use, distribution, and reproduction of material from published articles, provided the original authors and source are credited, and subject to any copyright notices concerning any third-party content. More information about CC-BY can be found here: <http://creativecommons.org/licenses/by/4.0/>.

You can therefore freely reuse your article, or parts of it, in your thesis.

Best regards,

Frontiers Editorial Office

2) . **Kathleen KM Glover** and Kevin M Coombs. (2017). ZIKV infection: a review of available techniques towards early detection. Journal of Molecular Biochemistry. 6: 26-32.

Dear Kathleen,

You do not need to ask for permission, the journal assigns the copyrights to the authors.

Best,

Spiros

3) **Glover KKM**, Gao A, Zahedi-Amiri A, Coombs KM. (2018). Vero cell Proteomic Changes Induced by ZIKV Infection. Proteomics. 19(4): 1-16.

You are hereby granted a personal, non-exclusive, non-sub licensable (on a stand-alone basis), non-transferable, worldwide, limited license to reproduce the Wiley Materials for the purpose specified in the licensing process.

4) **Kathleen Glover**, Kevin M Coombs. (2020). ZIKV (ZIKV) infection induces DNA damage response and alters the proteome of gastrointestinal cells. *Viruses*.

Dear Kathleen,

Thanks for contacting us regarding copyright. MDPI is publishing only open-access journals, and this includes *Viruses*. The content mentioned below was then published and is distributed under the terms and conditions of the Creative Commons Attribution License (<http://creativecommons.org/licenses/by/4.0/>). It means that anybody is free to use the material if they appropriately credit it.

As authors of this paper, you are copyright holders. Please feel free to use it in your thesis and provide proper citation to the referred publication. Thank you.

Kind regards,

Allison

Dr. Allison Yang

Managing Editor,

Viruses (<http://www.mdpi.com/journal/viruses>)

Impact Factor 3.816 (2020 Journal Citation Reports®)

Chapter: 1

1.1 Introduction

1.1.1 Historical background of ZIKV

ZIKV is an arbovirus that belongs to the family *Flaviviridae*. Other viruses in this family include the West Nile virus, Dengue virus, Japanese encephalitis virus, and Yellow Fever virus (1–3). ZIKV was first identified in the Zika forest of Uganda in 1947 by a group of scientists during a routine sentinel survey of rhesus monkeys for the Yellow Fever virus (4,5). Human infections caused by ZIKV were found in Africa, the Americas, Asia, and the Pacific between the 1960s and 1980s(6–8). Fagbami in 1979 published a report of detection of ZIKV infection in 30% of patient sera from four communities in Oyo state, Nigeria, along with three other Flavivirus namely, Yellow Fever (50%), West Nile (46%), and Wesselsbron (59%) (9).

The first major outbreak of Zika infection outside Africa was reported in the Yap Islands of Micronesia in 2007 (10). Patients were presenting Dengue-like symptoms with conjunctivitis. Thus, they were initially diagnosed serologically as being infected with the Dengue virus (10). However, molecular diagnoses by RT-PCR and sequencing confirmed ZIKV infection, based on approximately 90% nucleotide identity with the ZIKV genome (10). In French Polynesia, a woman with Guillain-Barré syndrome as well as influenza-like symptoms, was reported to be positive for ZIKV and negative for all four serotypes of Dengue by the test of plaque reduction neutralization (11).

In Brazil, the first confirmed case of ZIKV was reported in a patient initially exhibiting Dengue-like symptoms (12). The serological and molecular analyses of patient samples was negative for Dengue and Chikungunya, a pathogenic re-emerging arbovirus, but were positive for Zika by RT-PCR after detecting a 364 bp amplicon expected only for ZIKV. However, in 2015, the world's attention was drawn to Brazil when there was an increase in the number of microcephalic babies being born to pregnant women (13). In comparison to previous years, the 2015 ZIKV epidemic in Brazil resulted in a 20-fold rise in the number of infants born with microcephaly (14). According to the Brazilian Ministry of Health, these continued to rise in subsequent years (14)

Following the outbreak in Brazil, the WHO declared this virus a public health threat and asked for immediate attention because of its increasing spread to other countries and the high incidence of microcephaly in these places (15–17).

1.1.2 ZIKV Structure and Proteins

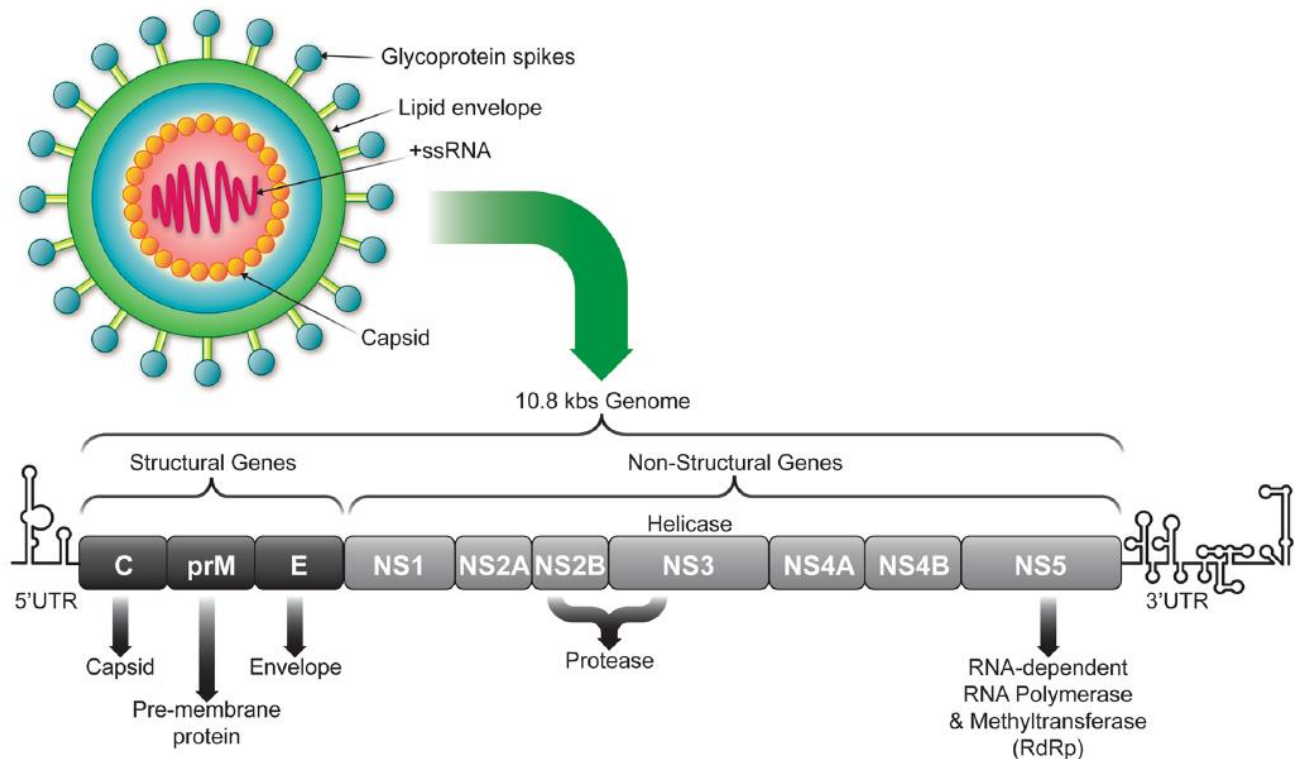


Figure 1: The Zika virus genome.

The Zika virus genome consists of 10.8 kb, coding for three structural proteins—capsid (C), precursor of membrane (prM) and envelope (E) proteins and seven non-structural proteins—NS1, NS2A, NS2B, NS3, NS4A, NS4B, and NS5 (267)

Zika has a single-stranded RNA genome with a positive sense polarity and falls in group four according to the Baltimore system of classifying viruses (2,3,18,19). The Zika viral genome is composed of 10,794 nucleotides which code for 3,419 amino acids (19,20) (Figure 1.). It contains one openreading frame flanked by a 5' and 3' UTR at both ends of the genome (8,18,20). The 5' UTR is polyadenylated and contains a conserved dinucleotide AG while the 3' end of the transcript is not polyadenylated and terminates with a conserved CUOH (18,21). The ZIKV genome, which acts as mRNA upon reaching the cytoplasm, is immediately translated into a polyprotein in the endoplasmic reticulum (ER). The polyprotein is cleaved by host and viral proteases into three structural (capsid protein (C) premembrane (prM) and envelope (E) protein) and seven non-

structural proteins (NS1, NS2A, NS2B, NS3, NS4A, NS4B, and NS5) (8,18,19,22–24) (Figure 1.).

1.1.3 ZIKV Structural Proteins

The capsid is known to protect and deliver the viral genomic material into the cytoplasm during its replicative cycle. ZIKV capsid is icosahedral in shape and surrounded by a spherical lipid bilayer membrane derived from the host (18). It is a 12kDa, 122 amino acid protein and is the first protein translated in the single viral polypeptide chain (22,25,26). ZIKV capsid binds the elements of viral genomic RNA (or viral genomic RNA) forming the nucleocapsid like other viruses and then undergoes uncoating removing the capsid; thus, it releases the viral genome into the cytoplasm initiating translation of the genomic RNA. ZIKV capsid during the maturation stage of its life cycle also buds into the endoplasmic reticulum (ER) lumen to produce the immature virus particle containing viral prM and E proteins (27,28). The immature virus particles traffic via the secretory pathway are processed in the late Golgi compartment by a furin-like protease that cleaves the prM protein into M and pr to produce mature viral particles (27,28).

The Envelope protein is a 54kDa protein and the major virion surface protein involved in host cell binding and membrane fusion (29). Differences between ZIKV and other flaviviruses have been reported at the site of amino acid glycosylation within the envelope protein. Dengue virus, for instance, is glycosylated at Asparagine (Asn) 67 and 154 respectively within the envelope protein important for viral binding and release (30). ZIKV, on the other hand, lacks glycosylation at these sites except in Asn 154 (31–33). The region of glycosylation is an important determinant for antibody specificity and a major target for neutralizing antibodies (34,35).

1.1.4 ZIKV Nonstructural-Proteins

The nonstructural-proteins (NS1-NS5) form the replicative complex and play a role in host innate immunity antagonism (18). ZIKV NS1 shares a lot of structural similarities with NS1 from other flaviviruses; however, it has a distinct divergent electrostatic potential on its loop surface, which is involved in binding host factors and producing protective antibodies making it an antiviral target (18). ZIKV NS1 is glycosylated, associated with lipids and forms homodimers inside the cell, while it forms hexameric lipoprotein particles when it is secreted into the extracellular space (36). ZIKV NS1 protein is necessary for viral replication and evasion of the immune response (18,37).

NS2A, NS2B, NS4A and NS4B are membrane-associated hydrophobic proteins. (18). ZIKV NS2A forms part of the replication complex and is involved in modulating host antiviral response (38). NS3 has two structurally separate functional domains namely, the C-terminal

helicase domain which is responsible for dsRNA unwinding during viral RNA synthesis and the N-terminal protease domain which interacts with the hydrophobic domain of NS2B. This interaction results in the formation of the viral NS2B–NS3 protease complex, which is responsible for the cleavage and processing of the polyprotein (36,38).

NS4A regulates the ATPase activity of the NS3 helicase activity while NS4B like in other flaviviruses, induces the formation of ER-derived membrane vesicles where the viral replication takes place (18,39). ZIKV NS5 protein is the largest (~100 kDa) and most conserved ZIKV protein, with 94% sequence identity between the two major ZIKV lineages, Asian and African (18,40). The NS5 protein has two known domains namely a methyltransferase domain involved in the 5' RNA-capping process and an RNA-dependent RNA polymerase (RdRP) domain involved in genome replication (40–43). NS5 is also involved in interferon suppression during the ZIKV life cycle(44).

1.1.5 Epidemiology and Pathogenesis of Zika Infection.

The vector that has been globally identified to transmit ZIKV is the *Aedes* mosquito. The virus was first recovered from the *Aedes (Stegomyia) africanus*, caught on a tree platform in the Zika forest during a sentinel survey of rhesus monkeys for Yellow Fever virus (4,45). The *Aedes* mosquito is known to survive both tropical and temperate climate conditions (3,46,47); two of these parasites, *Aedes aegypti* and *Aedes albopictus*, have a wider global coverage as they can survive both climatic conditions (3). The mosquito *Aedes aegypti* has been implicated in the transmission of ZIKV; its feeding habit of biting several hosts to complete its blood meals spreads the virus (48). Apart from the 2007 ZIKV outbreak in Gabon, *Aedes albopictus* has not been related to most cases of ZIKV (49).

Besides vector transmission, various research groups have shown evidence of other modes of transmission of the ZIKV. Transplacental transmission has been confirmed and is currently a global concern as infected babies are born with microcephaly (50). Sexual transmission due to the persistence of ZIKV in the male genital tract has also been reported (51,52). The majority of sexually transmitted ZIKV cases have been linked to infection by a ZIKV-infected partner within 20 and 41 days of onset of illness in ZIKV infected male partner (53,54). The persistence of ZIKV in males has been linked to the persistence of infectious virus and viral RNA in the semen after 69 and 370 days respectively after the onset of disease symptoms (52,55,56) .

ZIKV has also been identified as one of the possible transfusion transmissible infections in addition to the potential transmission of HIV and hepatitis B (57). ZIKV was detected by PCR in 42(3%) of the 1505 blood samples donated from asymptomatic donors in French Polynesia (58). This finding suggested that ZIKV is a transfusion transmissible virus, which should be considered as a screening factor prior to a blood transfusion to patients.

Cells of the skin (fibroblasts and epidermal keratinocytes) are highly permissive to ZIKV infection (59) and the three primary immune cells targeted by flaviviruses, including ZIKV, are monocytes, macrophages, and dendritic cells (60–64), although, CD14+ monocytes have been reported as the main targets of ZIKV during infection (65–68).

Transmission of ZIKV starts when an infected mosquito bites an animal. The virus then migrates into the lymph nodes and undergoes further replication, (69) and migrates into the circulatory system where it crosses the blood–brain barrier and enters the central nervous system (70). The first line of host cell defense to ZIKV, as well as to other viral infections, is the innate immune response which includes secretion of type I interferons (IFNs) and inflammatory cytokines, complement responses, and Natural Killer cell immunity (70). Arboviruses like ZIKV are known to hijack other innate responses such as apoptosis, autophagy, and unfolded protein response to their benefit during infection and replication (71)

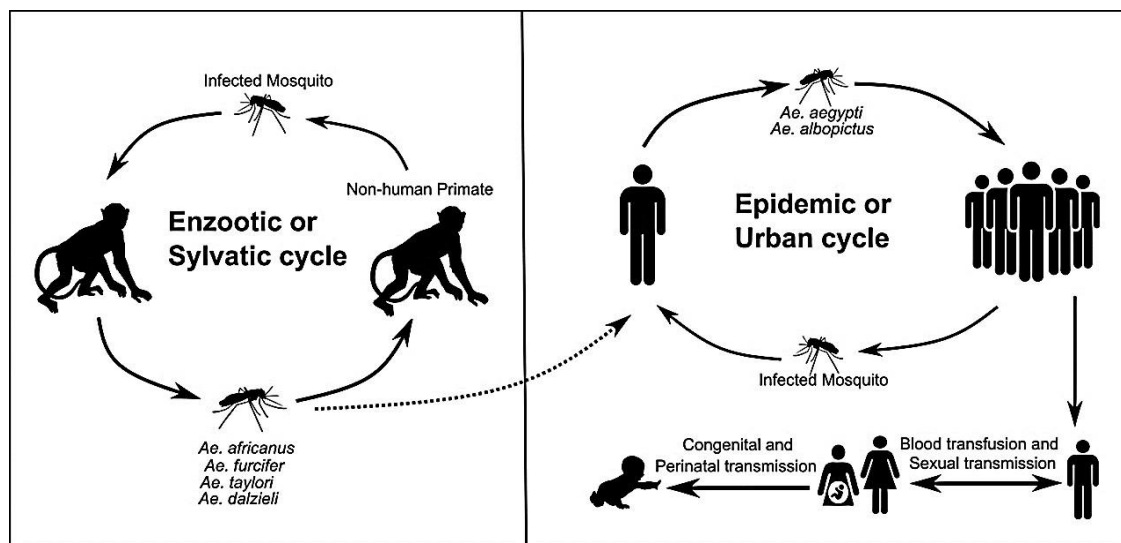


Figure 2: Transmission cycle of ZIKV (72).

ZIKV is spread mostly through mosquito bites. However, infected blood transfusion, sexual transmission, and maternal-fetal transfer have all been reported as mechanisms of transmission.

The enzootic or sylvatic cycle, as well as the epidemic or urban cycle, have both been described for ZIKV.

1.1.6 Clinical Manifestation of ZIKV Infection

With regards to symptoms, Zika infection mimics that of Dengue (48). Thus, Zika was previously misdiagnosed in patients as Dengue infection (11). The period between ZIKV infection and the onset of its associated clinical symptoms is approximately 3 to 12 days (73). However, infection is asymptomatic in approximately 80% of ZIKV infection cases (10,48). The clinical symptoms manifest as a self-limited febrile syndrome associated with rash, conjunctivitis and arthralgias (11). Rash, a prominent feature, is maculopapular and pruritic in most cases; it begins proximally and spreads to the extremities with spontaneous resolution within 1–4 days of onset while Fever is typically low grade (37.4°C – 38.0°C) (74–76). Other clinical complications reported in infected patients are gastrointestinal complications such as diarrhea nausea, abdominal pain, diarrhea, and vomiting (77). Zika induced renal complications in humans are being investigated due to the detection of the virus in the/a urine sample and the permissive of renal cells to ZIKV (78). Liu and his colleagues reported ZIKV causes acute kidney injury (AKI) in both newborn and adult mouse models by increasing the levels of AKI-related biomarkers (79).

Microcephaly and Guillain–Barré syndrome are the diseases reported to be caused by ZIKV infection. Microcephaly is a condition that results when the virus attacks the neural progenitor cells, disrupting their development and thereby affecting the complete formation of the fetal brain (80–82). Neural progenitor cells (NPC) are self-renewing neural stem cells in the brain which differentiate into neurons, astrocytes, and oligodendrocytes (83). Several research findings, such as detection of viral RNA in the amniotic fluid of Zika infected pregnant women as well as in brain tissues from microcephalic babies, have established the link between ZIKV and microcephaly (81,84). *In vivo* experiments in which pregnant mice were infected with Zika led to neuronal death, cell cycle arrest and apoptosis of NPCs leading to embryonic microcephaly and growth restriction (85–87).

Guillain–Barré syndrome is a rare but serious autoimmune disorder in which the immune system attacks healthy nerve cells in the peripheral nervous system (88). This leads to weakness, numbness, and tingling which can eventually result in paralysis. ZIKV epidemics in French Polynesia in 2013 and in Latin America and the Caribbean in 2015–2016 were linked to an increase in individuals being diagnosed with GBS (88–90). The WHO on Feb 1, 2016, declared Zika

associated microcephaly and Guillain-Barre syndrome as a Public Health Emergency of International Concern (PHEIC). This declaration was not based on the current information of Zika associated cases but on what is not known of clusters of microcephaly, Guillain-Barré syndrome, and possibly other neurological defects reported by country representatives from Brazil and French Polynesia (11,14).

1.1.7 Diagnosis of ZIKV Infection

Clinical presentations of patients infected with Zika are nonspecific as other infectious diseases also elicit the same clinical presentations. Thus, suspicion of ZIKV infection in the/a symptomatic patient will be based on the person confirming travel to a ZIKV endemic region. Laboratory diagnosis by RNA nucleic acid testing, using reverse transcription-quantitative polymerase chain reaction (RT-qPCR) is used to confirm Zika infection in blood or serum, which are currently used for detection of Zika infection in patients (91). Viremia is detectable between 3 to 5 days post-infection. Other samples with Zika diagnostic potential are cerebrospinal fluid (CSF), urine, saliva, amniotic fluid, semen, and fetal brain tissue (73). Urine and saliva, which are noninvasive samples, offer an alternative for diagnosis as compared to blood and cerebrospinal fluid, which are invasively collected from patients (92). Urine samples are currently recommended for diagnosis of ZIKV infection as viral RNA persists longer in urine compared to blood (57,92). One study reported that ZIKV RNA was detected in urine up to 20 days post-infection after viral RNA was undetectable in the blood (73). Thus, a patient urine sample must also be tested to confirm a/the diagnosis when a negative blood test is reported for a Zika suspected patient. Detection of Zika viral RNA in the saliva is best during the acute phase of the infection but is not ideal during the late stage. Musso et al. (2015) screened 182 Zika suspected patients' saliva and urine samples. Zika viral RNA was positive for 35 (19.2%) of their saliva while negative in their blood (58). On the other hand, 16 (8.8%) of the patients tested positive for Zika viral RNA in their blood but were negative in their saliva. This indicates that blood samples should also be screened in cases where saliva is used for Zika diagnosis.

Detection of ZIKV in the blood or serum by molecular techniques, namely RT-PCR, is best during the acute stage of the infection when the patient is in viremic status (93). Serology and molecular diagnoses are also currently the techniques being used for confirming Zika infection in patients. However, serologic testing has a major limitation because cross-reactivity with other

flaviviruses particularly Dengue, limits specificity. In addition, serology cannot be used as ZIKV IgM may be undetectable during the acute phase of the infection (94). Therefore, positive serologic test results should be confirmed with molecular testing. The plaque reduction neutralization assay, a sero-neutralization assay, generally has improved specificity over serology, but may still yield cross-reactive results in secondary Flavivirus infections (73).

Urine samples are also tested before the 14th day after the onset of symptoms. A positive result is confirmatory of Zika infection. A negative result, however, does not exclude infection (3) and additional serum IgM testing must be done to rule out infection. In the case of pregnant women who fall under the high-risk group, RNA nucleic acid testing is recommended on both serum and urine two weeks after any visit to a Zika endemic region. In addition, RNA testing is also done for those who are IgM positive for Zika after exposure. Pregnant women are routinely screened for Zika as part of their antenatal care in areas where Zika is endemic, the fetus is vulnerable to the developmental processes especially during the 1st and 2nd trimester of pregnancy (3).

1.1.8 Prevention (Antiviral and Vaccine Development against ZIKV)

ZIKV has been known for several decades (1947 till today) and causes serious clinical manifestations; however, there are no FDA-approved therapeutic interventions against it (89,95). It was unexpected that more than two years after WHO declared ZIKV a public health threat, global ZIKV prevalence dropped drastically (96). One question that comes to mind is that, could global decline in ZIKV prevalence be because of underdiagnosing of ZIKV cases due to lack of rapid diagnostic kits for the/a region which do not have the technical expertise or resource for ZIKV RNA nucleic acid testing by RT-PCR in suspected infected patient samples or could the current global attention on the still ongoing COVID-19 have shifted the world's attention from ZIKV?

Despite this drastic decline in global prevalence, considerable concerns remain to indicate a need to develop effective therapeutic interventions against ZIKV and other arbovirus infections to hijack potential viral outbreak and their clinical complications. This will mitigate probable future epidemics and pandemics, as almost occurred during the 2014–2016 Ebola virus outbreak, which fortunately did not result in a global pandemic due to an effective vaccine against Ebola (97,98).

Several factors which might result in the occurrence of a potential ZIKV pandemic include changes in the virulence of this virus, increased global travel and changes in climate conditions

leading to the geographic spread of the *Aedes* mosquito species (99). Patients infected with ZIKV are provided with supportive treatment where symptoms—such as fever, pain, pruritic rashes—among others and their symptoms are managed with various treatments—such as the use of acetaminophen, antihistamines, fluids replacement to prevent dehydration in ZIKV-infected patients, among others (100). However, more preventative measures must be considered hence the focus of my PhD research.

Different multifaceted libraries, FDA-approved drugs as well as natural compounds are being screened to determine their antiviral efficacy against ZIKV (101). These compounds are grouped as (i) direct-acting antivirals, directed against viral targets, or (ii) host-targeting antivirals, aimed at targeting cellular components needed for the viral cycle (102). Compounds being utilized in these two categories are being tested using *invitro* assays and animal models. Very few have gotten to the clinical trial stage for testing to ensure safety and efficacy when used in infected human populations (103).

ZIKV vaccine group candidates being tested include DNA Vaccines, Purified, Inactivated Virus Vaccines, mRNA Vaccines, Live Attenuated Vaccines, and Viral-Vectored Vaccines (104). Most of the various vaccine candidates in the various groups listed above as of September 2020 are unfortunately still at phase I clinical trials except one VRC5283, a DNA vaccine that has advanced to an international placebo-controlled phase II trial. The efficacy of this vaccine candidate is being assessed in both flavivirus endemic and nonendemic areas (105).

Concerns of people with preexisting flavivirus immunity developing vaccine-mediated Antibody-dependent enhancement (ADE) especially in Dengue infection due to antibody cross-reaction with ZIKV have been raised (106,107). Also, whether some people might later in life develop Guillain–Barré-like neurological side effects or developing fetus having congenital malformations are some of the points raised regarding the vaccine candidate which are still in the/a clinical trial. All these concerns must be addressed by the ZIKV vaccine trials which will pass phase III clinical trial and will be administered to ensure that it is safe and protective especially to the high-risk populations including women of childbearing age, pregnant women, young children, the elderly, and immune-compromised individuals (104).

1.1.9 Proteomics

Biomarker discovery and identification are being explored for the development of therapeutic modalities. Past and current research are designed to gain further insight into the virus-host interaction, and the impact of one on the other leading us to gain more understanding of the virus lifecycle, as well as the impact of the virus on the host cell's proteome and the transcriptome. These can be explored by use of various omics techniques and approaches as shown in Figure 3. Detection of these biomarkers facilitated by various 'omics techniques, include metabolomics, transcriptomics, metagenomics, proteomics, secretomics, and many others. Proteomics is one of the omics tools that have successfully been used to identify protein biomarkers, which are targeted during viral infections making them a promising and effective therapeutic candidate (3). Also, information generated by proteomic analyses have provided more understanding on changes in protein expression profile and has added to existing knowledge about how viruses hijack their host cell during replication via direct and indirect pathways. The advantages of seeking such protein biomarkers in this case is because all viruses depend on their host cell machinery to survive; thus, blocking access to these essential host factors will halt the virus life cycle, hence protecting the patient.

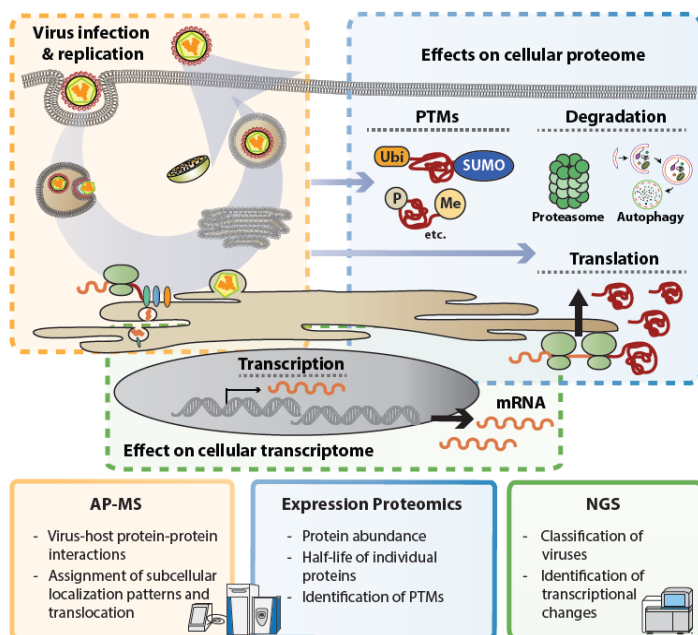


Figure 3: Omics methods to study virus-induced cellular perturbations (128).

1.1.9a SOMAScan Proteomic Analysis.

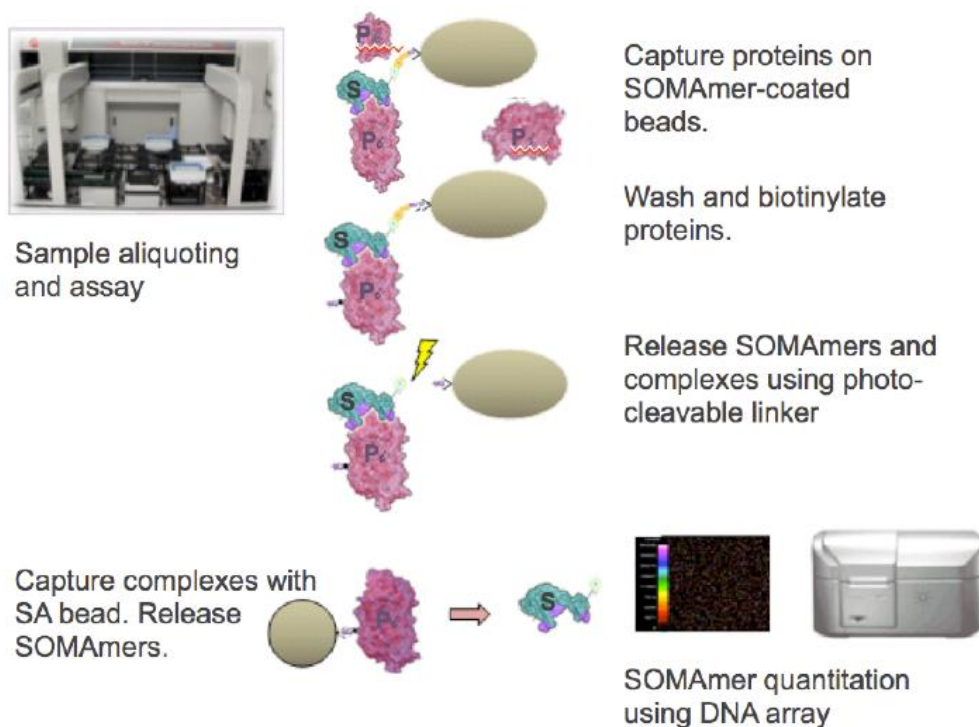


Figure 4: General steps of the SOMAScan Assay. (109) .

The SOMAScan is a highly multiplexed protein discovery tool that employs slow off-rate modified aptamers (SOMAMers; Soma-Logics, Inc., Denver, CO) (108). Aptamers are short nucleotides selected for their highly selective binding to specific proteins which can be measured using microarrays (109). This proteomic tool is highly sensitive, quantitative, and reproducible and has been successfully used to identify disease biomarkers for drug discovery. They are provided in a 96-well format (SOMAScan) and thus allows for simultaneous detection and measurement of more than 1,300 proteins in up to 92 different samples. It can also be utilized for various infection agents in large scale. Marion et al., 2016 and Coombs et al., 2019 used the SOMAScan platform, which was designed to screen 1,129 and > 1300 host proteins that were dysregulated following infection by various IAV strains, respectively (268,269). Recently, due to the COVID-19 outbreak, SomaLogic, the company that designed the SOMAScan announced that it increased the number of host proteins that can be screened from a previous ~1300 to ~7000

human cellular proteins (110).

The workflow of the SOMAScan analysis involves incubating diluted biological samples to be analyzed with SOMAmers which are pre-immobilized onto streptavidin (SA)-coated beads. The beads are then washed to remove unbound proteins and tagged by an NHS-biotin reagent. The tagged beads are exposed to an anionic competitor solution that prevents non-specific interactions from reforming after they are disrupted. The streptavidin (SA)-coated beads are then exposed to UV light which releases the SOMAmers protein complex and unbound SOMAmers from the beads. SOMAmers protein complex are re- incubated with SA coated beads and washed to remove unbound SOMAmers. The protein bound SOMAmer reagents are released from their cognate proteins using denaturing conditions and finally quantified by hybridization to custom DNA microarrays (111)

1.1.9b Tandem Mass Tagging Mass Spectrometry.

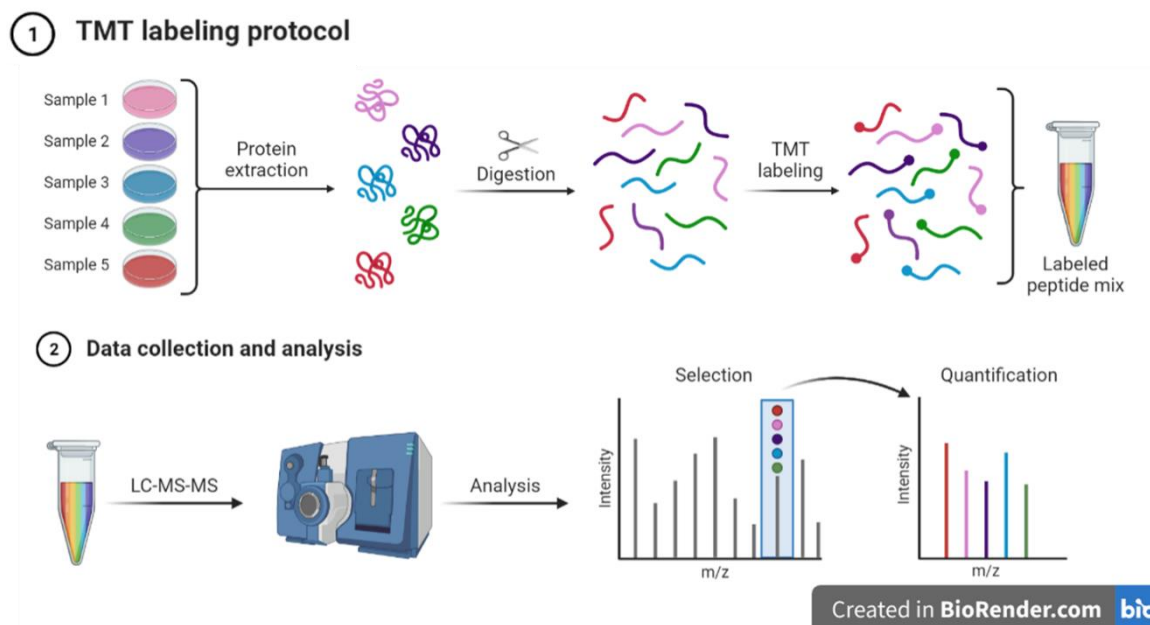


Figure 5: TMT Labeling Protocol. By Bio Render, July 2020, retrieved from <https://app.biorender.com/biorender-templates/t-5f4963c5b59c7a00ad18b5fd-tmt-labeling-protocol> Copyright 2021 by Bio Render.

Mass spectrometry has been a powerful technique for identifying large numbers of proteins in a non-biased manner as a preliminary screening tool (60). One drawback of mass spectrometry is that there is generally poor overlap between experimental replicates and the more abundant proteins are usually identified while low abundant proteins may be missed (112,113). Tandem Mass Tag Reagents are

isobaric tags which enables more accurate and multiplexed quantification of proteins in different samples by Tandem Mass Spectrometry (114). Labeled samples are analyzed on a high-resolution Orbitrap LC-MS/MS mass spectrometer before data analysis to identify peptides and quantify relative abundance of reporter ions (114). The TMT reagent consists of a mass reporter, a mass normalizer, and an amine reactive group. The advantage of TMT Mass Spectrometry is that different samples can be simultaneously labelled and analyzed at the same time hence there are 6, 10, 11 and 16 plex TMT labelling of samples (115).

1.1 Hypothesis and Aim of Study

ZIKV infection will induce dysregulation of host cell proteins in cellular pathways required for viral replication across multiple time points of ZIKV infection. The aim of my PhD research was therefore to use proteomic techniques to identify host proteins that were dysregulated during ZIKV infection and determine the various cellular pathways of these proteins.

1.2 Specific Objectives.

1. To determine protein expression profiles during ZIKV infection using proteomic techniques namely the SOMAScan and TMT Mass Spectrometry. This enabled identification of host proteins that were dysregulated and provided a clearer understanding of proteomic targets of the virus during its replication.
2. To determine specific cellular signal pathways and the proteins that were significantly dysregulated because of Zika infection at multiple time points.
3. To perform functional *in vitro* testing of proteins, which are most profoundly associated with Zika to gain better insight into the molecular mechanisms of Zika infection and their use as biomarkers for Zika infection.

1.3 Significance of study.

In Brazil, newborns delivered to ZIKV-infected pregnant mothers had a significant prevalence of microcephaly in 2015. Microcephaly occurs when ZIKV targets neural progenitor cells, altering their development and, as a result, influencing the creation of the fetal brain, which affects the development of the newborn (60,81,82). Identification of impacted proteins is being investigated in order to acquire a better knowledge of ZIKV biology. Because all viruses require host cellular machinery to reproduce, modifying essential cellular protein components may disrupt the ZIKV

replicative cycle and/or pathogenesis, resulting in an alternate therapy option. In comparison to earlier published ZIKV proteomic research, my PhD thesis examined alterations within the host cell proteome at several time periods and revealed previously unknown host proteins and pathways that are dysregulated and activated by the virus during infection.

Chapter 2: Materials and Methods

2.1 Cells and Viruses

2.1.i Cells.

All cell lines used in my PhD research were maintained as described by Glover et al., 2018 and 2020 (60,116,117). Vero cells (ATCC Number: CCL-81) and Caco-2 cells (ATCC® HTB-37™) were each cultured in DMEM and EMEM (ATCC® 30-2003™) respectively. Each culture medium was supplemented with 10% heat-inactivated fetal bovine serum (FBS), filter sterilized and 2 mM non-essential amino acids, sodium pyruvate and L-glutamine. All cell lines were maintained at 37 °C with 5% CO₂ ; cells were separated from each other and the container by trypsinization every 2–3 days.

2.1.ii Virus:

The Asian strain of ZIKV gifted from Dr. David Safronetz, Chief of Special Pathogens, the National Microbiology Laboratory, Public Health Agency of Canada was used in my ZIKV proteomic PhD research. Vero cells were infected with initial Zika stock to produce high viral titers. ZIKV infected Vero cells were then maintained in serum starved culture media. Cells were observed for cytopathology, and culture supernatants containing infectious viral particles were harvested by centrifugation; 20% FBS was then added to the harvested supernatants. ZIKV stock titer was determined by plaque assay and stored at -80°C.

2.2 Infection.

ZIKV growth curves were individually performed in each cell line to determine time points for peak ZIKV titer production in each cell line. Growth curve was done by infecting cells with ZIKV using low multiplicities of infection (MOI) namely, 1, 0.1, 0.01, and 0.0001. Titer of ZIKV produced in each cell lines was determined by plaque assay after day 1,2,3,4, and 5 days of infection.

For proteomic analyses, cells were infected at a higher MOI of 3 which by Poisson calculation, is

predicted to result in >90% of cells being infected. ZIKV and time-matched mock-infected cells were initially harvested at 6, 12, 24, 48, and 72 h post infection (hpi). Proteomic analyses were however performed on three separate biologic replicates after 12,24 and 48 hpi based on the cell viability by trypan blue staining and percentage of infected cells after ZIKV infection after immunofluorescent staining after these time-points respectively (60). Photomicrographs of Mock and infected cells were microscopically observed for cytopathic effect (CPE) using a Nikon TE-2000 inverted microscope. All images were taken with a Canon A-700 digital camera and exported into PowerPoint for minimal adjustment of brightness and contrast.

2.3 Protein Quantification:

Proteins from Mock- and ZIKV-infected cells for each cell line and time point were extracted by lysing cells with MPER (Pierce; Rockford, IL) supplemented with 1 × HALT Protease inhibitor (Pierce; Rockford, IL). Prior to cell lysis cells were washed thrice with sterile PBS to get rid of FBS in media used to culturing each cell line which would have interfered with interpretation of proteomic findings. After cell lysis, total protein from each cell lysate was estimated using Bicinchoninic acid assay (BCA) Protein Assay (Pierce; Rockford, IL).

2.4. Immunofluorescent Staining

Approximately 10,000 cells for each cell line were seeded on spotted slides and kept for 24 h at 37 °C in 5% CO₂. Cells were mock- and ZIKV infected after 24hrs of incubation of seeded cells and maintained in serum starved media. Time matched mock and ZIKV were fixed using 4% paraformaldehyde and permeabilized with 0.1% TritonX-100 in PBS for 5min. Each spot was blocked in 3% BSA overnight at 4 °C. After overnight blocking, cells were incubated with primary anti-ZIKV-NS1 antibody in 3% BSA overnight at 4 °C. After overnight incubation, cells were washed with 0.2% Tween 20 and 1% BSA in sterile PBS, incubated for 60 min with Alexa Fluor546 and Phalloidin for 20min and finally mounted with DAPI-containing mountant. Slides were imaged using a Zeiss Axio Observer Z1 inverted microscope.

2.5. Cell Viability

To determine the cell viability post ZIKV infection for time point selected for ZIKV proteomic analysis (12,24,48hrs) the trypan blue staining method was used. Time matched mock and ZIKV infected cells were harvested by brief trypsinization, resuspending in fresh culture media, and stained with equal volume of trypan blue. After 3 min of trypan blue staining, cells were counted with a hemocytometer. Total numbers of dead (blue) cells for each cell line were

compared to the total numbers of cells counted.

2.6. Immunoblotting

To verify infection status of cells, Western blots were performed to probe for ZIKV non-structural protein NS1 (Cat No Bio Front Technologies; cat # BF-1225-06). Proteins from ZIKV-infected and mock-infected samples were separated by SDS-PAGE and transferred to 0.2µm nitrocellulose membranes. Membranes were blocked in 5% skim milk for 1hr after which viral proteins were probed. GAPDH and/or β-actin (Cell Signaling # 2118l and 3700S respectively) were used as controls to estimate equal amount of proteins loaded as well as quantify expression intensity of viral proteins based on time points.

2.7. SOMAScan Analyses.

Protein concentrations of BCA-determined cell lysates were adjusted to 200 µg mL and 70 or 200 µL of each sample submitted for SOMAScan analysis. Analyses were performed in-house on a SomaLogic's -licensed platform in the Manitoba Centre for Proteomics and Systems Biology, using a SOMAScan version 1.3 platform capable of measuring quantities of more than 1,300 proteins. The SOMAScan assay consists of mixing each biologic sample with SomaLogic's proprietary slow off-rate modified aptamers (SOMAmers). Each SOMAmer was selected for its capacity to selectively recognize and bind to a specific human protein. Many SOMAmers also are known to bind monkey, feline, and mouse proteins (108). After mixing and binding each sample in an individual 96-well, which allows simultaneous analysis of up to 92 samples (plus four control wells), the SOMAmers were washed, released, hybridized to DNA microarrays and quantified (108,109). Results were reported in RFU which were directly proportional to the amounts of target proteins in the initial samples, as confirmed by a standard curve generated for each protein-SOMAmer pair (108).

2.8 Tandem Mass Tagging (TMT) Mass Spectrometry (MS) Analyses

Quantified proteins from 12, 24, and 48 hpi samples were digested into peptides using the SP3 (single-pot solid-phase-enhanced sample preparation) procedure described by Sielaff (118). Briefly, proteins were trypsin digested for 14 h at 37 °C and peptides were eluted. Tandem mass tags (TMT) labeling was performed as specified by the manufacturer (Thermo Fisher Scientific), except that TMT labels were dissolved in DMSO. Individual 6-plex TMT labeling was performed on 80 mg of each of three replicates of

mock and three replicates of infected at each time-point, making a total of 18 samples analyzed by TMT M/S. Equivalent amounts of labeled samples within each TMT time set were mixed prior to 2D LC/MS/MS.

An Agilent 1100 series LC system with UV detector (214 nm) and 1mm X 100mm XTerra C18, 5 μ m column (Waters, Ireland) was used for pH 10 first dimension reversed-phase separation. A gradient of 1.80% acetonitrile per minute (0.1– 59.9% acetonitrile in 30 min) was delivered at a flow rate of 150 μ L/min. Both eluents A (water) and B (1:9 water: acetonitrile) contained 20 mM ammonium formate at pH 10. Twenty 1-min fractions were collected and concatenated into 10 (#1 mixed with # 11, etc.) to provide optimal orthogonal separation. These fractions were lyophilized and resuspended in 0.1% formic acid for the second-dimension analyses. Analyses of TMT-labeled peptides were performed on an Orbitrap Q Exactive HF-X instrument (Thermo Fisher Scientific, Bremen, Germany). The sample was introduced using an Easy-nLC 1000 system (Thermo Fisher Scientific) at 1 μ g per injection. Mobile phase A was 0.1% (v/v) formic acid and mobile phase B was 0.1% (v/v) formic acid in 80% acetonitrile (LC-MS grade). Gradient separation of peptides was performed on a C18 (Luna C18; 3 μ m particle size [Phenomenex, Torrance, CA]) column packed in-house in Pico- Frit (100 μ m X 30 cm) capillaries (New Objective, Woburn, MA, United States). Peptides were separated by the following gradient: 5% phase B over 2 min, 5–7% increase of phase B over 2 min, 7–25% over 60 min, 25–60% over 15 min, 60–90% over 1 min, with a final elution of 90% B for 10 min at a flow rate of 300 nL/min. Data acquisition on the Orbitrap Q Exactive HF-X instrument was configured for data-dependent method using the full MS/DD-MS/MS setup in a positive mode. Spray voltage was set to 1.85 kV, funnel RF level at 40, and heated capillary at 275°C. Survey scans covering the mass range of 350–1500 m/z were acquired at a resolution of 120,000 (at m/z 200), with a maximum ion injection time of 60 ms, and an automatic gain control (AGC) target value of 3e6. For MS2 scan triggering, up to 20 of the most abundant ions were selected for fragmentation at 32% normalized collision energy, with intensity threshold kept at 6.3e4. AGC target values for fragment spectra were set at 1E5, which were acquired at a resolution of 30,000, with a maximum ion injection time of 80 ms and an isolation width set at 1.2 m/z. Dynamic exclusion of previously selected masses was enabled for 20 s, charge state filtering was limited to 2–6, peptide match was set to preferred, and isotope exclusion was on.

2.9 Peptide and Protein Identification and Quantification.

A database of protein sequences for ZIKV (Thai strain) and human (Uniprot 2016) was used for peptide/protein identification (116). For each time point every 1D LC-MS run in the 2D-LC-MS experiment was converted into an MGF file using the Proteome Discoverer bundled tool, as we have previously described (119–121). These were then concatenated into a single MGF per time point. These three concatenated MGFs files were each searched against the database using X! tandem (cyclone 2012.10.01.1). Spectra files in MGF format, the peptide identification results, and the overall protein expression matrix are stored under accession MSV000085057 at the UCSD Centre for Computational Mass Spectrometry repository (<https://massive.ucsd.edu>). Standard peptide identification settings were used: single missed cleavage tryptic peptides were permitted, with a parent and fragment mass tolerance of 10 ppm. A fixed posttranslational modification of C+ 57.021 was applied, and variable PTMs including N-terminal acetylation, deamidation, phosphorylation, and oxidation were permitted. Peptide assignment into source proteins was managed by X! tandem. Peptide level TMT6 reporter tag intensities were integrated across window of ± 3 mDa each and corrected for isotopic overlap between channels using the supplied batch-specific correction matrix. Protein quantitation required at least two unique peptides with expectation values $\log(e) \leq -1.5$ each, yielding highly confident protein assignments of at least $\log(e) \leq -3$. The sum of peptide level TMT6 reporter tag intensities for each protein was converted into a log2 scale for simplified differential analysis.

2.10 Statistical and Bioinformatics Analysis

RFU for each of the more than 1,300 proteins identified after SomaLogic analysis, in each of three biologic replicates, each consisted of a ZIKV-infected sample and a time matched non-infected mock sample at 12, 24, and 48 hpi (18 total samples) were imported into Excel and converted to log2 values (60,116). Fold-changes were determined for each of the nine infected samples compared to their time-matched mock samples. The fold-changes were analyzed for significance by both Students t-test with two tails, and by Z-score analysis, essentially as described (122). Briefly, all fold-changes not deemed to be significant by t-test were examined by Z-score, expressing each value as its number of standard deviations away from the population mean. Each protein's Z-score was considered significant if it met the following conditions: (1) The Z-score was $> 1.96\sigma$ in each of $\geq \frac{1}{2}$ the replicates and was $> 0.98\sigma$ in the remaining replicate, or was $< -1.96\sigma$ in each of $\geq \frac{1}{2}$ the replicates and was $< -0.98\sigma$ in the remaining replicate; and (2) the

average Z-score for all replicates was $> 1.96\sigma$ or $< -1.96\sigma$. For increased stringency, a fold-change cut-off of 1.25-fold dysregulation (≥ 1.25 - fold if up-regulated, or ≤ 0.80 -fold if down-regulated) was also applied to those proteins deemed significantly dysregulated. Fold changes and p-values were imported into PANTHER and IPA for additional bioinformatics and pathway analyses.

Chapter 3: Results

3.1 Vero Cell Proteomic Changes Induced by ZIKV Infection.

Number of citations from this publication: 11

3.1.i Contributory Role.

Contributed to designing and performing all experiment prior to SomaLogic analysis which was done by Gao Ang, one of the listed coauthors of this publication. Also contributed to analyzing the data generated and writing up the manuscript prior to submission for publication.

3.1.ii Kinetics of Virus-Induced Cytopathology and Virus Replication.

ZIKV growth curves, Western blotting, and immunofluorescent staining were initially performed in Vero cells to determine the optimal times for subsequent proteomic screens. Using an MOI of 3, which by Poisson calculation is predicted to result in >90% of cells being infected, Vero Cells were ZIKV-infected. Cytopathologic changes were microscopically observed from 24 to 72 hours of ZIKV infection, shown in Figure 6. Cytopathologic changes were moderate after 24hpi and extensive after 48 to 72 hpi. There were, however, no visible cytopathologic changes after 12hrs, which was then chosen as the early time point for ZIKV infection.

To ensure cells after ZIKV infection remained viable prior to proteomic analysis, cell viabilities of mock and time-matched ZIKV infected Vero cells were determined by Trypan Blue Exclusion Test of Cell Viability (Figure 6B). There were no significant differences in cell viabilities of mock or time-matched ZIKV Vero cells at earlier time points namely 6, 12, or 24 hrs., with the proportion of dead cells below 10%. Very significant differences were however observed after 48 hpi where only about 8% of mock cells were dead compared to approximately 20% of ZIKV infected cells. Cell viability was however below 50% after 72 hrs. of ZIKV infection where almost half of the infected cells were dead.

Viral replication kinetics were also assessed by immunoblotting for ZIKV non-structural protein 1 (NS1) and measuring infectious viral particle production by plaque assay. ZIKV NS1 expression, as well as high titers of ZIKV, were observed at later times (Figure 6C). Protein signal increased with longer incubation. Viral titer also increased as a function of incubation time (Figure 6D).

Since significant global proteomic screens to evaluate infection-mediated protein dysregulation require that most cells in the population are infected, we used immunofluorescent microscopy to

look for viral NS1, which is only expressed during productive infection, and concluded that nearly all our cells were infected by 24- and 48-hours post-infection (Figure 6E)

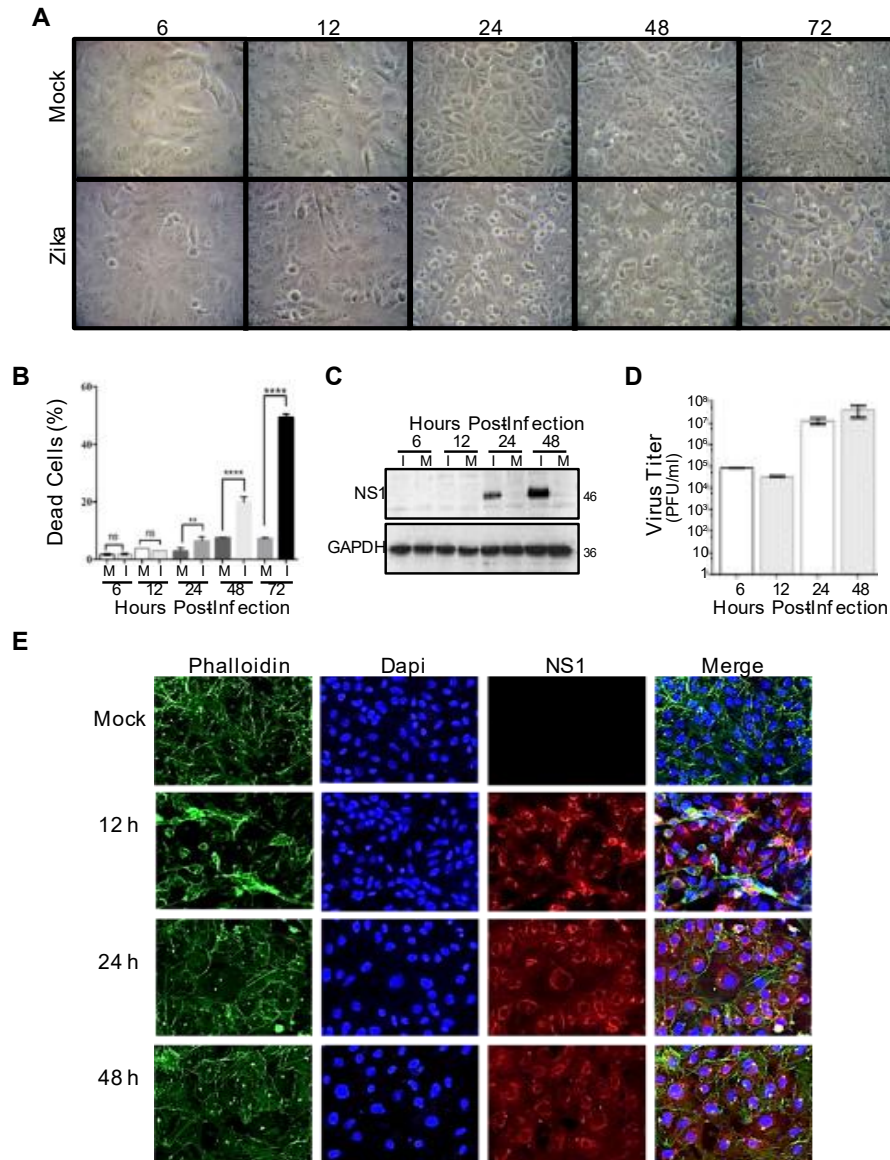


Figure 6: Kinetics of virus induced cytopathology and virus replication in Vero cells.

A) Cytopathic effect induced by ZIKV. Vero cells were infected with ZIKV at MOI = 3 and overlaid with serum-starved DMEM. Infected and parallel mock-treated cells were observed microscopically at indicated times for appearance of cytopathic effect after ZIKV infection. Images were captured with a Canon A-700 camera, and those shown are representative of three biologic replicates. B) Cell viability after ZIKV infection. Mock- and ZIKV-infected cells were harvested at indicated time points and stained with trypan blue. The percentages of live and dead cells in both mock and infected flasks were counted using a hemocytometer. $n = 3$, error bars represent S.E.M. C) Immunoblot confirmation of successful infection. Viral non-structural protein

NS1, a marker of productive infection, was probed at indicated times to confirm infection status of the cells. Molecular weight marker locations are indicated to the right. The blot is representative of three biologic replicates. M = mock, I = ZIKV-infected. D) Determination of infectious viral particle production. Supernatants from ZIKV-infected Vero cells were harvested at indicated time points and infectious viral particle production determined by standard plaque assay. $n = 3$, error bars represent S.E.M. E) Immunofluorescent detection of proportions of ZIKV-infected cells. Vero cells were infected at an MOI = 3 for indicated periods of time and immunoprobed to determine proportions of productively infected cells. DAPI (blue) for nucleus, Phalloidin (green) for cytoskeleton and Alexa 546 (red) for ZIKV NS1.

3.1.iii ZIKV Induction of Proteomic Dysregulation.

SOMAScan analyses of triplicate replicates were performed on time-matched mock-infected compared ZIKV infected Vero cells after 12, 24, and 48 hpi. Host proteins were considered “dysregulated” based on their fold changes which were determined by the difference between time-matched mock log2 expression values from the infected. This criteria for considering a protein “dysregulated” has been successfully used in several published omics studies from our lab (proteomics) as well as other research groups (119,123–126). The first replicate's proteomic data for 12 and 24 hours were skewed away from the second and third replicates, according to a PCA. The proteomic data from all three replicates at 48 hpi were however more consistent. Based on the PCA findings, bioinformatic analysis was done using all three replicates, or only replicate #2 and #3, and compared results from these two analyses to each other (Appendix: Figure S1A, Supporting Information). To validate that fold changes values were virus-induced, hence the term dysregulates, Western blotting was done for host proteins with folds greater or less than the fold values cut-off which was reflective of the value reported after SOMAScan analysis. Heatmap of fold-changes across all three time points showed the most dysregulation of host proteins was at 48 hpi, while depending on which datasets were used, there were variations in apparent dysregulation of certain proteins at 12 and 24 hpi (Appendix: Figure S1B, Supporting Information).

Similarly, regardless of whether all three datasets were used or whether the first dataset was omitted, several biological processes, molecular function events, and protein classes were classified as highly enriched when these datasets were uploaded into bioinformatics pathway analysis tools (Appendix: Figure S1C, Supporting Information). This was particularly true for the down-regulated classes, where most were similarly enriched. Similar enrichments were also found in the up-regulated functions although the degree of enrichment was more variable. Thus, because

of the significant skewing of some of the datasets in replicate #1, all data analyses were based on replicates 2 and 3. Based upon t-test and Z-score analyses, 125 unique Vero proteins were significantly dysregulated by ZIKV infection (Figure 7, Table 1). For analyses of such datasets, we usually also consider each protein's differential fold-change along with its significance. For example, if proteins whose fold-change is less than 10% in either direction are excluded from all proteins considered significant, the number of unique significantly dysregulated proteins is reduced to 107, with two up-regulated at 12 hpi, 19 down-regulated at 12 hpi, etc. However, if the cut-off is set as a twofold change in either direction, the number of unique significantly dysregulated proteins is reduced to only 11, with no proteins significantly dysregulated until 48 hpi. Thus, for a more detailed analysis of this data set, we set the cut-offs as p-value < 0.05 and fold-change of ≥ 1.25 (up-regulated to ≥ 1.25 ($= \geq 0.322 \log_2$) or down-regulated to ≤ 0.80 ($= \leq -0.322 \log_2$)). Using these criteria, one protein was significantly up-regulated and ten were significantly down-regulated at 12 hpi, three proteins were significantly up-regulated, and one was significantly down-regulated at 24 hpi, and 39 proteins were significantly up-regulated and 28 were significantly down-regulated at 48 hpi (Tables 1 and 2).

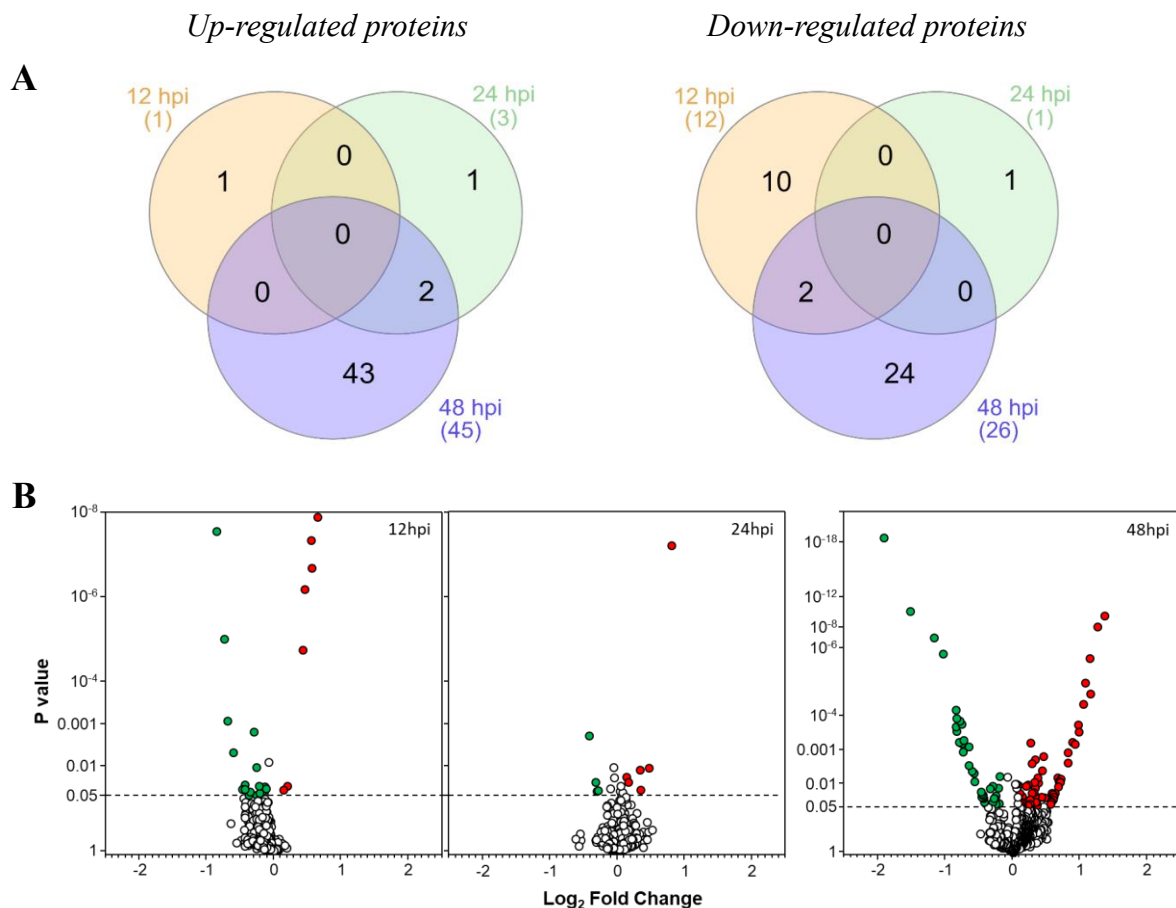


Figure 7: Characteristics of dysregulated proteins.

A) Venn diagram of total numbers of significantly dysregulated (up and down) cellular proteins identified by SOMAScan analysis at 12, 24, and 48 hpi infection, showing numbers of common proteins across all three time points. B) Volcano plots displaying p-values and log2-fold changes of each protein at each time point after compiling and merging data from biologic replicates #2 and #3, because, as indicated in text and in Figure S1, Supporting Information, PCA showed two of the three time points in replicate #1 were skewed away from data in replicates #2 and #3. Red dots correspond to proteins considered significantly up-regulated (fold-change ≥ 1.25 ; $\log_2 \geq 0.322$) and green dots correspond to proteins considered significantly down-regulated (fold-change ≤ 0.80 compared to mock; $\log_2 \leq -0.322$). The horizontal dashed lines correspond to p-value of 0.05.

Table 1: Numbers of significantly dysregulated ZIKV-infected Vero proteins.

Number that are significant	Total Unique	12 hpi	24hpi	48hpi
And Fold-change > 1.000	125	3	9	59
And Fold-change < .9999		21	7	40
And Fold-change > 1.100	107	2	5	51
And Fold-change < .9091		19	4	39
And Fold-change > 1.250	77	1	3	39
And Fold-change < .8000		10	1	28
And Fold-change > 1.500	45	0	0	24
And Fold-change < .6667		4	0	17
And Fold-change > 2.000	11	0	0	7
And Fold-change < .5000		0	0	4

Significance was determined by t-test and Z-Score as detailed in Materials & Methods after compiling data from Replicates #2 and #3.; Shaded values, corresponding to significant dysregulation and up- or down-regulated; ≥ 1.25 -fold, were used for subsequent analyses.

Table 2: Vero cell proteins significantly affected by ZIKV infection, measured by SOMAmers.

Entrez Gene Symbol	Protein	12 h		24 h		48 h	
		Fold Change	P-value	Fold Change	P-value	Fold Change	P-value
CA6	Carbonic anhydrase 6	1.38	6.9E-07	1.03	0.693	1.10	0.595
KLKB1	Plasma kallikrein	0.78	0.040	0.99	0.910	0.98	0.867
MMP12	Macrophage metalloelastase	0.76	0.048	0.95	0.786	1.12	0.111
	Polymeric	0.74	0.035	0.93	0.820	0.65	0.0009
PIGR	immunoglobulin receptor	0.73	0.028	1.04	0.800	1.01	0.781
FGR	Tyrosine-protein kinase Fgr	0.73	0.050	1.04	0.797	2.24	0.004
CXCL11	C-X-C motif chemokine 11	0.72	0.036	1.10	0.729	0.95	0.728
LTA LTB	Lymphotoxin alpha1:beta2	0.66	0.005	0.94	0.951	1.20	0.415
PES1	Pescadillo homolog	0.62	0.0009	0.91	0.846	0.85	0.329
HIST1H1C	Histone H1.2	0.60	9.8E-06	0.87	0.670	0.75	0.029
FER	Tyrosine-protein kinase Fer	0.55	2.9E-08	0.87	0.288	1.25	0.072
KLK7	Kallikrein-7	1.14	0.867	1.39	0.011	0.87	0.014
FN1	Fibronectin	0.96	0.945	1.27	0.037	1.62	0.013
EPHA3	Ephrin type-A receptor 3	0.87	0.597	1.27	0.013	1.28	0.038
RASA1	Ras GTPase-activating protein 1	0.85	0.327	0.75	0.002	1.11	0.178
TGM3	Protein-glutamine gamma-glutamyltransferase E	0.71	0.575	1.19	0.480	2.60	0.001
CCL5	C-C motif chemokine 5	0.90	0.042	1.03	0.826	2.43	6.6E-08
CSNK2A2 CSNK2B	Casein kinase II 2-alpha':2-beta heterotetramer	0.77	0.646	1.04	0.965	2.25	2.4E-05
HMGN1	Non-histone chromosomal protein HMG-14	0.92	0.742	1.26	0.471	2.14	0.026
APOE	Apolipoprotein E (isoform E4)	0.93	0.763	1.21	0.535	2.10	0.037
NUDCD3	NudC domain-containing protein 3	1.03	0.878	1.36	0.573	2.00	0.0003
PKM2	Pyruvate kinase PKM	0.91	0.164	1.04	0.754	1.99	0.037
EIF5A	Eukaryotic translation initiation factor 5A-1	0.90	0.542	1.31	0.369	1.92	0.0008
PARK7	Protein deglycase DJ-1	0.86	0.151	1.06	0.828	1.87	0.040
METAP2	Methionine aminopeptidase 2	0.90	0.821	0.97	0.919	1.79	0.003
WNK3	Serine/threonine-protein kinase WNK3	0.99	0.984	1.19	0.620	1.79	0.016
APOE	Apolipoprotein E (isoform E2)	0.84	0.149	1.11	0.738	1.66	0.027
PRKACA	cAMP-dependent protein kinase catalytic subunit alpha	0.87	0.495	1.04	0.864	1.65	0.009
PEBP1	Phosphatidylethanolamine-binding protein 1	0.75	0.190	0.87	0.659	1.63	0.009
SSRP1	FACT complex subunit SSRP1	0.89	0.662	1.02	0.840	1.56	0.045
PAK6	Serine/threonine-protein kinase PAK 6	1.04	0.880	1.20	0.736	1.55	0.027
EPHA2	Ephrin type-A receptor 2	0.93	0.414	1.02	0.777	1.54	0.031
ANXA5	Annexin A5	0.89	0.411	1.15	0.086	1.54	0.023
HSPA1A	Heat shock 70 kDa protein 1A	0.94	0.906	1.23	0.671	1.52	0.021
CDK2 CCNA2	Cyclin-dependent kinase 2:Cyclin-A2 complex						

ITGA1 ITGB1	Integrin alpha-I: beta-1 complex	1.10	0.737	1.22	0.132	1.51	0.038
PPID	Peptidyl-prolyl cis-trans isomerase D	0.93	0.766	0.99	0.970	1.51	0.032
UBE2N	Ubiquitin-conjugating enzyme E2 N	0.90	0.576	0.98	0.822	1.50	0.020
CKB	Creatine kinase B-type	0.90	0.161	1.06	0.107	1.50	0.043
DCTPP1	dCTP pyrophosphatase 1	0.81	0.598	0.97	0.904	1.41	0.028
IDE	Insulin-degrading enzyme	0.92	0.504	1.02	0.939	1.39	0.002
YWHAB,YWHAE,YWHAG, YWHAH,YWHAQ,YWHAZ, SFN	14-3-3 protein family	0.89	0.192	1.03	0.670	1.37	0.004
FAS	Tumor necrosis factor receptor superfamily member 6	0.99	0.977	1.08	0.734	1.36	0.026
CSNK2A1 CSNK2B	Casein kinase II 2-alpha:2-beta heterotetramer	0.96	0.909	0.96	0.844	1.32	0.010
GRB2	Growth factor receptor-bound protein 2	0.96	0.201	1.02	0.755	1.31	0.007
PA2G4	Proliferation-associated protein 2G4	0.89	0.033	1.04	0.827	1.30	0.048
GPI	Glucose-6-phosphate isomerase	0.89	0.096	1.05	0.699	1.30	0.038
XPNPEP1	Xaa-Pro aminopeptidase 1	0.93	0.739	1.06	0.761	1.28	0.024
UCHL1	Ubiquitin carboxyl-terminal hydrolase isozyme L1	0.93	0.672	1.09	0.600	1.27	0.014
CAPN1 CAPNS1	Calpain I	0.93	0.659	1.04	0.880	1.27	0.002
CDC37	Hsp90 co-chaperone Cdc37	0.75	0.550	0.95	0.931	1.27	0.010
UFC1	Ubiquitin-fold modifier-conjugating enzyme 1	0.88	0.396	0.97	0.797	1.26	0.020
IGF1R	Insulin-like growth factor 1 receptor	0.92	0.252	1.16	0.553	0.79	0.050
IMPDH1	Inosine-5'-monophosphate dehydrogenase 1	0.88	0.641	0.89	0.437	0.76	0.038
IGFBP2	Insulin-like growth factor-binding protein 2	0.90	0.799	0.85	0.497	0.75	0.023
MDK	Midkine	0.84	0.745	0.98	0.971	0.74	0.028
CNTN1	Contactin-1	0.97	0.882	1.07	0.709	0.74	0.021
TNFRSF21	Tumor necrosis factor receptor superfamily member 21	0.89	0.714	0.97	0.931	0.73	0.026
LGALS3BP	Galectin-3-binding protein	0.89	0.713	0.94	0.822	0.73	0.019
AKR1A1	Alcohol dehydrogenase [NADP(+)]	0.89	0.635	0.94	0.767	0.73	0.031
PDPK1	3-phosphoinositide-dependent protein kinase 1	0.99	0.993	1.08	0.944	0.68	0.009
SPINT2	Kunitz-type protease inhibitor 2	0.93	0.890	0.91	0.849	0.68	0.005
L1CAM	Neural cell adhesion molecule L1	0.85	0.310	0.89	0.544	0.66	0.005
IGFBP3	Insulin-like growth factor-binding protein 3	0.90	0.841	0.89	0.530	0.64	0.003
GRN	Granulins	0.96	0.925	1.01	0.987	0.61	0.007
STAT3	Signal transducer and activator of transcription 3	0.91	0.880	0.81	0.041	0.61	0.001
HSPB1	Heat shock protein beta-1	0.90	0.630	0.97	0.909	0.60	0.0007
IGFBP7	Insulin-like growth factor-binding protein 7	0.89	0.768	0.90	0.819	0.60	0.0002
LYZ	Lysozyme C	0.83	0.686	1.03	0.934	0.59	0.015
GSN	Gelsolin	0.88	0.710	1.01	0.978	0.58	0.0006
IGFBP5	Insulin-like growth factor-binding protein 5	0.84	0.736	0.88	0.338	0.57	0.0001
EIF4H	Eukaryotic translation initiation factor 4H	1.10	0.036	0.92	0.693	0.57	0.0003
EIF4A3	Eukaryotic initiation factor 4A-III	0.89	0.689	0.96	0.878	0.56	7.4E-05
SNX4	Sorting nexin- 4	0.92	0.837	0.83	0.039	0.56	0.0002
C3	Complement C3	0.89	0.820	0.92	0.893	0.49	1.6E-06

EIF4G2	Eukaryotic translation initiation factor 4 gamma 2	0.86	0.557	0.80	0.025	0.45	2.9E-07
C3	C3a anaphylatoxin des Arginine	0.90	0.913	0.91	0.925	0.35	7.9E-12
C4A C4B	Complement C4	0.89	0.385	0.81	0.573	0.27	0.014

Fold-change values represent protein dysregulation of ZIKV-infected compared to mock-infected. Significant fold-changes >1.25-fold are indicated in shaded cells and larger bold font. Red text corresponds to up-regulation compared to mock; green corresponds to down-regulation. Significant p-values shown in red. Significance was determined by T-test and by Z-Score as detailed in Materials & Methods. Proteins are sorted by time point (early to late) with up-regulated at top and down-regulated below. Fold-changes determined from two biologic replicates.

3.1.iv Validation of Protein Dysregulation ZIKV.

Western blots were performed on five selected proteins to validate SOMAScan data (Figure 8). These proteins were selected to represent up-regulated, down-regulated, and non-regulated proteins and on antibody availability. β -actin was used as a loading and normalization control. There was generally good agreement between the SOMAScan data and the immunoblot data for the chosen proteins. Fibronectin was measured as up-regulated significantly only at 24 hpi by SOMAScan (1.39, p-value 0.011), and Western blot also showed a major band intensity increase in the 24 h infected sample compared to the time-matched mock control. STAT3 was measured as mildly down-regulated in the 12 and 24 hpi samples (0.91 p-value 0.90, 0.81 p-value 0.04) and significantly down-regulated in the 48 hpi sample (0.61 p-value 0.001) by SOMAScan.

Western blot also showed a major band intensity decreased in the 48-h infected sample compared to the time-matched control and provided more detail about the α and β forms. There were clear differences in the α/β ratio, with the β form declining with increased incubation time, irrespective of infection status. The remaining proteins PSMA2 (12hpi 0.90 p-value 0.30, 24hpi 1.00 p-value 0.94, 48hpi 1.02 p-value 0.84) and GAPDH (12hpi 0.94 p-value 0.53, 24hpi 0.97 p-value 0.73, 48hpi 0.96 p-value 0.25) were not significantly dysregulated according to both SOMAScan and Western blot. Although Western blotting suggested CLIC1 (12hpi 0.87 p-value 0.34, 24hpi 0.98 p-value 0.52, 48hpi 1.21 p-value 0.03) was mildly dysregulated, this was not found to be significant, also in agreement with the SOMAScan data.

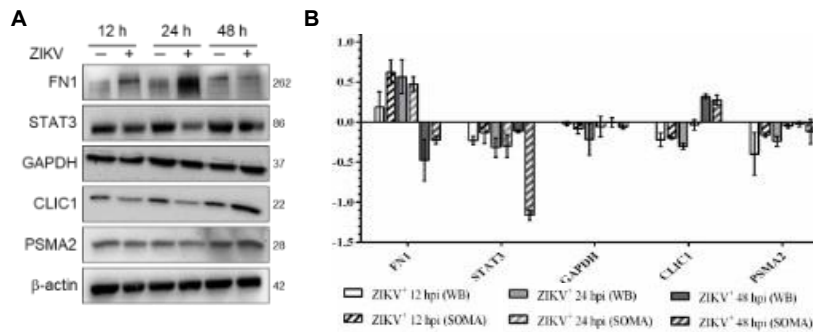


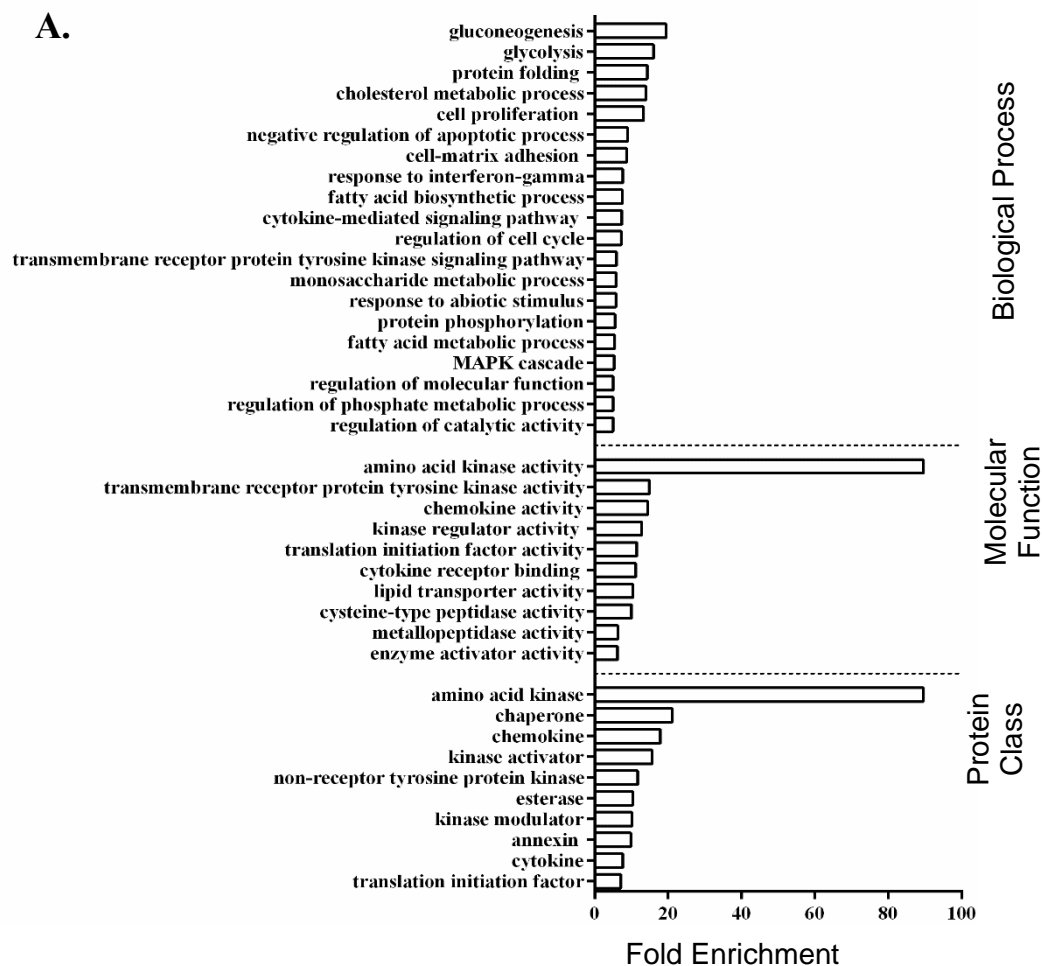
Figure 8: Validation of protein dysregulation.

A) The indicated proteins (up-regulated FN1, down-regulated STAT3, and non-regulated GAPDH, PSMA2 and CLIC1) were harvested at indicated times from mock- and ZIKV-infected Vero cells at 48 hpi, lysed, proteins resolved in SDS-PAGE, transferred to nitrocellulose membranes, and membranes probed with indicated antibodies. Molecular weight marker locations are indicated to the right. These blots are representative of three biologic replicates. B) Densitometric comparison of immunoblot-determined protein quantities compared to SOMAScan determined protein quantities.

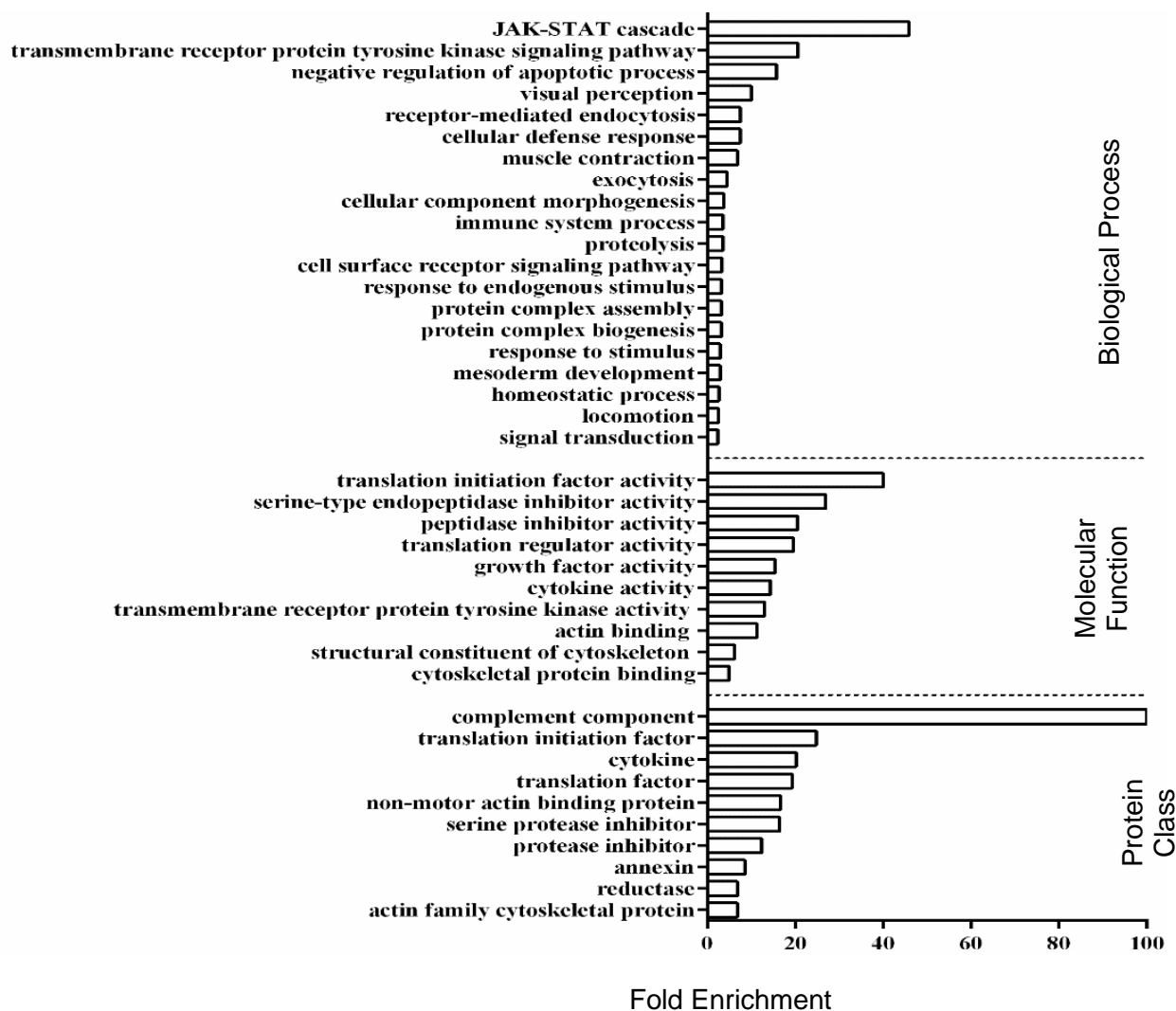
3.1.v Bioinformatic and Pathway Analyses Highlight Multiple Cellular Processes and Pathways Affected by ZIKV Infection.

Because of the small numbers of proteins measured as dysregulated at 12 and 24 hpi, no prominent cellular pathways were reliably identified by IPA at these time points. Numerous processes were identified at 48 hpi. The two most prominent biologic processes up regulated by ZIKV infection by 48 hpi were gluconeogenesis and glycolysis (fold enrichment values >10) (Figure 9A, top). Amino acid kinases also were up-regulated and were enriched >80-fold and chaperones were enriched 20-fold. The most prominent biologic process down-regulated by ZIKV infection by 48 hpi was the JAK-STAT cascade (fold enrichment value >40) (Figure 9A, bottom). Translation initiation factor activity and complement components also were significantly enriched among down-regulated functions. Only two prominent cellular networks were identified by IPA namely, (1) Cellular movement, organismal injury and abnormalities, cell-to-cell signaling and interaction, and (2) Cell death and survival, cellular development, cellular growth, and proliferation (Figure 9B, 9A, and B). Each of these cellular processes had scores >30 and contained ten or more focus molecules (significantly dysregulated).

Numerous canonical pathways also were identified as significantly activated or inhibited (Figure 10C). Activated pathways included IGF-1 signaling, PI3K/Akt signaling, NF- κ B signaling, and Tec kinase signaling (involving >1.25-fold up-regulation of ITGB1, PAK6, GRB2, and FAS, and >1.25-fold down-regulation of TNFRSF21 and STAT3) (Figure 10D). Inhibited pathways included PTEN signaling, IL-6 signaling, and growth hormone signaling. Tec kinase signaling was predicted to activate neuronal and motor neuron cell death, and apoptosis of neuroglia and oligodendrocytes (Figure 10E).



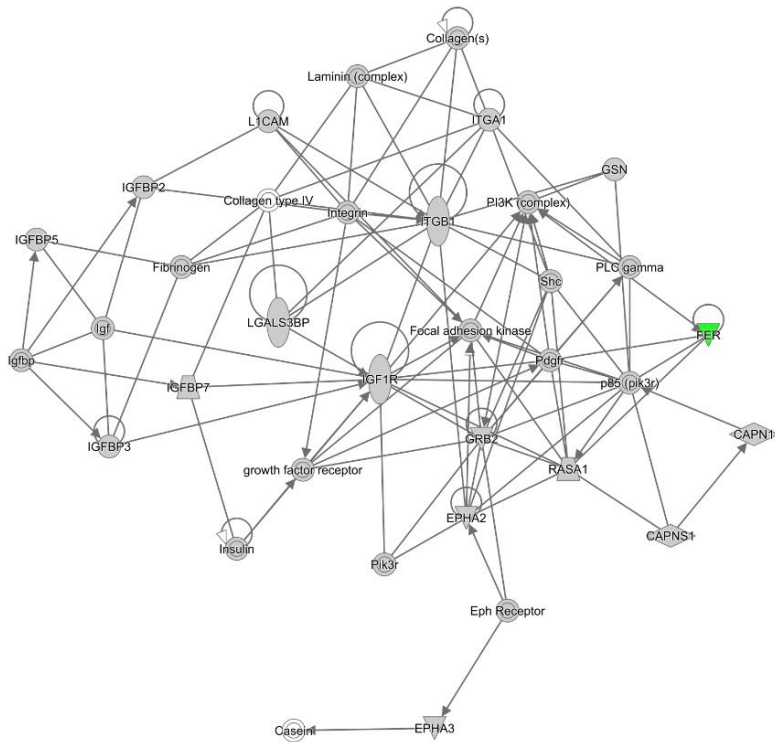
B.



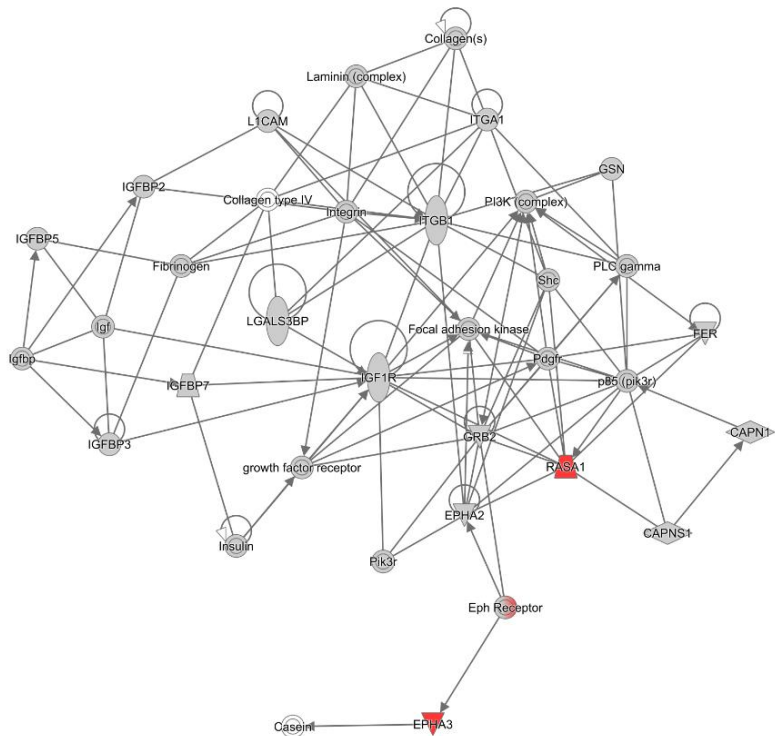
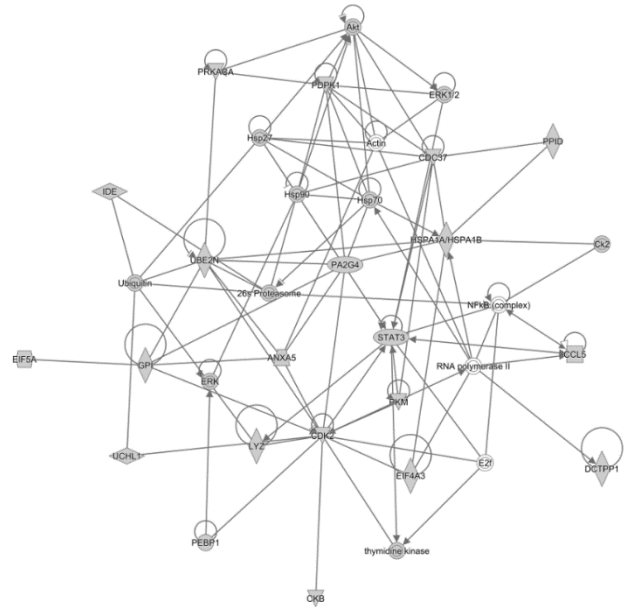
B

Cellular Movement, Organismal Injury
and Abnormalities, Cell-To-Cell Signaling
and Interaction

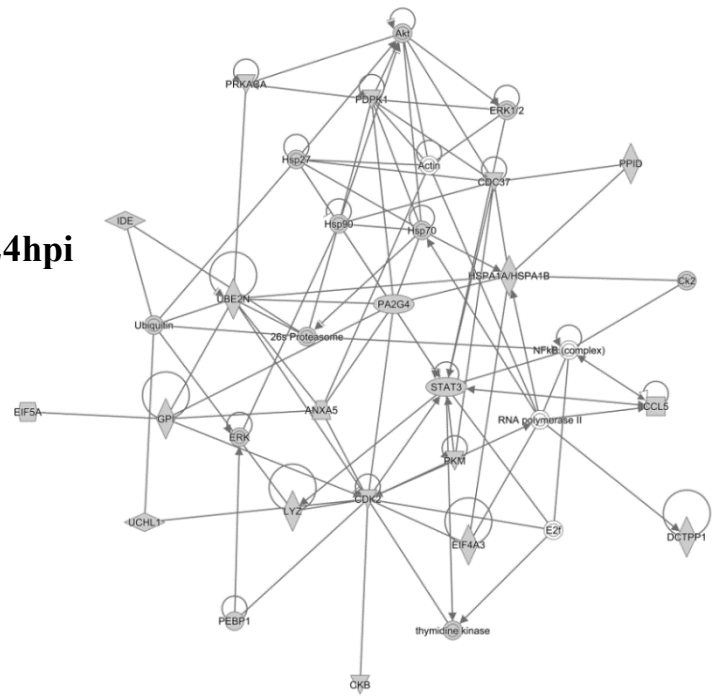
Cell Death and Survival, Cellular Development,
Cellular Growth and Proliferation



12hpi



24hpi



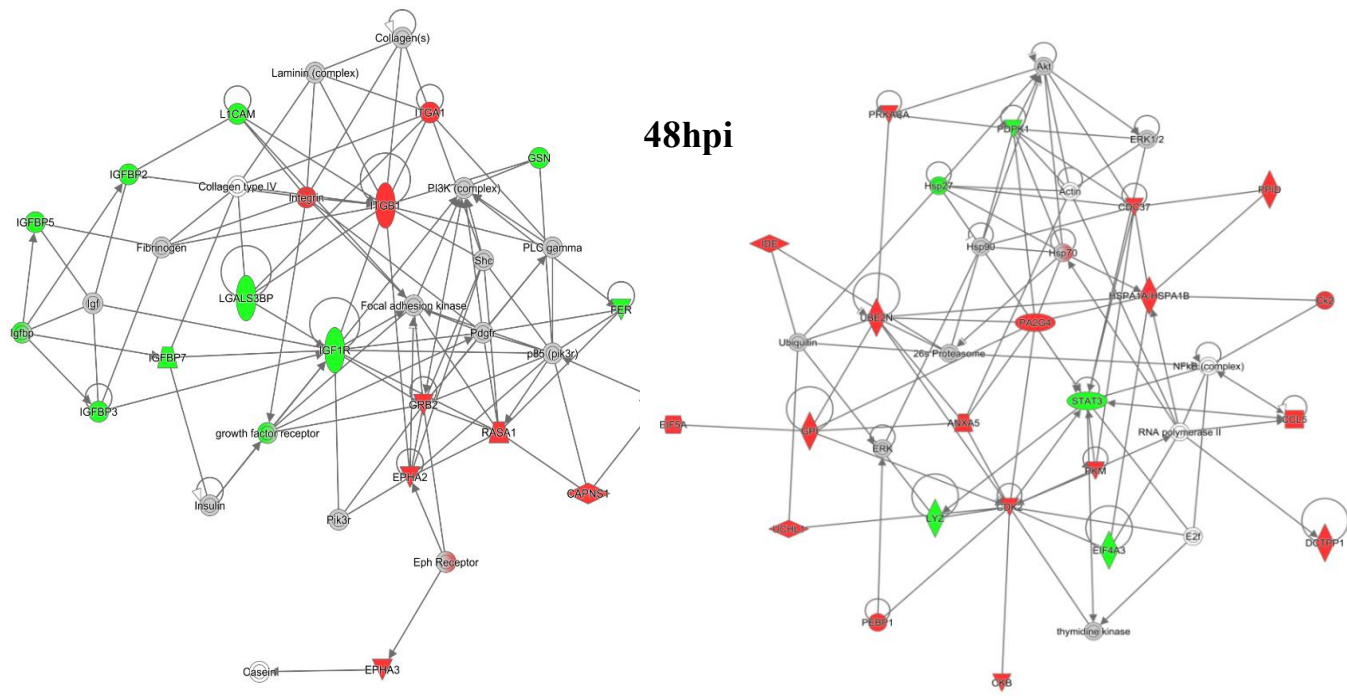
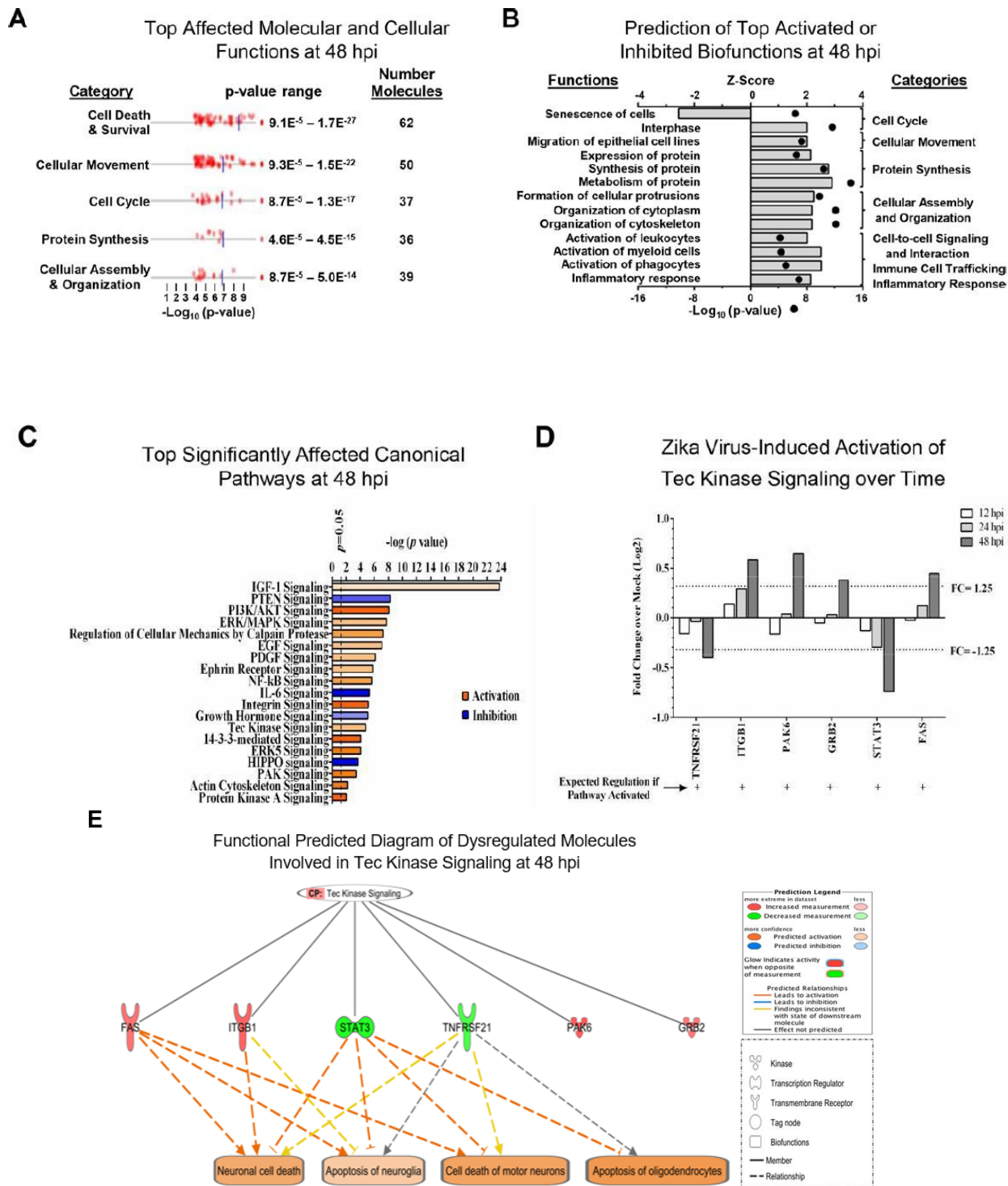


Figure 9: GO determined by Panther classifications and IPA generated top networks of dysregulated Vero cell proteins.

Lists of significantly dysregulated proteins were imported into PANTHER. Bar charts show the various biological processes, molecular functions and protein classes, and their fold enrichment, affected by up-regulated proteins (top) and down-regulated proteins (bottom) at 48 hpi. B) Selected IPA networks of dysregulated Vero cell proteins. Networks with scores >20 we determined from proteins dysregulated at 48 hpi and are identified. Data from earlier time points were overlaid onto these networks to visualize progression of dysregulation during infection. Solid lines indicated direct interactions between molecules. Green-colored molecules are down-regulated, red-colored molecules are up-regulated, grey-colored are non-regulated, and white are not part of the SOMAScan panel.



biofunction (senescence of cells) is indicated by negative Z-Score. Major biofunction categories are indicated at right. C) Top affected canonical pathways with log₁₀ p-value indicated at top. Orange corresponds to activation and blue corresponds to inhibition, with the degree of coloration corresponding to Z-Score. D) ZIKV-induced activation of selected proteins within the Tec kinase signaling pathway as a function of time post-infection. Note that by 48 hpi, all proteins are dysregulated ≥ 1.25 -fold. E) Predicted effects of indicated Tec kinase pathway proteins on neuronal and motor neuron cell death, and on neuroglia and oligodendrocyte apoptosis

3.2. ZIKV disrupts proteins involved in the neurosensory system.

Number of citations from this publication: 3

3.2.i Contributory Role.

Performed all experimental work except, the mass spectrometry analysis and peptide identification as well write-up section under the methodology done by Ying Lao and Victor Spicer, who were co-authors on this publication which was also part of my PhD thesis. Contributed to writing and reviewing the entire manuscript before and after submission for publication. All Figures and Tables were generated by me and Ali Zahedi-Amiri, with whom I co-shared the first authorship on this paper.

3.2. ii. ZIKV causes specific temporal changes in the cellular proteome.

A non-biased mass spectrometry (MS)-based proteomic analysis of ZIKV-infected Vero cells to extend and complement the proteomic data generated after SomaLogic analysis of ZIKV infected Vero cells. We identified a total of 7,455 cellular protein hits across all time points, with 6,443, 6,402, and 6,382 proteins identified at 12, 24, and 48hpi, respectively. ZIKV proteins, including non- structural ones, also were identified in the virus-infected samples but not in the mock samples, confirming the infection status of the appropriate cells. Because the TMT analysis reports ZIKV: mockpeptide and protein ratios, and ZIKV proteins are not expected in the mock samples, the ZIKV proteins were not considered hereafter. The number of significantly dysregulated cellular proteins was highest at 48hpi, as earlier seen in our targeted studies (127,128) (Figure.11A, Tables 3, 4).

Statistical tests indicated several thousand proteins were significantly dysregulated, although the vast majority had small fold-changes (Table 3). We, and many others, have previously applied fold-change cut-offs ranging from 1.5-fold to 2.0-fold for increased stringency, and we did likewise. Thus, nearly 400 proteins were significantly dysregulated using a 1.5-fold cut-off, which provided a rich source for subsequent bioinformatics analyses. Proteins dysregulated at a higher stringency of ≥ 2.0 -fold are shown in Table 4. Less than 1% of the measured proteome underwent significant modifications within the first 24h of infection. Most early dysregulated proteins were not significantly dysregulated at later time points, although the amount of MED13L (Mediator of

RNA polymerase II transcription subunit 13-like) in ZIKV infected cells was significantly higher than in mock cells at both early and late time points, but not significantly dysregulated at 24hpi. We generated inter-time point heatmaps to facilitate interpretation of protein dysregulation patterns over the 48h observation window and observed that except for MED13L, none of the significantly dysregulated proteins at either 12 or 24hpi were significantly dysregulated in the same direction at later time points (Figure. 11 A, B).

Several proteins (i.e., PLAUR, ARID5B, AHNAK, and ABLIM1) were significantly dysregulated in opposite directions across two-time points (Figure.11B). Moreover, interaction networks obtained from protein data at 12 and 24hpi identified 5 and 17 interacting molecules, respectively (Figure.11B, right panels), suggesting that these temporally altered proteins may interact with other biological process regulators during the early phases of ZIKV infection. Immunoblots were performed to validate differential amounts of selected proteins at most time points (Figure. 11C). Although there were differences in absolute dysregulation values, likely representing the different methods used, most protein dysregulations trended in the same direction. Enzymes and other unspecified molecule types were the most frequently observed proteins significantly differentially expressed at all time points investigated (Figure. 11D). Most of the regulated proteins at 12hpi were mapped to the nucleus, while significantly altered proteins at 24 and 48hpi mapped mainly to the cytoplasmic compartment (Figure. 11E). This proteomic overview of dysregulated proteins indicated that ZIKV infection could cause significant temporal alterations in the proteome of infected Vero cells.

Table 3: Numbers of ZIKV-induced significantly dysregulated proteins

	Total Unique	12h	24h	48h
Number w/ p-value < 0.05		72	393	2252
and F.C. > 1.05	2565	66	162	1094
and F.C. < .952		6	229	1156
and F.C. > 1.25	1355	27	44	534
and F.C. < 0.80		1	120	660
and F.C. > 1.33	855	20	29	317
and F.C. < 0.75		1	68	432
and F.C. > 1.50	374	10	13	120
and F.C. < .667		0	22	209
and F.C. > 2.00	78	4	6	21
and F.C. < 0.50		0	3	41

and F.C. > 2.50		1	4	7
and F.C. < 0.40	30	0	2	13

Significance was determined by T-test and Z-Score as detailed in Materials & Methods.
Specific proteins dysregulated ≥ 2.0 -fold are listed in Table 4.

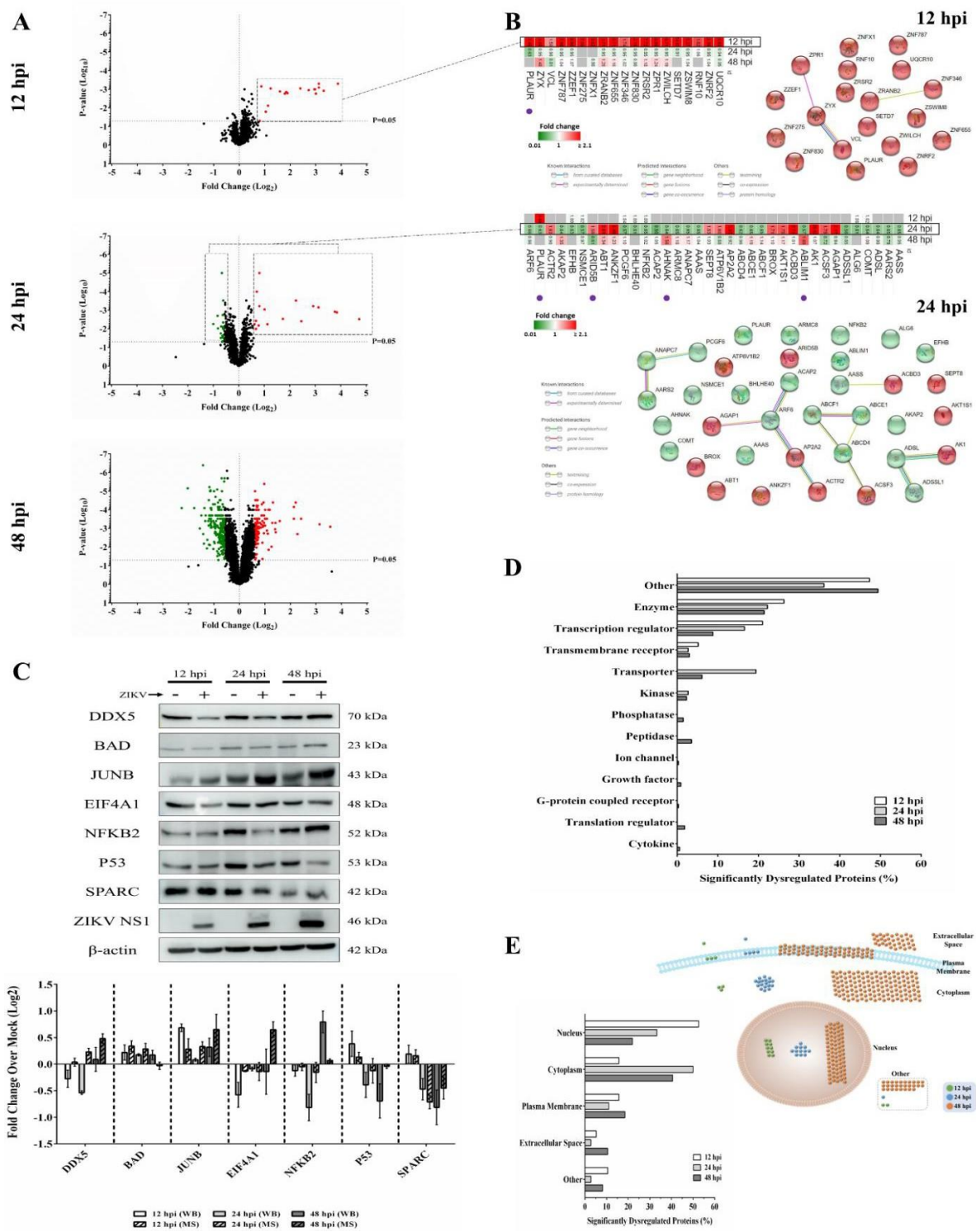


Figure 11: Mass spectrometry proteomic analysis of ZIKV-infected Vero cells.

(A) Volcano plots displaying ZIKV-induced log₂-fold protein level changes and significance of differentially regulated proteins at 12 (upper panel), 24 (middle panel), and 48 (lower panel) hours post-infection (hpi) (p-value < 0.05). (B) The quantitative comparison heatmaps indicating fold changes and protein-protein interaction networks of differentially dysregulated proteins across two time points (12 and 24 hpi). The protein-protein interaction network of the large number of differentially dysregulated proteins at 48 hpi is shown in Supplementary Figure S2. Proteins labeled with purple dots below heatmaps were significantly differentially expressed in the opposite direction at either earlier or later time points. (C) Western blot validation of selected differentially dysregulated proteins from mass spectrometry results. Representative blots are shown. Different loading controls were used for the densitometry normalization and analysis. Protein fold changes and availability of antibodies were considered for validation. ZIKV NS1 was probed to confirm the infection. (D) Classification of significantly dysregulated protein type at different time points after ZIKV infection. (E) The subcellular localizations of dysregulated proteins at different time points represented both quantitatively (left panel) and graphically (right panel).

Table 4: Vero cell proteins dysregulated ≥ 2.0 -fold by ZIKV infection.

		12h		24h		48h	
Gene	Protein	Fold Change	P-value	Fold Change	P-value	Fold Change	P-value
Up-regulated proteins							
MED13L	Mediator of RNA polymerase II transcription subunit 13-like	9.96	1.2E-03	1.04	0.229	11.82	8.3E-04
MON1B	Vacuolar fusion protein MON1 homolog B	2.18	7.5E-03	0.86	0.290	0.90	0.190
GPR126	G-protein coupled receptor 126	2.09	5.6E-07	0.75	0.065	nd	nd
CAPN8	Calpain-8	2.06	0.016	nd	nd	nd	nd
AK1	Adenylate kinase isoenzyme 1	0.96	0.734	26.42	3.0E-03	1.07	0.176
ACBD3	Golgi resident protein GCP60	0.97	0.608	8.73	7.0E-04	1.01	0.884
ANKZF1	Ankyrin repeat and zinc finger domain-containing protein 1	nd	nd	5.48	3.9E-03	1.23	0.067
AP2A2	AP-2 complex subunit alpha-2	1.04	0.449	3.32	2.9E-03	0.92	0.055
AGAP1	Arf-GAP with GTPase, ANK repeat and PH domain-containing protein 1	nd	nd	2.17	5.6E-03	0.94	0.313
ABT1	Activator of basal transcription 1	1.12	0.362	2.01	9.5E-04	1.34	0.021
HIST1H1C	Histone H1.2	nd	nd	1.04	0.646	4.39	6.6E-05
NSL1	Kinetochore-associated protein NSL1 homolog	1.27	0.063	0.89	0.041	4.39	3.2E-04
CTDP1	RNA polymerase II subunit A C-terminal domain phosphatase	0.96	0.250	1.04	0.494	3.00	3.9E-04
GJA1	Gap junction alpha-1 protein	1.12	0.372	0.89	0.261	2.68	1.6E-03
TRMT2A	tRNA (uracil-5-)-methyltransferase homolog A	1.45	0.032	0.94	0.592	2.66	4.7E-04
ITFG2	Integrin-alpha FG-GAP repeat-containing protein 2	0.91	0.317	0.91	0.097	2.64	1.1E-03
SZRD1	SUZ domain-containing protein 1	1.05	0.598	0.98	0.835	2.49	4.3E-05

AGFG1	Arf-GAP domain and FG repeat-containing protein 1	0.88	0.025	1.08	0.204	2.45	4.5E-04
SLC7A6OS	Probable RNA polymerase II nuclear localization protein SLC7A	nd	nd	nd	nd	2.39	9.5E-03
MKI67	Antigen KI-67	1.12	0.302	0.90	0.149	2.28	9.9E-05
DENND4C	DENN domain-containing protein 4C	1.03	0.826	0.92	0.280	2.21	0.014
RALGAPA1	Ral GTPase-activating protein subunit alpha-1	nd	nd	0.99	0.951	2.20	1.5E-04
RRM2	Ribonucleoside-diphosphate reductase subunit M2	1.03	0.794	0.83	0.431	2.16	1.9E-03
CXorf56	UPF0428 protein CXorf56	1.11	0.610	1.04	0.511	2.11	2.7E-04
NCAPD3	Condensin-2 complex subunit D3	0.94	0.434	0.91	0.397	2.11	1.3E-03
C19orf53	Leydig cell tumor 10 kDa protein homolog	1.12	0.434	1.16	0.055	2.03	2.8E-04
CHTF8	Chromosome transmission fidelity protein 8 homolog isoform 2	nd	nd	nd	nd	2.02	2.6E-04
FAM21C	WASH complex subunit FAM21C	nd	nd	nd	nd	2.01	1.2E-04
EMD	Emerin	1.17	0.368	1.20	0.041	2.01	6.5E-04
HMG1	Non-histone chromosomal protein HMG-14	1.05	0.613	0.92	0.410	2.00	2.8E-04

Down-regulated proteins

PGPEP1	Pyroglutamyl-peptidase 1	nd	nd	0.18	1.2E-17	0.86	0.104
FARSB	Phenylalanine--tRNA ligase beta subunit	0.95	0.415	0.39	7.2E-06	1.01	0.779
ACAP2	Arf-GAP with coiled-coil, ANK repeat and PH domain-containing protein 2	1.02	0.751	0.50	5.5E-03	1.05	0.305
PLAGL2	Zinc finger protein PLAGL2	nd	nd	1.01	0.908	0.21	7.9E-05
CTSD	Cathepsin D	0.94	0.259	1.18	5.3E-03	0.25	6.8E-06
KRT16	Keratin, type I cytoskeletal 16	1.41	0.045	nd	nd	0.25	5.4E-08
CTSL	Cathepsin L1	1.02	0.872	0.81	0.124	0.29	7.8E-05
HRNR	Hornerin	1.66	0.002	1.00	0.982	0.33	1.4E-05
RDH10	Retinol dehydrogenase 10	nd	nd	0.92	0.461	0.34	9.7E-04
MCFD2	Multiple coagulation factor deficiency protein 2	1.10	0.312	1.02	0.631	0.36	2.5E-04
KRT6C	Keratin, type II cytoskeletal 6C	nd	nd	nd	nd	0.37	1.6E-04
GRN	Granulins	0.92	0.069	1.04	0.492	0.37	2.0E-03
SCD	Acyl-CoA desaturase	1.24	0.225	0.98	0.641	0.38	6.5E-03
DHRS3	Short-chain dehydrogenase/reductase 3	nd	nd	1.00	0.979	0.39	7.8E-05
EIF1	Eukaryotic translation initiation factor 1	0.93	0.494	1.03	0.758	0.40	4.4E-04
BCAM	Basal cell adhesion molecule	1.03	0.795	0.87	0.139	0.40	1.6E-04
MAGED1	Melanoma-associated antigen D1	0.96	0.636	nd	nd	0.41	0.012
SLCO2A1	Solute carrier organic anion transporter family member 2A1	nd	nd	nd	nd	0.42	4.1E-03
UBL5	Ubiquitin-like protein 5	0.97	0.776	0.95	0.607	0.43	4.0E-04
CEBPB	CCAAT/enhancer-binding protein beta	1.04	0.748	0.86	0.208	0.43	6.6E-04
NPC2	Epididymal secretory protein E1	0.96	0.716	0.85	0.343	0.44	2.9E-05
LGALS3BP	Galectin-3-binding protein	0.96	0.615	0.90	0.358	0.44	7.4E-03
TAP2	Antigen peptide transporter 2	1.06	0.605	0.94	0.525	0.44	1.6E-04
SPINT2	Kunitz-type protease inhibitor 2	1.05	0.298	0.94	0.508	0.44	3.1E-04
RBM3	RNA-binding protein 3	1.06	0.496	0.91	0.230	0.44	2.4E-04
SERPINI1	Neuroserpin	0.94	0.588	0.93	0.417	0.45	7.8E-03
EPHA7	Ephrin type-A receptor 7	1.06	0.449	0.90	0.088	0.45	3.5E-04
CPQ	Carboxypeptidase Q	1.04	0.719	0.88	0.243	0.45	1.1E-05
PSAP	Prosaposin	1.11	0.559	0.89	0.293	0.45	6.4E-04

TPP1	Tripeptidyl-peptidase 1	nd	nd	1.00	1.000	0.45	1.4E-05
CYP27A1	Sterol 26-hydroxylase, mitochondrial	1.04	0.424	0.90	0.112	0.46	1.7E-04
FADS1	Fatty acid desaturase 1	1.13	0.573	1.03	0.428	0.46	4.2E-04
SPAG1	Sperm-associated antigen 1	1.02	0.661	0.99	0.941	0.46	8.9E-04
ASAH1	Acid ceramidase	1.08	0.452	0.75	0.036	0.46	1.8E-04
VCAN	Versican core protein	1.10	0.308	0.93	0.645	0.46	4.6E-04
CDH6	Cadherin-6	1.05	0.696	1.02	0.825	0.46	7.3E-04
CLN5	Ceroid-lipofuscinosis neuronal protein 5	0.97	0.778	0.86	0.192	0.47	7.6E-05
COLEC12	Collectin-12	1.05	0.434	1.03	0.682	0.47	7.6E-04
KCT2	Keratinocyte-associated transmembrane protein 2	1.07	0.488	0.83	0.268	0.47	1.1E-04
MRPL28	39S ribosomal protein L28, mitochondrial	1.09	0.298	1.05	0.359	0.47	8.7E-04
HEXA	Beta-hexosaminidase subunit alpha	1.06	0.440	1.06	0.119	0.48	2.1E-04
GLB1	Beta-galactosidase	1.13	0.341	1.10	0.197	0.49	4.1E-04
ECHDC3	Enoyl-CoA hydratase domain-containing protein 3, mitochondrial	nd	nd	0.83	0.175	0.49	5.4E-05
PPT1	Palmitoyl-protein thioesterase 1	0.94	0.169	0.91	0.205	0.49	0.013

Only proteins dysregulated ≥ 2.0 -fold are listed. Entries are sorted, first by time, from 12hpi to 48hpi, then by degree of dysregulation within each set. Values determined from three biological replicates. Proteins with significant p-value are red in T-Test column, those significantly up-regulated are shown in bold red and those significantly down-regulated are shown in bold blue. n.d. = not detected.

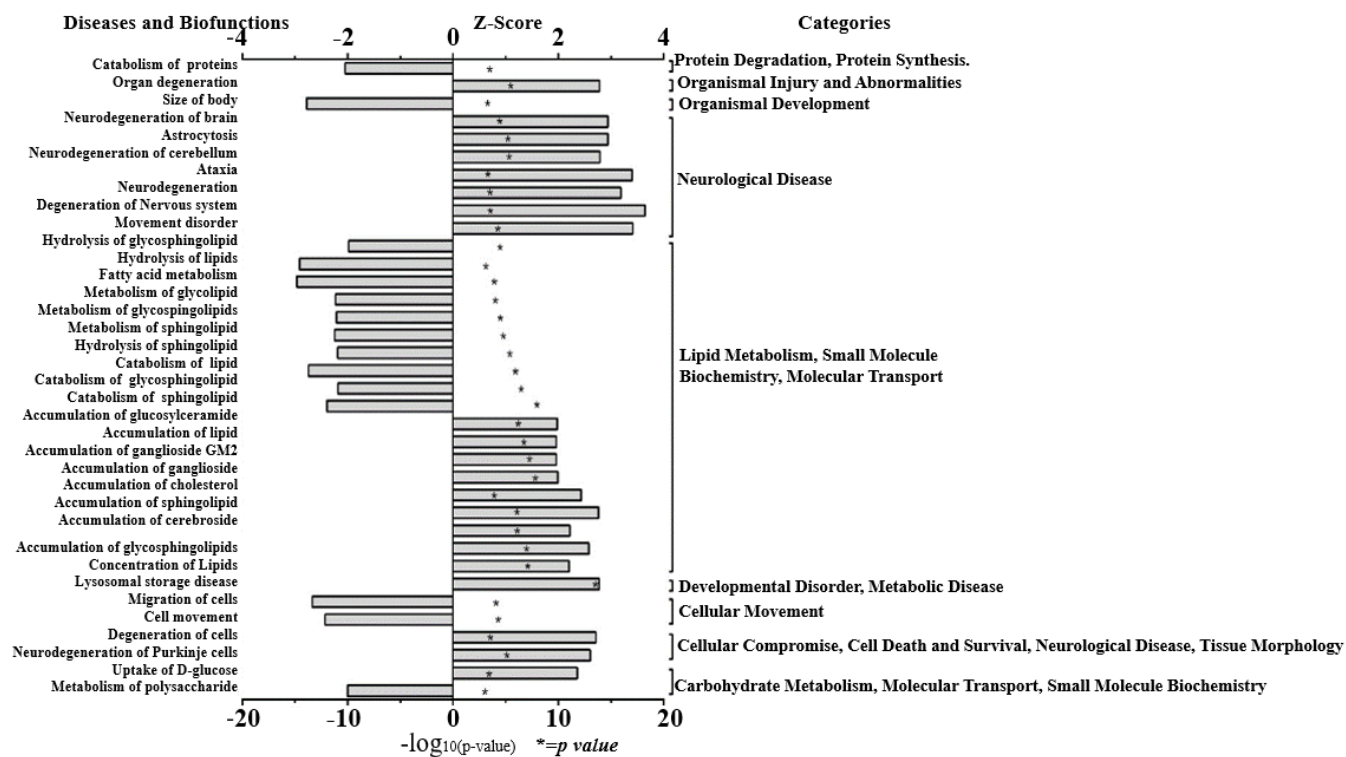
3.2.iii ZIKV Infection Dysregulates a Wide Variety of Bio-functions and Pathways.

Functional analyses of dysregulated proteins identified bio-functions predicted to be highly affected by ZIKV infection. Due to the small number of modified proteins at early time points of ZIKV infection, IPA did not recognize any significant changes in bio-functions at 12 and 24hpi. However, numerous functional alterations among a wide variety of bio-functions were predicted at 48hpi. Among the largest number of affected bio-functions were protein alterations associated with neurological diseases and lipid metabolism (Figure. 12A; Supplementary Table S1). Proteins linked to neurological abnormalities were predicted exclusively to be activated based on Z-score at 48hpi, whereas proteins associated with lipid metabolism functions were almost equally divided into inhibited and activated functional states. Dysfunctions such as movement disorders, ataxia, neurodegeneration, astrocytosis, and lysosomal storage disease were among the top activated diseases (Z-scores $\geq +2.7$), and some functions including migration of cells, catabolism of lipid, size of the body, hydrolysis of lipid, and fatty acid metabolism were among the top inhibited biofunctions (Z-scores ≤ -2.6) (Supplementary Table S1). The higher number of altered bio-

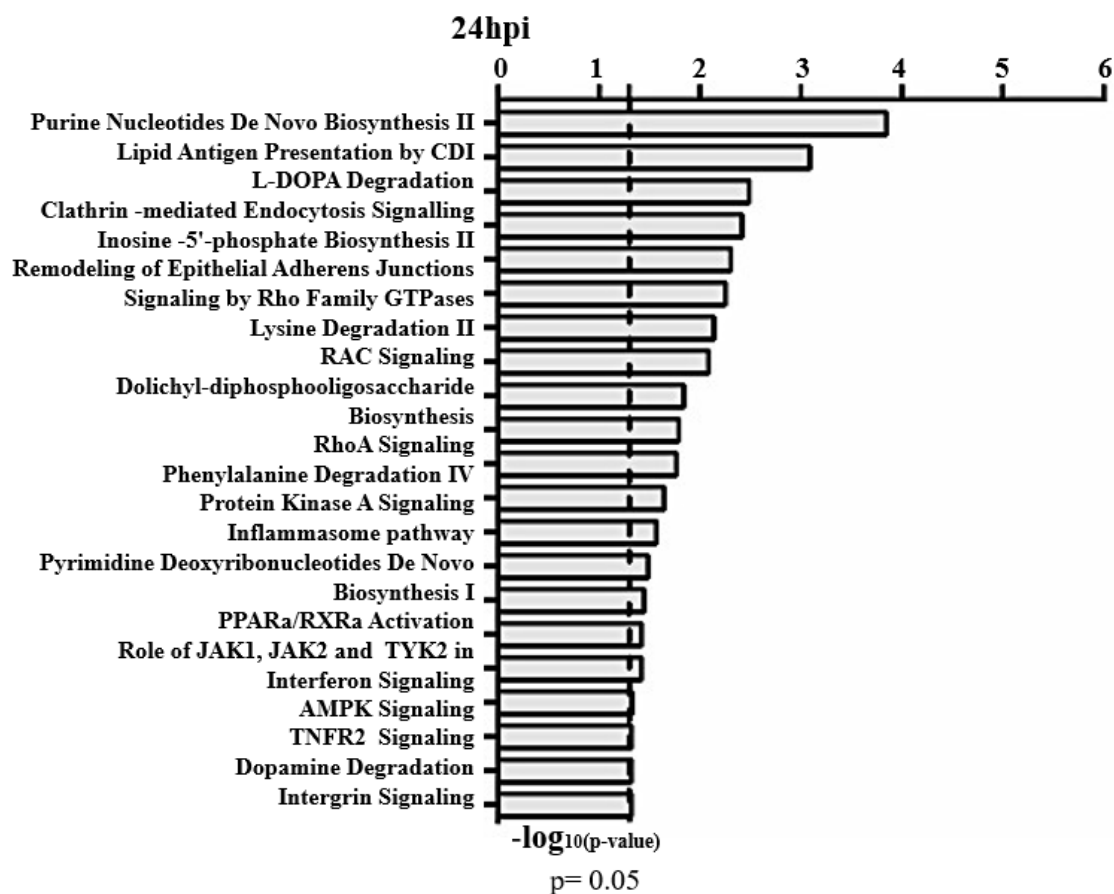
functions and diseases involving lipid metabolism and neurological complications may suggest new links between the function of host cellular lipids and the development of ZIKV-induced cellular malfunctions. Analysis of the top 21 affected canonical pathways did not indicate commonalities across infection times since entirely different sets of proteins were significantly dysregulated at each time point after ZIKV infection (Figure. 12B). IPA could not establish confident inhibition or activation trends for ZIKV-modulated canonical pathways because there were too few ZIKV modified pathway member proteins compared to background proteins. Nevertheless, with the increasing duration of ZIKV infection, we observed more diversification of signaling pathways by 48hpi compared to 24hpi. Dysregulated pathways at 24hpi were mainly assigned to metabolic processes, while pathways controlling immune responses, autophagy, endocytosis, phosphorylation, metabolism, visual phototransduction, cell movement, and others were among the top ZIKV-affected canonical pathways at 48hpi. When compared with the first day of infection, the increasing diversity and specificity of altered pathways by 2dpi indicates a dynamically evolving and increasingly complex host response during later stages of ZIKV infection that recruits and engages an increasing number of different cellular pathways.

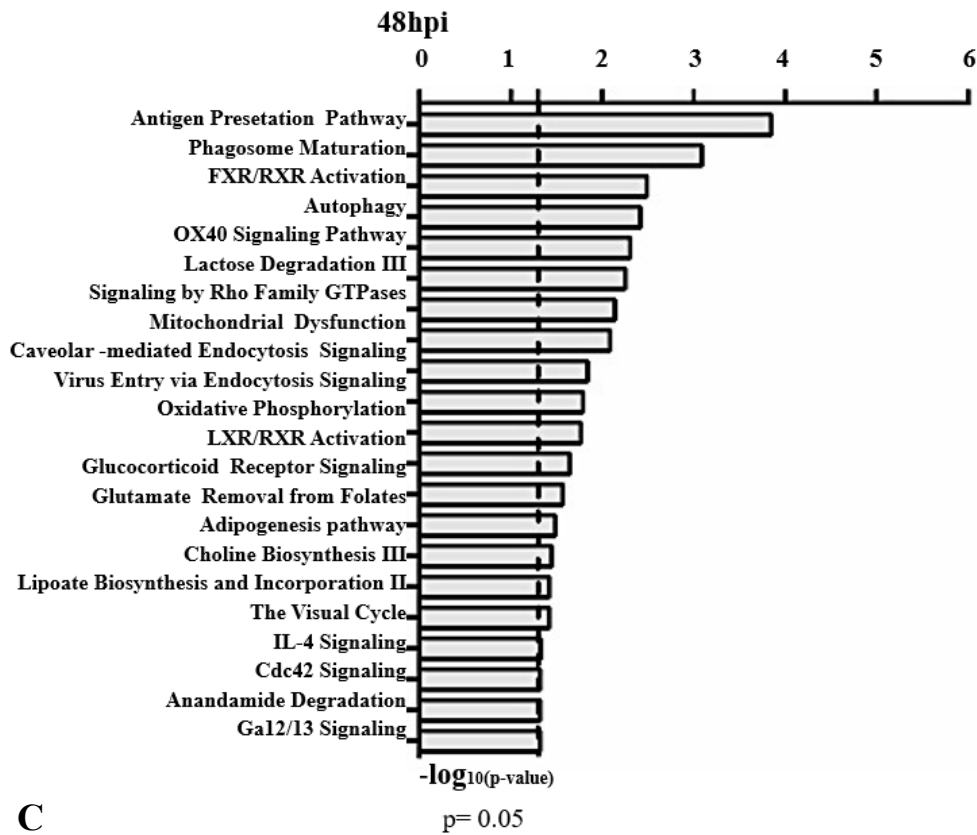
IPA predicted 7 elevated activity functions ($Z\text{-scores} \geq +1.97 \sigma$) and 30 elevated inhibitory functions ($Z\text{-scores} \leq -1.96 \sigma$) (Figure. 11C) from the lists of ZIKV-modulated proteins. About 35% of the affected upstream molecules were designated as regulators of transcription. One-third of these transcriptional regulators are predicted to be activated, whereas the remaining $\frac{2}{3}$ are predicted to be inhibited by ZIKV. Interestingly, nuclear transcription factor NKX2-3 and NF- κ B inhibitor alpha (NFKBIA) were the most activated and inhibited factors, respectively. IPA predictions above suggests that ZIKV can influence the host cell transcriptional machinery by coordinating different mechanisms of action. At least for NFKBIA, this has been linked to the regulation of NF κ B mediated immunoregulatory and anti-inflammatory responses (59). We interrogated the ability of affected upstream regulators to engage in an interconnecting network (Figure. 12D). Most upstream regulators are predicted to interact with at least one other regulator molecule. NFKBIA and CDKN2A may serve as “master regulators” in this upstream network because they have the highest number of intermolecular interactions.

A

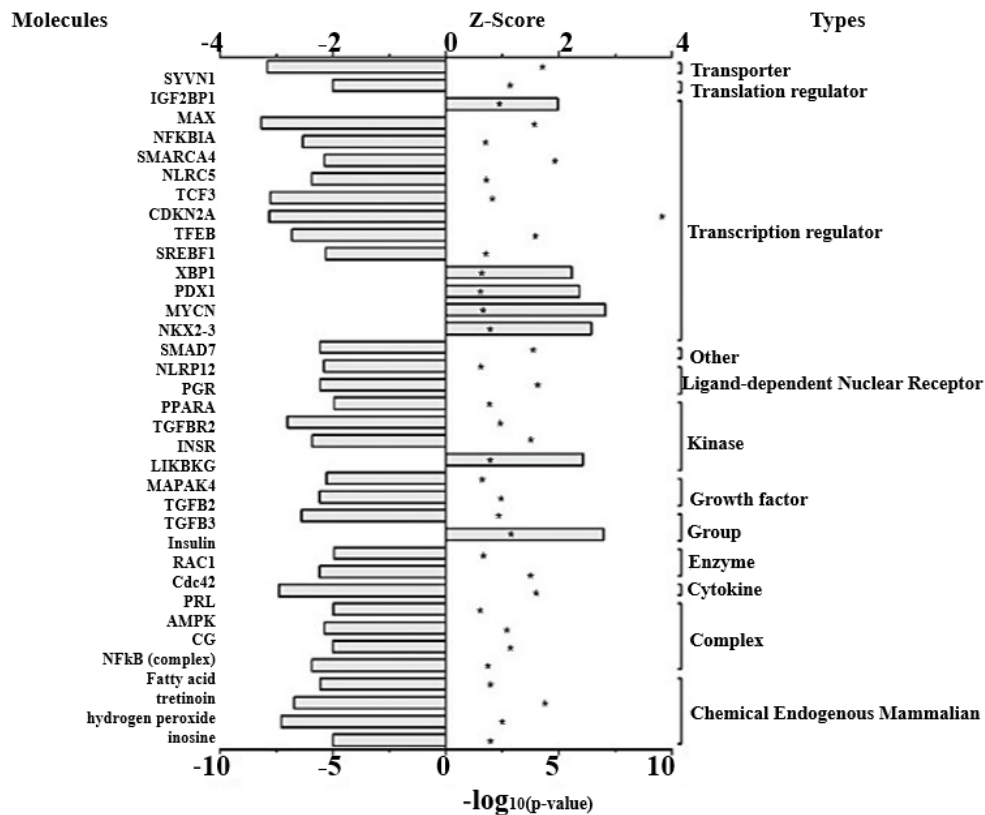


B





C



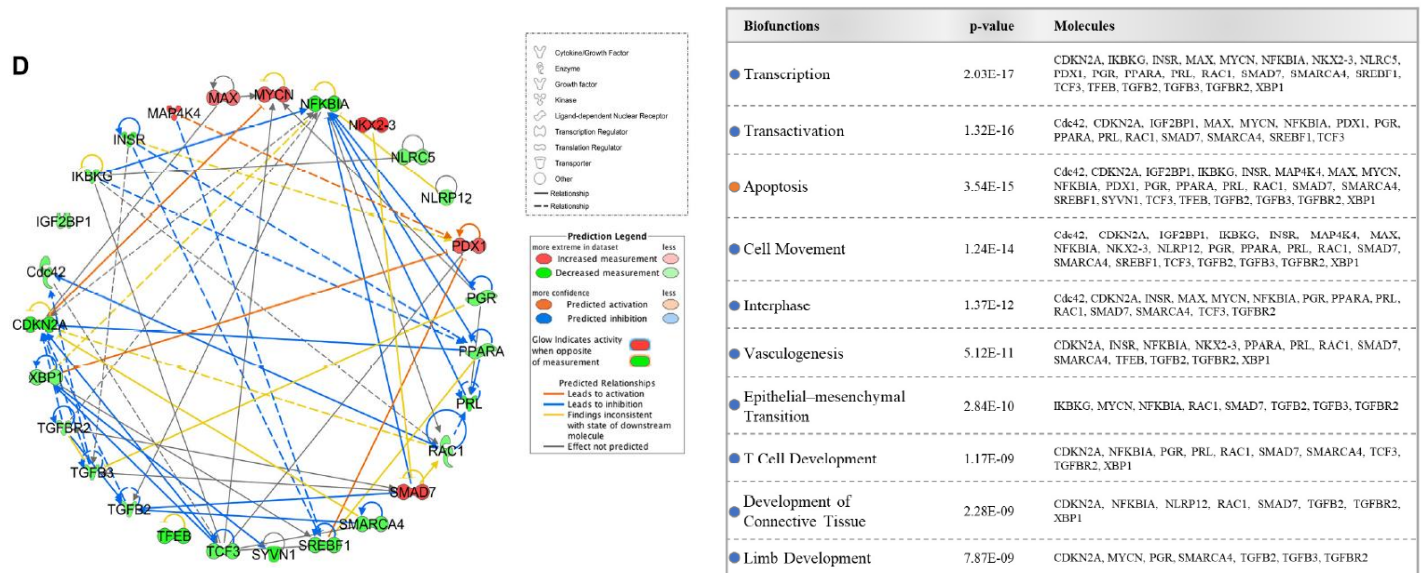


Figure 12: Proteomic prediction of top affected biofunctions, canonical pathways, and upstream molecules in Vero cells after ZIKV infection.

A) Predicted activation or inhibition patterns of top affected biofunctions at 48 hpi based on Z-scores (upper x-axis) and log10 p-values (lower x-axis indicated by asterisk). Influenced biofunctions are grouped using major parental categories of functions (shown at right). B) Prediction of top affected canonical pathways by ZIKV at 24 (upper panel) and 48 (lower panel) hpi. C) Prediction of top affected upstream molecules and their possible activation or inhibition based on expression patterns of downstream proteins at 48 hpi. D) Interaction network of top predicted upstream molecules (upper panel) and their related biofunctions (table in lower panel). Activation or inhibition patterns of connected biofunctions and interaction types of predicted molecules are measured according to Z-scores calculated from IPA software, which is based on the expression of differentially regulated downstream proteins at 48 hpi.

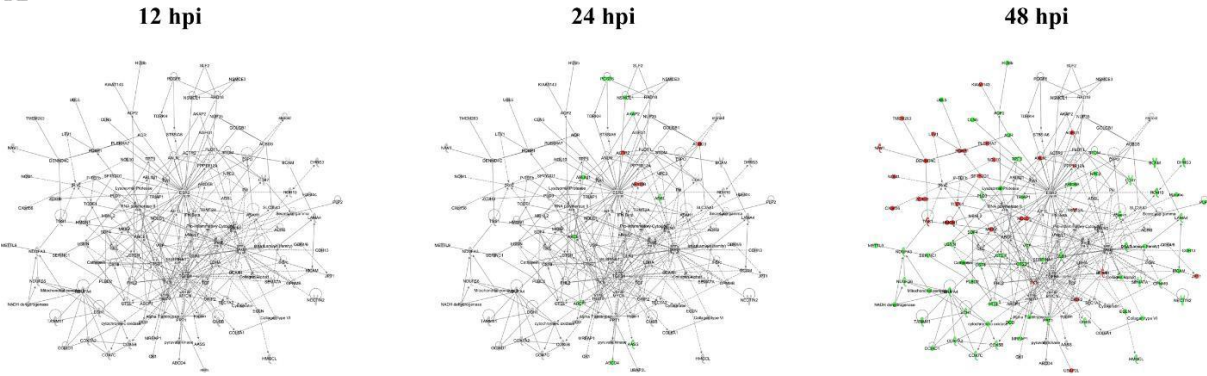
3.2. iv. ZIKV alters protein interaction networks linked to developmental processes.

We identified several protein interaction networks comprising ≥ 20 focus molecules ($p\text{-score} \leq \text{Loge } -30$) associated with a broad spectrum of cellular functions, including lipid metabolism, inflammatory responses, and embryonic development. Those protein members of interaction networks with highly significant alterations corresponding to developmental disorders were selected and merged for temporal analysis (Figure: 13A). No notable changes were detected at 12hpi in this merged network. However, as time progressed to 48hpi, significant increases and decreases in protein quantity patterns among interacting proteins indicated a complex and dynamic response profile of proteins associated with developmental processes in host cells exposed to ZIKV. The IPA prediction feature also suggested inhibition and activation of other member molecules in this network that was not experimentally identified by MS by 48hpi (Figure: 13B). TGF2, Akt, ESR2, Vegf, ERK1/2, TK1, and Hsp70 were among the proteins with the largest

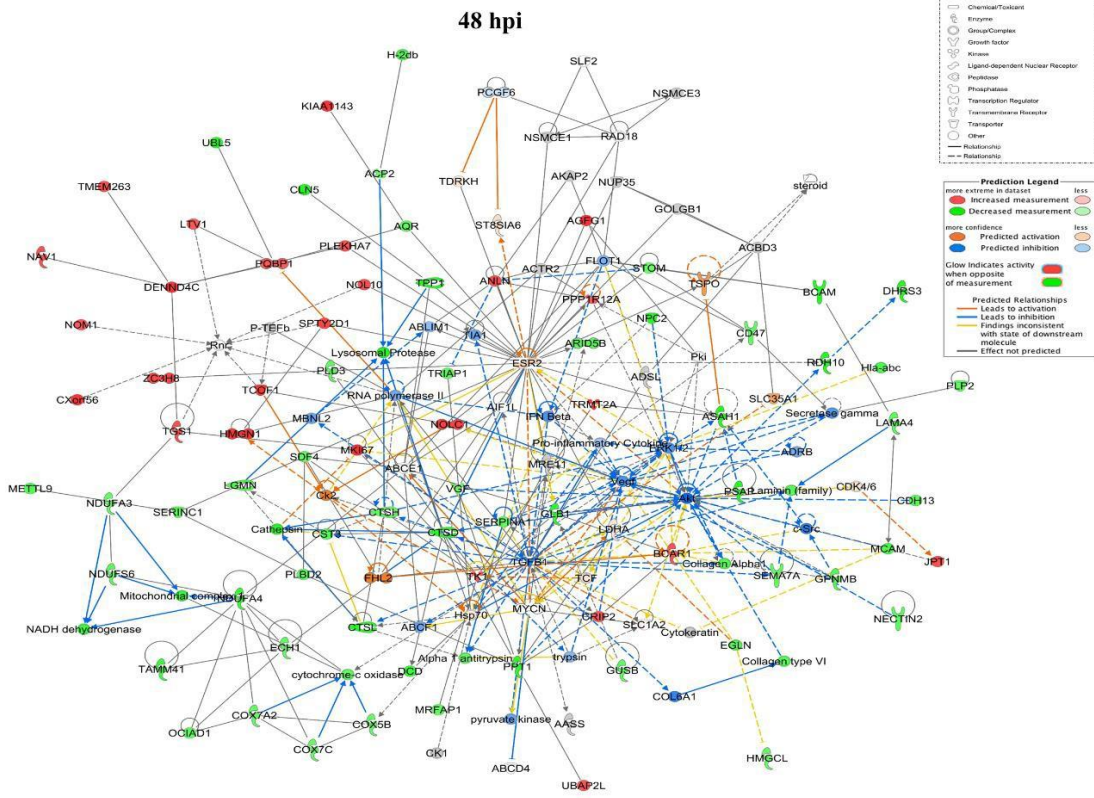
number of intermolecular interactions in this network.

We then connected the developmental disorder merged network to developmental phenotypes. Intriguingly, craniofacial and brain development scored among the highest, followed by gonad formation, lung development, and bone-resorbing osteoclast formation (Figure. 13C). Pathway analyses of this network also revealed the involvement of several canonical biochemical pathways known to be important regulators of cellular differentiation, inflammatory processes, DNA repair, stress response, cell death, metabolism, and behavioral functions (Figure. 13D).

A



B



C

Biofunctions	p-value	Molecules
● Development of Head	8.39E-04	ARID5B, CST3, CTSD, DHRS3, ERK1/2, ESR2, MYCN, PPT1, PSAP, RDH10, SDF4, Secretase gamma, SLC1A2, TCOF1, TGFBI, TSPO, Vegf
● Formation of Brain	1.13E-03	CST3, ERK1/2, ESR2, MYCN, PPT1, RDH10, SDF4, SLC1A2, TCOF1, TGFBI, Vegf
● Gonadogenesis	1.12E-03	AGFG1, ARID5B, ESR2, NECTIN2, RAD18, RDH10, TDRKH, TKI, Vegf, VGF
● Formation of Lung	1.07E-04	ASAH1, CTSH, ESR2, MYCN, NPC2, RDH10, TGFBI, TKI
● Formation of Osteoclasts	1.29E-03	Akt, CD47, CST3, FHL2, IFN Beta, LGMN, Pro-inflammatory Cytokine, TGFBI

D

Pathway	Molecules
Sirtuin Signaling	Akt, ERK1/2, LDHA, Mitochondrial complex 1, MYCN, NADH dehydrogenase, NDUF3, NDUF4, NDUF56, Pro-inflammatory Cytokine, RNA polymerase II, TSPO
RAR Activation	Akt, c-Src, Ck2, DHRS3, ERK1/2, Pro-inflammatory Cytokine, RDH10, TGFBI, Vegf
Glucocorticoid Receptor Signaling	ADRB, Akt, Cytokeratin, ERK1/2, Hsp70, IFN Beta, Pro-inflammatory Cytokine, RNA polymerase II, TGFBI
Neuroinflammation Signaling	Akt, ERK1/2, H-2b, Hla-abc, IFN Beta, Pro-inflammatory Cytokine, Secretase gamma, SLC1A2, TGFBI
Aryl Hydrocarbon Receptor Signaling	Cathepsin, CDK4/6, CTSD, ERK1/2, ESR2, IFN Beta, Lysosomal Protease, Pro-inflammatory Cytokine, TGFBI

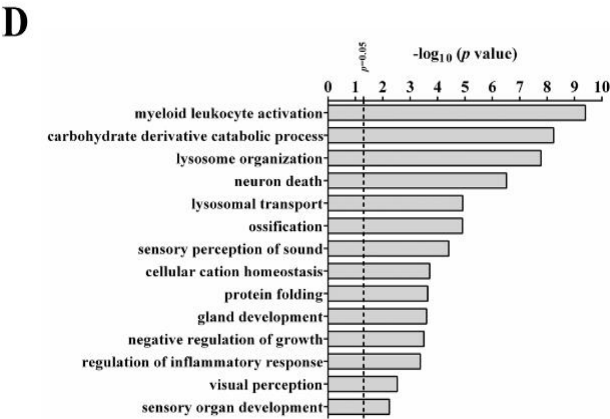
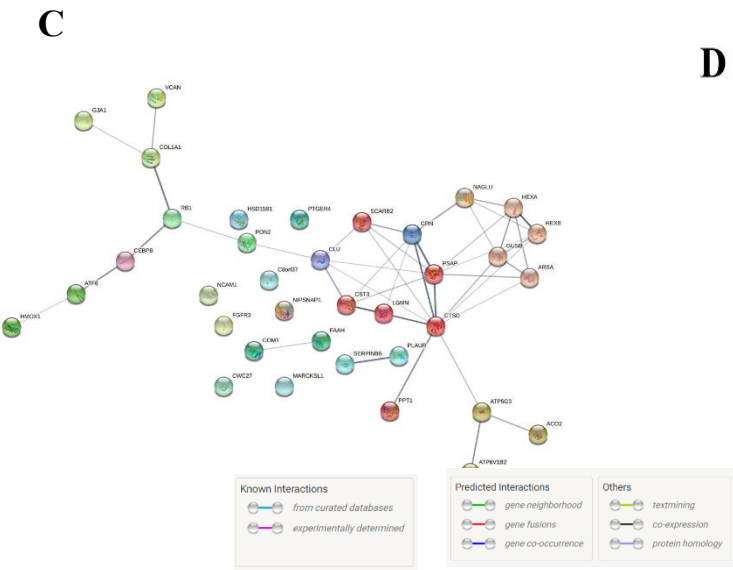
Figure 13: Effect of ZIKV infection on protein-protein interaction network of developmental abnormalities.

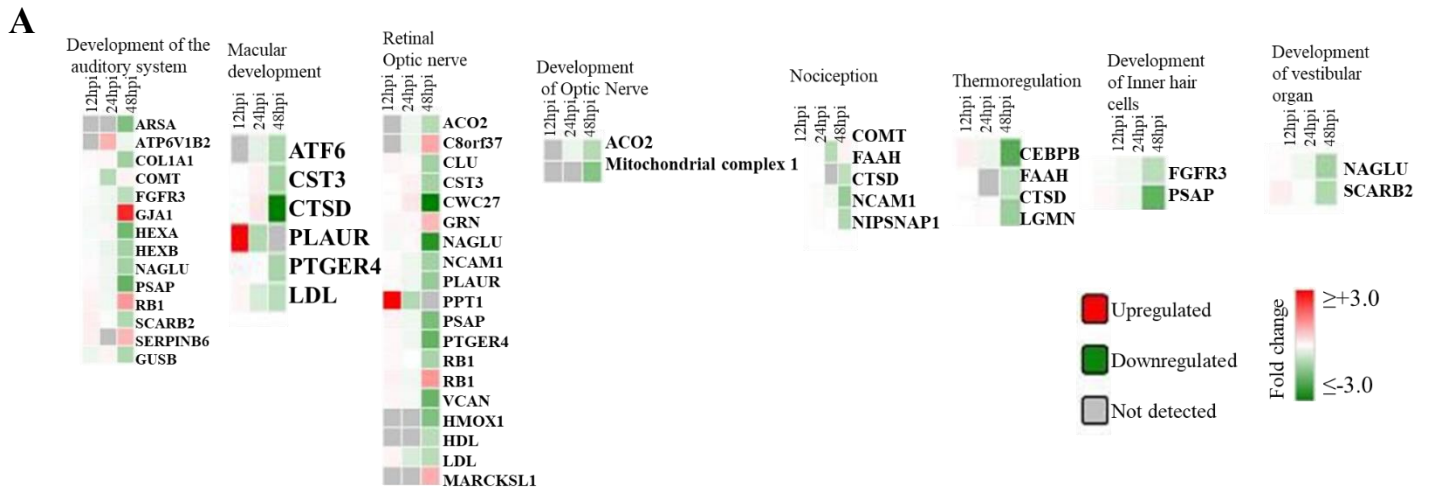
A) Alterations in the expression of molecules controlling developmental abnormalities network across three time-points. Up- and downregulated proteins are represented in red and green, respectively; gray proteins denote that they were recognized in the present study but not influenced significantly; colorless proteins interact with different molecules in the network but were not identified by mass spectrometry. B) IPA prediction on the regulation patterns of proteins that belong to developmental abnormalities interaction network but were not either differentially expressed or recognized in our mass spectrometry experiment. This prediction model was established through overlaying proteomic data at 48 hpi on the merged network pertaining to developmental abnormalities. Molecules shown in orange and blue represent predictions for activation and inhibition, respectively. C) Selection of certain biofunctions that were predicted to be inhibited based on ZIKV-mediated changes in molecules regulating this network. D) List of top-affected canonical pathways that could be connected to member proteins of developmental abnormalities network.

3.2. v. ZIKV infection targets proteins linked to neurosensory disorders.

Recent clinical evidence suggests that ZIKV infection may cause neurosensory disorder development and cognitive impairments in children, even in those children who survived neonatal infection and do not show apparent complications (80,129,130). Currently, no molecular study has attempted to link possible mediators and biomarkers of neurosensory diseases to ZIKV infection. We collated all known molecules related to the neurosensory system and its associated abnormalities and overlaid it with our proteomic data (Figure. 14A). Significant ZIKV-mediated dysregulation was seen mostly at 48hpi, impacting the levels of proteins controlling neurosensory system development. A graphical illustration of molecules involved in ZIKV-induced impairment of the neurosensory system and their multiple functions in different neurosensory diseases are depicted in Figure. 14B. A subset of proteins, including RB1, PSAP, NAGLU, FGFR3, SCARB2, LDL, CTSD, CST3, PTGER4, ACO2, NCAM1, and FAAH, were involved in at least two types of neurosensory dysfunctions. Moreover, proteins associated with cognitive impairments, like GRN, ARSA, NCAM1 and GUSB, showed marked differences in protein levels (Figure. 14B, lower panel). The largest numbers of identified dysregulated proteins were involved in retinal diseases and hearing loss. Bioinformatic assessment of all proteins corresponding to neurosensory diseases whose levels changed significantly between mock and infected showed that most of these proteins interacted with at least one other member (Figure. 14C).

GO analysis was also performed on this class of biological processes to provide an overview of the most affected pathways (Figure. 14D). In addition to auditory and visual perception, and sensory organ development, we noted significant enrichment of other critical pathways that involve neurons, ossification, growth, gland development, and others. GO analysis highlighted the complex functionality of ZIKV-affected host proteins and provided a first insight into molecular mechanisms and temporal events triggered by ZIKV infection that may drive the progression of neurosensory disorders and other developmental abnormalities. The protein members identified in this study and their affiliation with specific networks demonstrate, for the first time, an intricate relationship between ZIKV-induced host defenses and specific neuro-developmental processes and unveils novel mechanisms and pathways that qualify as potential new targets to combat ZIKV infection and downstream pathology.





Development of the Neurosensory system



B

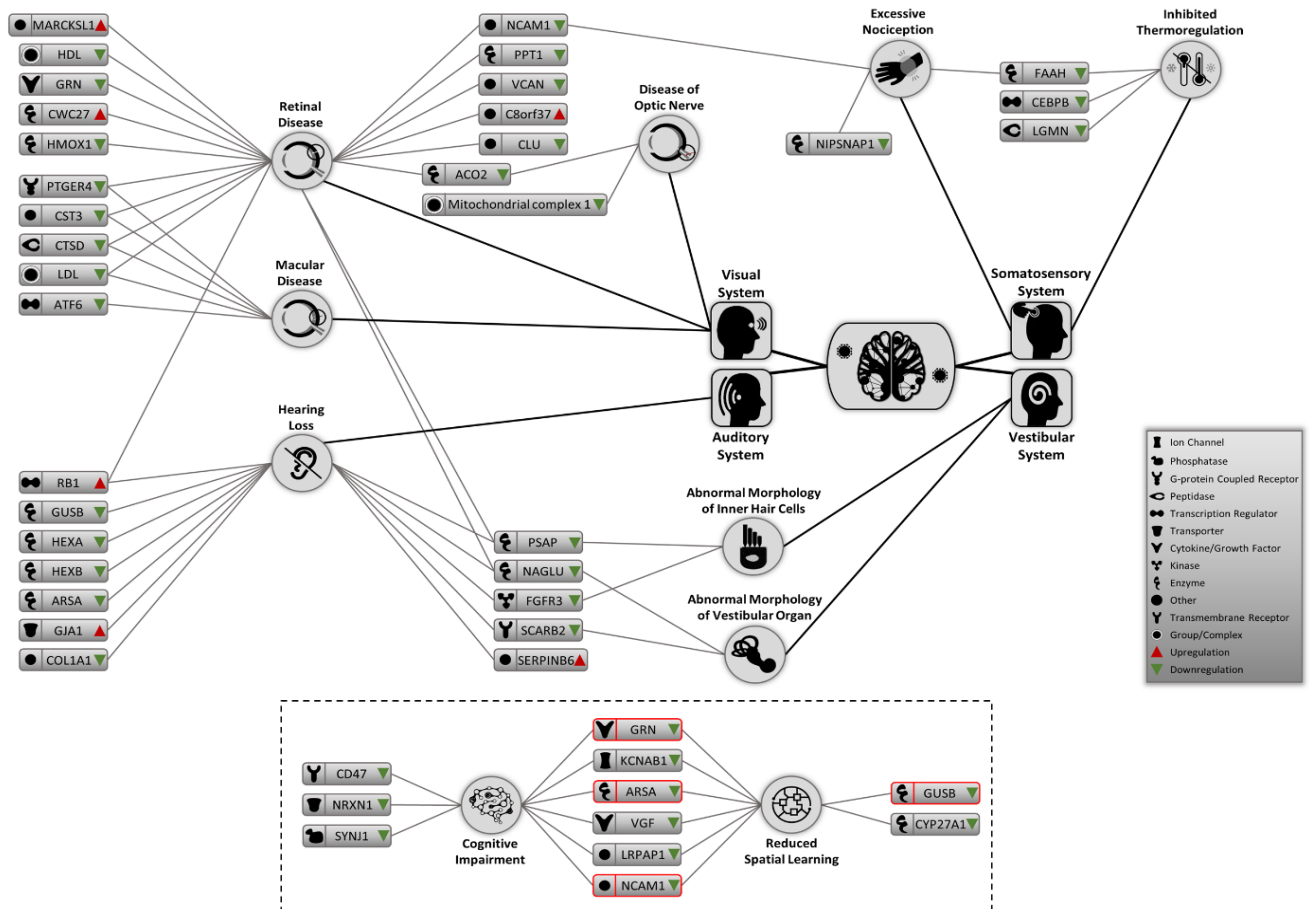


Figure 14: Proteomic prediction of ZIKV-induced changes in the neurosensory system. A) Heatmaps of significantly dysregulated proteins involved in the development of neurosensory system. Most significant changes belonged to the 48 hpi dataset. Specific heatmaps that cover different subsets of neurosensory system are shown in upper panels. Lower panel represents the global overview heatmap for all proteins regulating the development of neurosensory system across three time-points from ZIKV-infected Verocells. B) Graphic representation of predicted ZIKV-triggered dysregulations in different parts of the neurosensory system by 2 dpi. Lower bordered panel indicates that a few proteins (ones with red margins) within influences on sensory nervous system together with some other differentially expressed proteins at 48 hpi could influence cognitive and learning functions based on IPA predictions. C) Protein-protein interaction assessment of significantly regulated proteins causing neurosensory impairments based on their expression data at 48 hpi. D) Gene ontology analysis within the single class of biological process showing top affected pathways based on significantly expressed proteins with functions in neurosensory system at 48 hpi.

3.3. ZIKV Infection Induces DNA Damage Response and Alters the Proteome of Gastrointestinal Cells.

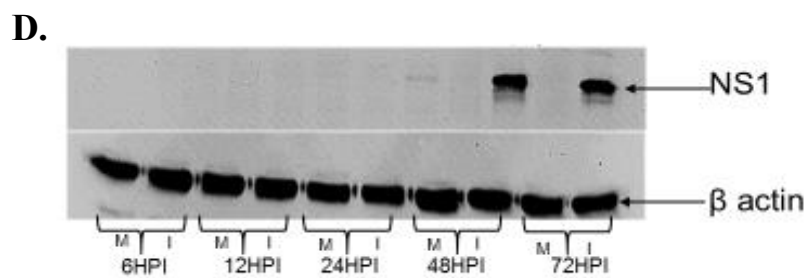
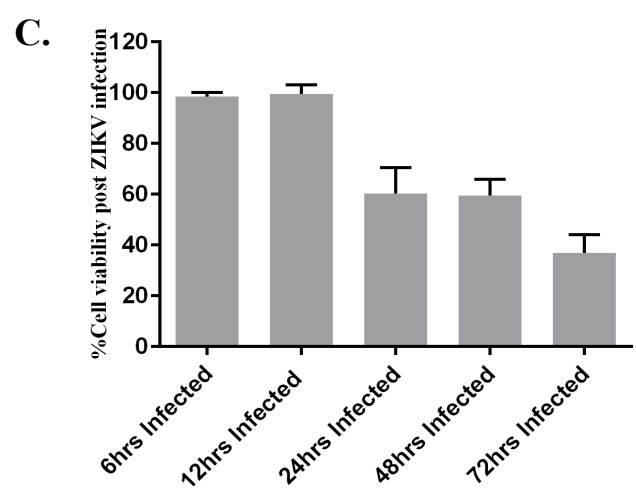
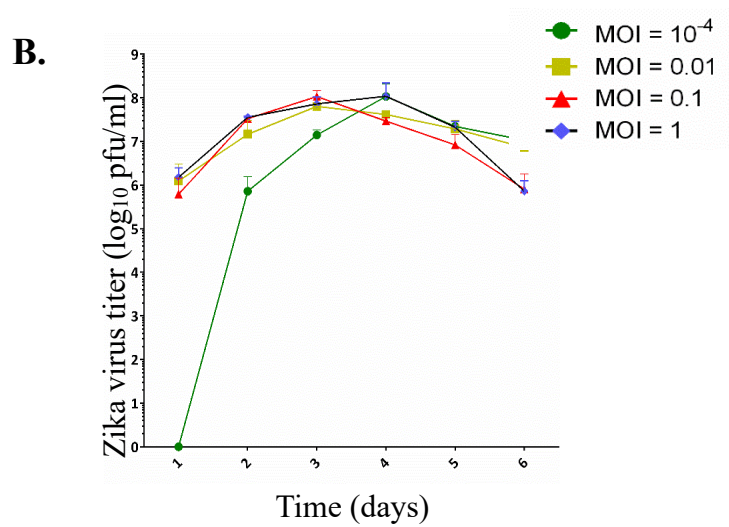
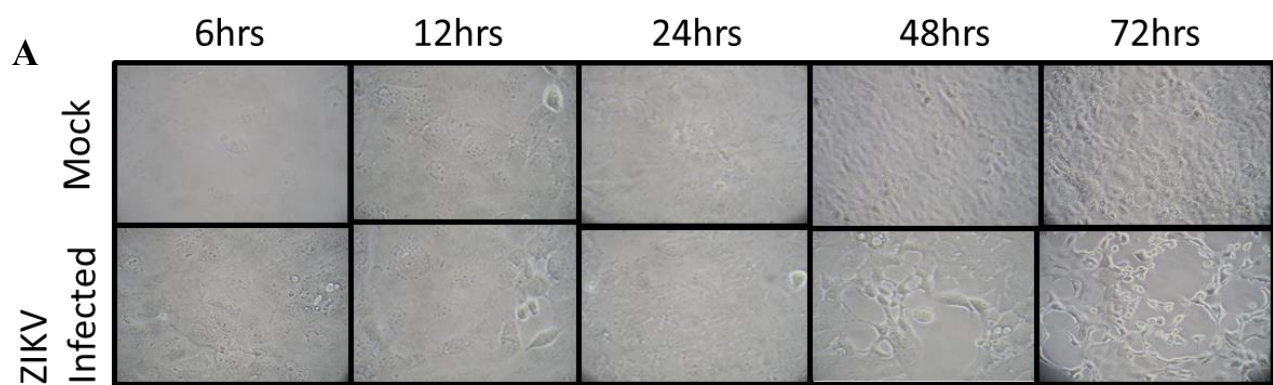
Number of citations from this publication: 3

3.3.i. Contributory Role.

Performed all experiments and contributed to the data analysis of proteomic data generated, as well as the drafting and reviewing of the manuscript of this publication which also formed part of my PhD thesis.

3.3. ii. ZIKV Virus Induces Cytopathology in Caco-2 with Increased Viral Titer

As done in our previously published ZIKV proteomic studies, time points for visible cytopathology, Western blotting, and immunofluorescent staining for ZIKV viral proteins were done prior to the proteomic screening. ZIKV-induced cytopathic effects (CPE) were noticeable by 24 hpi and were more pronounced after 48 hpi (Figure 15A). ZIKV growth curves also were performed to confirm our cells would support ZIKV replication and determine appropriate time points for subsequent analyses (Figure 15B). Peak titers exceeded 10^8 PFU/mL by days 3 and 4, even when cultures were infected at multiplicities of infection (MOI) < 0.01 . We then infected cells at an MOI of 3, predicted by Poisson distribution to result in $>90\%$ initial cell infection, as done in our previous ZIKV proteomic studies (60). Simultaneously, a WST-1 (4-[3-(4-iodophenyl)-2-(4-nitrophenyl)-2H-5-tetrazolio]-1, 3-benzene disulfonate; Pierce Biotechnology) cytotoxicity assay was performed to measure Caco-2 cell viabilities more precisely at various times after ZIKV infection. We observed no CPE up to 24 hpi, but CPE was apparent and increased from $\sim 50\%$ at 48 hpi to $\sim 70\%$ by 72 hpi (Figure 15C). ZIKV NS1 expression was examined, faint immunoreactive bands were observed at 24 hpi, and the signal was significantly stronger by later time points (Figure 15D). Immunofluorescence microscopy indicated that virtually every cell was infected by 48 hpi (Figure 15E), confirming that an MOI = 3 successfully infected every cell. Based on these cumulative data, we chose 12, 24, and 48 hpi as time points to probe by SOMAScan



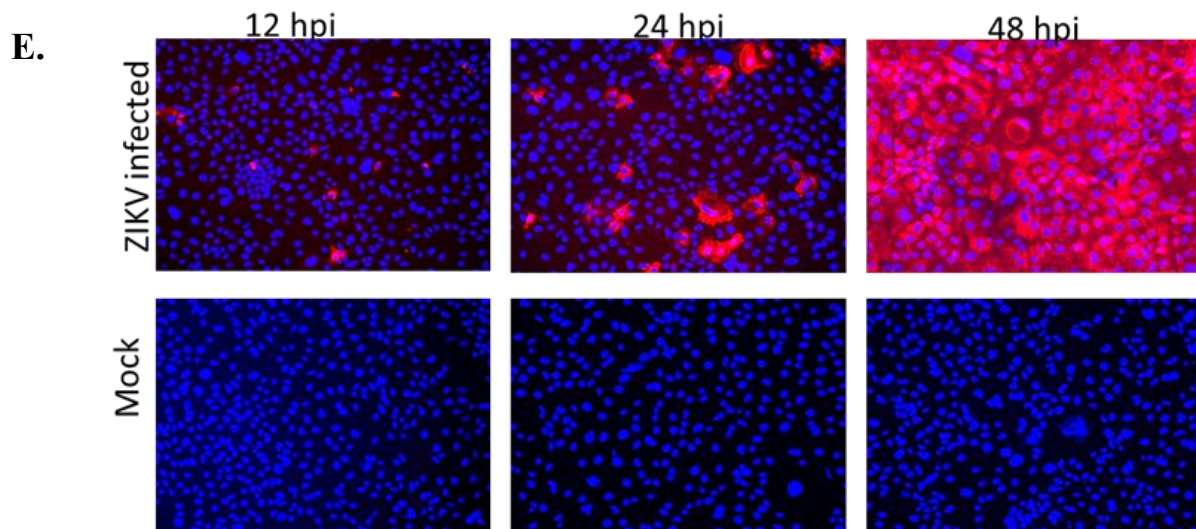


Figure 15:ZIKV growth kinetics in Caco-2 cells and proteomic validation

(A) Photomicrographs of Mock and ZIKV (ZIKV) infected Caco-2 cells at indicated times post-infection. (B) Kinetics of virus production after different MOI infections. Error bars represented S.E.M. of three replicates. (C) Cytopathology induced at different times post-infection, determined by WST-1 cell viability. Error bars represent S.E.M. of three replicates. (D) ZIKV non-structural protein-1 (NS1) expression in mock-infected (M) and in virus-infected (I) cells. (E) Immunofluorescence staining showing expression of ZIKV NS1 protein (red) as a function of time after ZIKV MOI = 3 infection. Nuclei were stained with DAPI (blue). Scale bars in A and E, (lower right micrographs) represent 100 μ m.

3.3.iii ZIKV Induces Proteomics Dysregulation of Caco-2 Host Proteins.

We screened and measured dysregulation of more than 1,300 Caco-2 proteins in triplicate from three different time points using the aptamer-based SOMAScan proteomic tool. Statistical analyses, using both Student's T-test and Z-score, identified 439 proteins dysregulated significantly at any time point (Table 5). The vast majority of these were upregulated at 12 hpi. More than 100 proteins were also significantly dysregulated at 48 hpi, and virtually all these also were upregulated. We routinely apply more stringent fold-change cut-off criteria to such lists of proteins (60). A total of 193 proteins were significantly dysregulated ≥ 1.30 -fold ($= \leq 0.7693$ -fold if downregulated) depicted in Figure 16A and imported into IPA for bioinformatics analyses. Table 6 displays the 71 total Caco-2 proteins significantly dysregulated ≥ 1.375 -fold ($= \leq 0.7273$ -fold if downregulated) across all three time points. Of the 71 proteins dysregulated, ≥ 1.375 -fold, 52 were upregulated at 12 hpi, 15 were upregulated at 24 hpi, 2 were upregulated at 48 hpi, and only 2 were downregulated at 48 hpi.

The entire dataset was imported into IPA for analysis. Figure 16B displays networks of the top Diseases and Functions with a score of >30 and >20 focus molecules. The most significantly affected networks at 12 hpi were cell death and survival, embryonic development, tissue morphology, amino acid metabolism, cell cycle, post-translational modification at 24 hpi and carbohydrate metabolism, developmental disorder, small molecule biochemistry at 48 hpi. Each network at each time point was overlaid with proteomic data from the other time points to visualize changes in expression profiles of the individual proteins in each network over time. Most of these significantly dysregulated proteins represented kinases, enzymes, cytokines, and other molecules predicted to reside in various subcellular compartments (Figure 16C). Most dysregulated host proteins were classified as “others” and located in the “extracellular space”.

IPA predicted several signaling pathways and linked various cellular processes that were activated or inhibited after 12 h of ZIKV infection (Figure 16D). Activation and inhibition of each pathway were based on positive or negative Z-scores. Pathways linked to immunity

included dendritic cell maturation, STAT3, chemokine, CD40, NF-kB, and p38 MAPK signaling (131–135). Other pathways, such as HMGB1, CDK5, ATM, and G2/M DNA damage checkpoint regulation, neuroinflammation and ErbB signaling, are linked to various cell cycle processes (136–141).

Table 5: Numbers of significantly dysregulated ZIKV-infected CaCo-2 proteins.

Number that are significant	Total Unique	12 hpi	24 hpi	48 hpi
and fold-change > 1.000and fold-change < .9999	439	252 4	52 0	150 4
and fold-change > 1.100 and fold-change < .9091	407	252 0	46 0	128 4
and fold-change > 1.250 and fold-change < .8000	261	230 0	23 0	6 3
and fold-change > 1.333 and fold-change < .7500	122	100 0	16 0	3 3
and fold-change > 1.375 and fold-change < .7273	71	52 0	15 0	2 2
and fold-change > 1.500 and fold-change < .6667	23	10 0	9 0	2 2
and fold-change > 2.000 and fold-change < .5000	2	0 0	2 0	0 0

Table 6: List of significantly dysregulated in Cacao-2 cells after ZIKV infection from 3 biological replicates

Gene	Swissprot	12hpi		24hpi		48hpi	
		Fold change	p-value	Fold change	p-value	Fold change	p-value
A2M	P01023	1.323	0.0190	1.094	0.5456	1.097	0.1882
ABL1	P00519	1.392	0.0272	1.186	0.4847	1.057	0.6067
ACAN	P16112	1.313	0.0491	1.079	0.2884	1.092	0.3545
ADAMTS5	Q9UNA0	1.320	0.0365	1.195	0.4933	1.192	0.0741
ADCYAP1	P18509	1.316	0.0201	1.104	0.5890	1.028	0.6535
AGER	Q15109	1.369	0.0371	1.097	0.2413	1.220	0.1933
AK1	P00568	1.721	0.0069	1.437	0.2480	1.408	0.4894
AKT1	P31749	1.523	0.1429	1.326	0.0301	1.304	0.3210
AKT3	Q9Y243	1.523	0.1429	1.326	0.0301	1.304	0.3210
ANG	P03950	1.437	0.3412	0.924	0.5369	0.651	0.0210
ANGPT4	Q9Y264	1.369	0.0356	1.067	0.5956	1.104	0.5448
ANGPTL3	Q9Y5C1	1.320	0.0465	1.099	0.4855	1.115	0.1608
ANP32B	Q92688	1.307	0.0424	1.033	0.7976	1.107	0.1464
APCS	P02743	1.369	0.0459	1.089	0.3282	1.089	0.3281
ARTN	Q5T4W7	1.424	0.0400	1.162	0.4011	1.097	0.2954
B2M	P61769	1.395	0.0433	1.181	0.1294	0.822	0.2865
BCAN	Q96GW7	1.382	0.0230	1.335	0.3332	1.120	0.3859
BMP10	O95393	1.313	0.0248	1.110	0.4484	1.173	0.0486
C2	P06681	1.335	0.0324	1.042	0.7476	1.112	0.5421
CA13	Q8N1Q1	1.488	0.0268	1.228	0.1593	1.454	0.2056
CA6	P23280	1.427	0.0134	1.019	0.9021	1.026	0.9332
CCDC80	Q76M96	1.353	0.0489	1.117	0.4144	1.050	0.2673
CCL14	Q16627	1.301	0.0342	1.089	0.7211	1.033	0.8071
CCL15	Q16663	1.326	0.0426	1.059	0.4871	1.203	0.0788
CCL2	P13500	1.326	0.0489	1.062	0.6098	1.122	0.1048
CCL21	O00585	1.310	0.0497	1.099	0.4909	1.110	0.1547
CCL22	O00626	1.320	0.0122	1.125	0.5154	1.067	0.4670
CCL25	O15444	1.310	0.0260	1.035	0.7256	1.077	0.5674
CCL4L1	Q8NHW4	1.431	0.0353	1.030	0.7884	1.084	0.5842
CD163	Q86VB7	1.363	0.0190	1.028	0.8890	1.099	0.2896
CD4	P01730	1.360	0.0151	1.104	0.4019	1.173	0.0427
CD40LG	P29965	1.376	0.0310	1.074	0.7730	1.136	0.3136
CDH12	P55289	1.316	0.0120	1.077	0.4832	1.133	0.0556
CDON	Q4KMG0	1.332	0.0215	1.104	0.2484	1.122	0.4187

CFH	P08603	1.353	0.0351	1.128	0.3805	1.122	0.2414
CFI	P05156	1.376	0.0230	1.026	0.9203	1.067	0.6144
CFL1	P23528	1.214	0.4098	1.866	0.0032	1.379	0.3762
CFP	P27918	1.307	0.0213	1.112	0.5692	1.077	0.3282
CHST15	Q7LFX5	1.395	0.0228	1.045	0.8005	0.940	0.6532
CHST2	Q9Y4C5	1.372	0.0355	1.059	0.5829	1.102	0.4799
CLEC1B	Q9P126	1.326	0.0328	1.050	0.8347	1.062	0.7333
CLEC7A	Q9BXN2	1.310	0.0442	1.067	0.4769	1.178	0.0208
CMA1	P23946	1.323	0.0497	1.038	0.7060	1.195	0.1799
CNDP1	Q96KN2	1.301	0.0374	1.102	0.2707	1.151	0.0254
CNTN5	O94779	1.304	0.0415	1.112	0.4204	1.128	0.0342
CRLF2	Q9HC73	1.313	0.0422	1.074	0.3117	1.151	0.0637
CSK	P41240	2.848	0.1290	2.543	0.0264	1.729	0.4505
CST7	O76096	1.392	0.0441	1.149	0.1283	1.133	0.1181
CTSS	P25774	1.360	0.0472	1.122	0.1155	1.157	0.2556
CTSV	O60911	1.441	0.0904	1.074	0.4759	0.606	0.0414
CXCL10	P02778	1.357	0.0357	1.089	0.4786	1.138	0.2892
CXCL16	Q9H2A7	1.310	0.0455	1.074	0.0721	1.094	0.1076
CXCL8	P10145	1.307	0.0444	1.064	0.4948	1.089	0.0518
DCN	P07585	1.313	0.0331	1.122	0.3047	1.149	0.0727
DCTPP1	Q9H773	1.640	0.1860	1.512	0.0783	1.819	0.0053
DHH	O43323	1.332	0.0435	1.092	0.3435	1.099	0.3559
DLL4	Q9NR61	1.388	0.0449	1.136	0.4127	1.138	0.1418
DNAJB1	P25685	1.717	0.1163	1.562	0.0470	1.280	0.5437
DNAJC19	Q96DA6	1.338	0.0240	1.110	0.3063	1.154	0.0617
DPT	Q07507	1.421	0.0347	1.112	0.5032	1.092	0.2463
EFNA4	P52798	1.350	0.0479	1.082	0.6204	1.014	0.8083
EGFR	P00533	1.301	0.0351	1.197	0.2464	1.141	0.0501
EIF4A3	P38919	1.666	0.1464	1.573	0.0161	1.266	0.5967
EIF4G2	P78344	2.229	0.0010	2.019	1.616E-05	1.485	0.6225
ESAM	Q96AP7	1.341	0.0131	1.162	0.1472	1.104	0.2297
ESD	P10768	1.347	0.0326	1.120	0.2862	1.283	0.3237
F11	P03951	1.332	0.0472	1.107	0.1894	1.248	0.1238
FABP3	P05413	1.558	0.0020	1.159	0.5529	1.301	0.4700
FCGR1A	P12314	1.363	0.0333	1.069	0.5476	1.112	0.1751
FCGR3B	O75015	1.464	0.0355	1.026	0.9296	1.120	0.3407
FCN1	O00602	1.323	0.0496	1.033	0.6840	1.151	0.0848
FER	P16591	1.505	0.0402	1.094	0.6893	1.251	0.3223
FGF1	P05230	1.360	0.0457	1.146	0.5957	0.979	0.9102
FGF10	O15520	1.366	0.0301	1.115	0.5910	1.087	0.2450
FGF16	O43320	1.404	0.0281	1.154	0.3774	1.178	0.2600

FGF17	O60258	1.344	0.0496	1.154	0.3890	1.077	0.4061
FGF18	O76093	1.335	0.0225	1.104	0.7066	1.072	0.3168
FGF4	P08620	1.372	0.0344	1.055	0.6979	1.087	0.6023
FGF7	P21781	1.411	0.0420	1.120	0.4558	1.128	0.4693
FGF9	P31371	1.372	0.0310	1.151	0.3144	1.159	0.0155
FOLH1	Q04609	1.320	0.2868	1.344	0.0357	1.035	0.8446
FSTL3	O95633	1.283	0.1786	0.869	0.6673	0.734	0.0320
GP6	Q9HCN6	1.350	0.0361	1.146	0.3413	1.143	0.2197
GPC2	Q8N158	1.414	0.0251	1.069	0.4929	1.203	0.3071
GZMB	P10144	1.316	0.0303	1.120	0.4523	1.084	0.2178
GZMH	P20718	1.347	0.0365	1.069	0.6728	1.104	0.1374
HAT1	O14929	1.341	0.4800	1.786	0.0010	1.136	0.7976
HFE2	Q6ZVN8	1.304	0.0200	1.112	0.3516	1.138	0.0807
HGF	P14210	1.307	0.0325	1.130	0.4144	1.102	0.2335
HK2	P52789	1.464	0.0824	1.573	0.0131	1.122	0.8761
HPX	P02790	1.598	0.0029	1.138	0.4567	0.975	0.8869
ICOS	Q9Y6W8	1.350	0.0471	1.107	0.1900	1.211	0.1381
IDE	P14735	1.372	0.2591	1.411	0.0062	1.289	0.2727
IFNGR2	P38484	1.313	0.0464	1.102	0.4859	1.110	0.0756
IFNL2	Q8IZJ0	1.408	0.0121	1.157	0.4801	1.197	0.2069
IL11	P20809	1.335	0.0240	1.059	0.6567	1.159	0.0815
IL12RB1	P42701	1.313	0.0453	1.089	0.4970	1.107	0.0602
IL15RA	Q13261	1.313	0.0418	1.021	0.8170	1.165	0.1254
IL18RAP	O95256	1.329	0.0368	1.074	0.7093	1.170	0.2241
IL1RL1	Q01638	2.051	0.2716	1.176	0.5661	1.523	0.0237
IL20	Q9NYY1	1.347	0.0445	1.030	0.7454	1.120	0.4229
IL20RA	Q9UHF4	1.329	0.0142	1.178	0.5021	1.084	0.5412
IL24	Q13007	1.326	0.0419	1.052	0.5572	1.097	0.4831
IL3RA	P26951	1.421	0.0467	1.206	0.3574	1.112	0.4364
IL6R	P08887	1.323	0.0474	1.089	0.4931	1.112	0.0900
IL7	P13232	1.498	0.0422	1.012	0.9674	0.989	0.1059
JAG1	P78504	1.357	0.0329	1.138	0.3512	1.028	0.4931
KIF23	Q02241	1.363	0.0221	1.176	0.3552	1.149	0.3040
KLK11	Q9UBX7	1.320	0.0189	1.110	0.2274	1.189	0.2484
KLK4	Q9Y5K2	1.307	0.0355	1.094	0.5116	1.120	0.0676
KLK8	O60259	1.329	0.0479	1.087	0.2766	1.162	0.0534
KNG1	P01042	1.329	0.0219	1.133	0.4130	1.077	0.3408
L1CAM	P32004	1.444	0.0323	1.059	0.7580	1.162	0.4324
LAG3	P18627	1.662	0.0126	1.026	0.9441	1.064	0.0335
LCN2	P80188	1.434	0.0480	1.165	0.2242	1.110	0.7437
LHB	P01229	1.326	0.0390	1.112	0.3914	1.128	0.0980

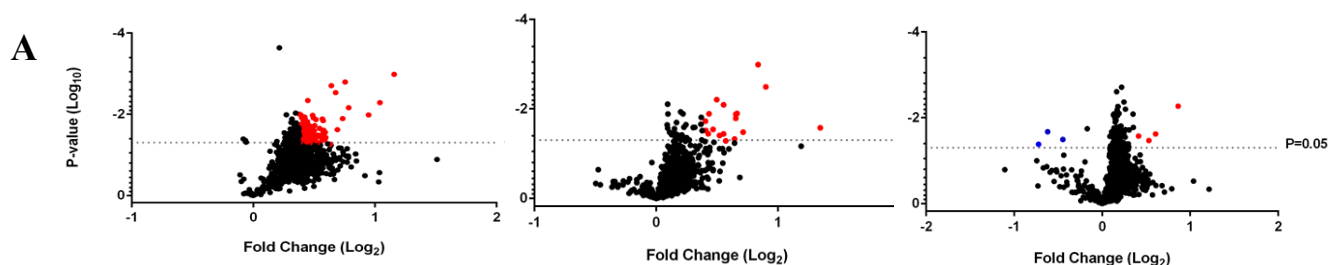
LRRTM3	Q86VH5	1.316	0.0174	0.918	0.7529	1.102	0.2278
LYZ	P61626	1.398	0.2120	1.382	0.0284	1.347	0.3589
MAP2K1	Q02750	1.417	0.1974	1.467	0.0360	1.307	0.0558
MAPK12	P53778	1.385	0.0427	1.149	0.4194	1.162	0.1107
MAPK13	O15264	1.509	0.0368	1.181	0.2048	1.206	0.7442
MAPK8	P45983	1.790	0.0942	1.434	0.0390	1.220	0.1805
MAPK9	P45984	1.686	0.0016	1.157	0.4720	2.051	0.3368
MATK	P42679	1.313	0.0287	1.059	0.6427	1.159	0.3184
MBL2	P11226	1.363	0.0399	1.122	0.4432	1.133	0.0260
MRC2	Q9UBG0	1.301	0.0286	0.998	0.9856	1.173	0.2591
MST1	P26927	1.481	0.0130	0.709	0.4638	1.047	0.5154
NAMPT	P43490	1.551	0.0607	1.323	0.0187	1.444	0.8138
NID1	P14543	1.417	0.0187	1.234	0.5189	0.973	0.0630
NID2	Q14112	1.363	0.0391	1.122	0.4993	1.087	0.3263
NME2	P22392	1.613	0.0238	1.357	0.2060	1.157	0.1280
NTF3	P20783	2.056	0.0051	0.809	0.5015	0.899	0.0407
NTF4	P34130	1.310	0.0104	1.072	0.7396	1.112	0.4040
NTN1	O95631	1.505	0.0276	1.159	0.5379	1.084	0.0935
NTRK3	Q16288	1.329	0.0255	1.136	0.4283	1.165	0.2284
PAK6	Q9NQU5	1.447	0.1414	1.104	0.5561	1.332	0.0266
PDE7A	Q13946	1.379	0.0444	1.162	0.3691	1.138	0.2518
PDGFRB	P09619	1.301	0.0434	1.170	0.3701	1.157	0.0713
PECAM1	P16284	1.304	0.0435	1.087	0.1982	1.151	0.0043
PGD	P52209	1.647	0.0677	1.350	0.0128	1.392	0.2546
PGLYRP1	O75594	1.357	0.0254	1.125	0.4856	1.136	0.5129
PLA2G2E	Q9NZK7	1.323	0.0417	0.827	0.4990	1.067	0.0941
PLA2G5	P39877	1.341	0.0442	1.102	0.4295	1.062	0.8544
PLAUR	Q03405	1.353	0.0494	1.104	0.1282	1.125	0.4730
PLG	P00747	1.329	0.0295	1.087	0.5887	1.107	0.1000
PLK1	P53350	1.335	0.0398	1.138	0.6127	1.107	0.1103
PON1	P27169	1.369	0.0398	1.062	0.6367	1.234	0.3485
POSTN	Q15063	1.401	0.0105	1.146	0.1906	1.220	0.7175
PPIF	P30405	1.488	0.0142	1.197	0.3350	1.028	0.9623
PRDX5	P30044	1.341	0.0402	1.084	0.5987	1.136	0.8677
PRKAA1	Q13131	1.347	0.0434	1.117	0.4535	1.084	0.5802
PRKAB1	Q9Y478	1.347	0.0434	1.117	0.4535	1.084	0.2085
PRSS2	P07478	1.310	0.0103	1.214	0.2840	1.089	0.1538
PRTN3	P24158	1.350	0.0330	1.102	0.3548	1.217	0.9693
PSMA2	P25787	1.310	0.0444	1.079	0.3234	1.133	0.1467
PSMA6	P60900	1.338	0.0163	1.120	0.3373	1.092	0.2114
PSPN	O60542	1.344	0.0443	1.052	0.7127	1.122	0.1816

PTK2	Q05397	1.301	0.0381	1.117	0.5438	1.064	0.0748
PYY	P10082	1.357	0.0183	1.162	0.6085	1.130	0.9416
RNASEH1	O60930	2.042	0.4602	1.932	8.439E-05	2.319	0.2245
RPS6KA5	O75582	1.491	0.0245	1.122	0.7708	1.055	0.8862
RSPO4	Q2I0M5	1.457	0.0221	1.097	0.7599	1.092	0.7762
SBDS	Q9Y3A5	1.632	0.1159	1.640	0.0329	1.408	0.7374
SELP	P16109	1.360	0.0372	1.125	0.3758	1.292	0.4439
SERPINE2	P07093	1.304	0.0472	1.115	0.0619	1.214	0.8814
SET	Q01105	1.363	0.0176	1.122	0.2756	1.035	0.4946
SEZ6L2	Q6UXD5	1.401	0.0392	1.195	0.3262	1.165	0.0766
SFRP1	Q8N474	1.376	0.0332	1.107	0.5859	1.203	0.3262
SHH	Q15465	1.478	0.0443	1.104	0.6775	1.130	0.9426
SIGLEC14	Q08ET2	1.385	0.0395	1.104	0.5562	1.062	0.1194
SKP1	P63208	1.303	0.0333	1.107	0.3527	1.112	0.3935
SLAMF7	Q9NQ25	1.301	0.0500	1.097	0.2046	1.211	0.1914
SLPI	P03973	1.326	0.0495	1.087	0.3886	1.104	0.0442
SOD1	P00441	1.307	0.0274	1.087	0.3595	1.122	0.1831
SPHK1	Q9NYA1	1.379	0.0452	1.320	0.2360	1.186	0.6927
SPTAN1	Q13813	1.304	0.0394	1.042	0.8299	1.087	0.3037
STAT1	P42224	1.516	0.2873	1.467	0.0081	1.431	0.2430
STX1A	Q16623	1.326	0.0394	1.107	0.2771	1.133	0.2168
THBS2	P35442	1.338	0.0116	1.110	0.6348	1.125	0.9031
THBS4	P35443	1.363	0.0045	1.087	0.6100	1.112	0.0479
TIE1	P35590	1.366	0.0247	1.047	0.7990	1.115	0.6769
TIMP1	P01033	1.376	0.0190	0.986	0.9418	1.104	0.2384
TIMP2	P16035	1.404	0.0316	1.167	0.1329	0.739	0.3286
TIMP3	P35625	1.478	0.0325	1.237	0.3142	0.982	0.2273
TNFRSF17	Q02223	1.360	0.0243	1.136	0.3668	1.069	0.3262
TNFRSF19	Q9NS68	1.411	0.0444	1.203	0.5692	1.079	0.0367
TNFRSF1A	P19438	1.424	0.0442	1.209	0.1000	1.082	0.0919
TNFSF15	O95150	1.307	0.0348	1.102	0.4192	1.130	0.4546
TNFSF4	P23510	1.301	0.0194	1.050	0.6665	1.138	0.0208
UBE2L3	P68036	1.307	0.0416	1.138	0.3614	1.130	0.2035
UNC5D	Q6UXZ4	1.927	0.0103	1.094	0.4992	0.946	0.5079
VEGFC	P49767	1.338	0.0196	1.112	0.4091	1.159	0.7365
WNK3	Q9BYP7	1.798	0.1401	1.584	0.0126	1.254	0.4788

Fold change cutoff used was ≥ 1.3 -fold and statistical significance level was p-value <0.05

Bolded red colored fold change represents significantly up-regulated Caco-2 proteins

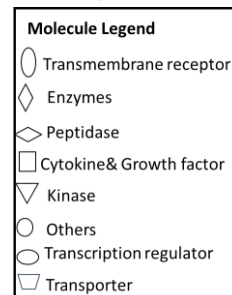
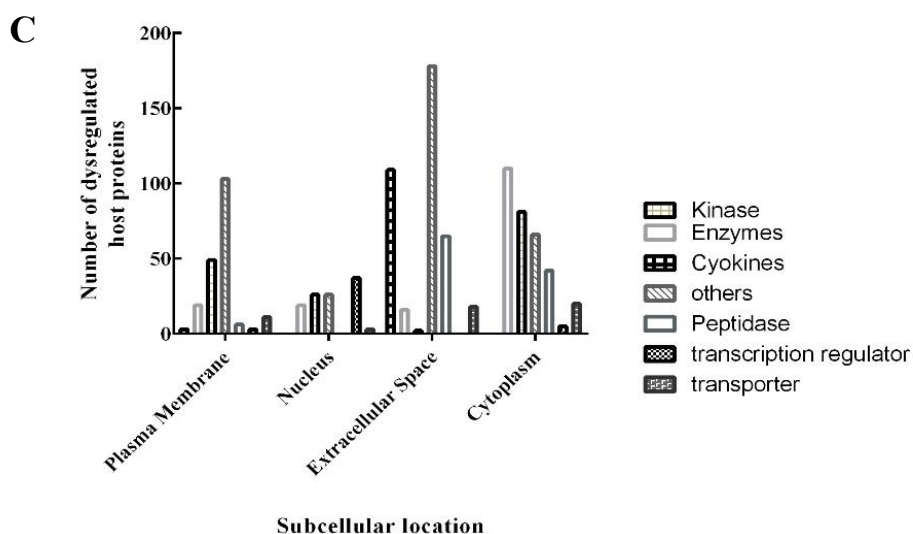
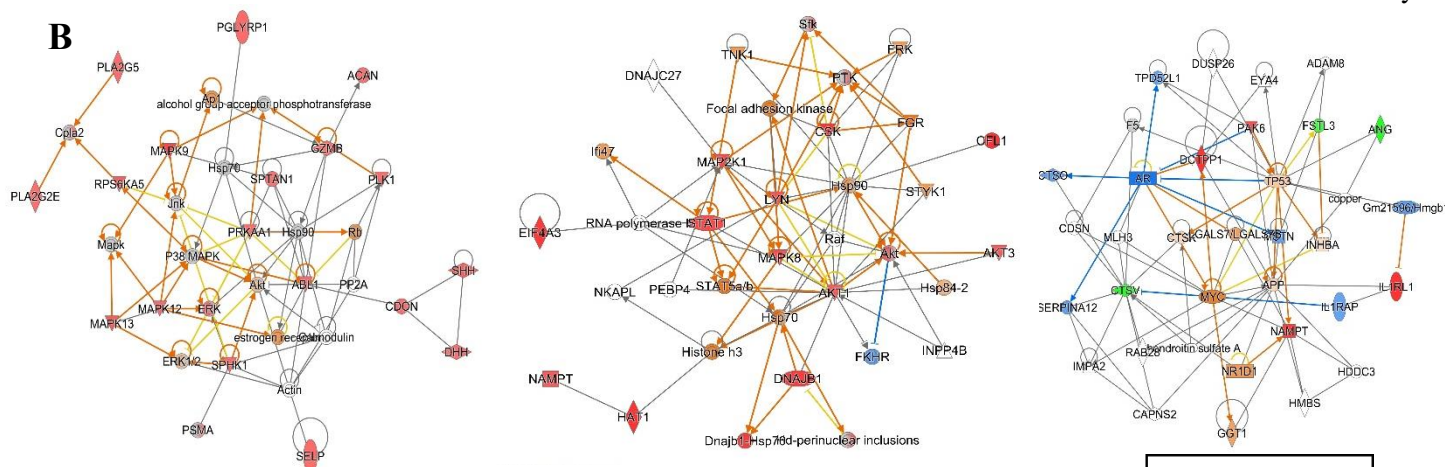
Bolded blue colored fold change represents significantly down-regulated Caco-2 proteins



Cell Death and Survival, Embryonic Development, Tissue Morphology

Amino Acid Metabolism, Cell cycle, Post-translational Modification

Carbohydrate Metabolism, Developmental Disorder, Small Molecule Biochemistry.



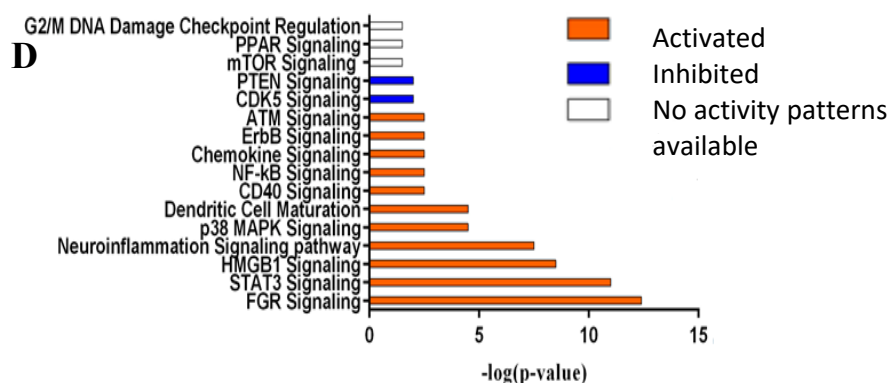


Figure 16: ZIKV dysregulated Caco-2 proteins and predicted signaling pathway.

ZIKV dysregulated Caco-2 proteins and predicted signaling pathway. (A) Volcano plots showing fold changes and p-values of Caco-2 proteins at each time point. Red dots are significantly upregulated proteins. The three blue dots in the 48-hrs plot are significantly downregulated. (B) IPA-determined interaction networks and focus molecules of top diseases and functions predicted to be affected after ZIKV infection. Orange proteins are upregulated, whereas downregulated proteins are green. Predicted pathway activations and inhibitions are depicted in orange and blue, respectively. (C) Subcellular locations of dysregulated host proteins and the nature of these proteins. (D) Bar charts showing signaling pathways predicted by IPA to be induced after 12 h of ZIKV infection. Orange bar and blue bars indicate activation and inhibition of pathways after infection, respectively. Clear bars indicate no activity prediction by IPA based on Z score.

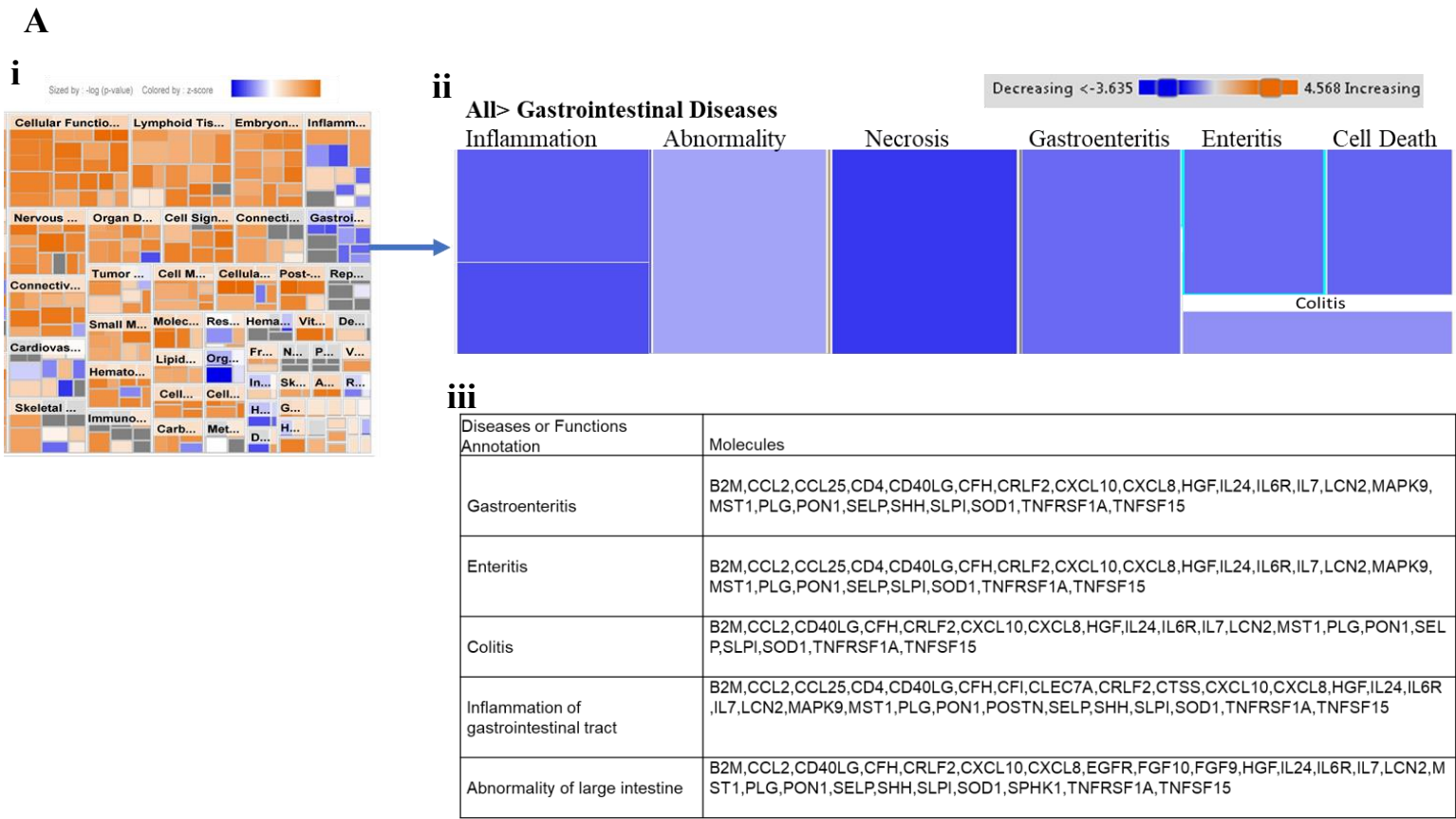
3.3.iv ZIKV Infection Results in Numerous Diseases and Alters Bio-functions.

Bioinformatic analysis of significantly dysregulated host proteins by IPA software, as done in our previous proteomic studies (60,116,119,126), predicted induction of several diseases and altered bio-functions because of ZIKV infection (117). Most of these alterations were observed at 12 hpi since more than 80% of host proteins dysregulated were at this early time point. Activation of all diseases and functions was based on their Z-scores. Diseases and functions with Z-score ≥ 2.0 are predicted to have increased activation, whereas those with Z-score ≤ -2.0 have decreased activation (Figure 16Ai). Bio-functions whose activations are predicted to be either increased or decreased include cell movement of dendritic cells, binding of T Lymphocytes, chemotaxis of neutrophils, the quantity of antigen-presenting cells, and inflammation of the body cavity. Previous ZIKV proteomic studies identified the development and quality of neurons, the sensory organ, sensory system development, and lipid synthesis (60,119).

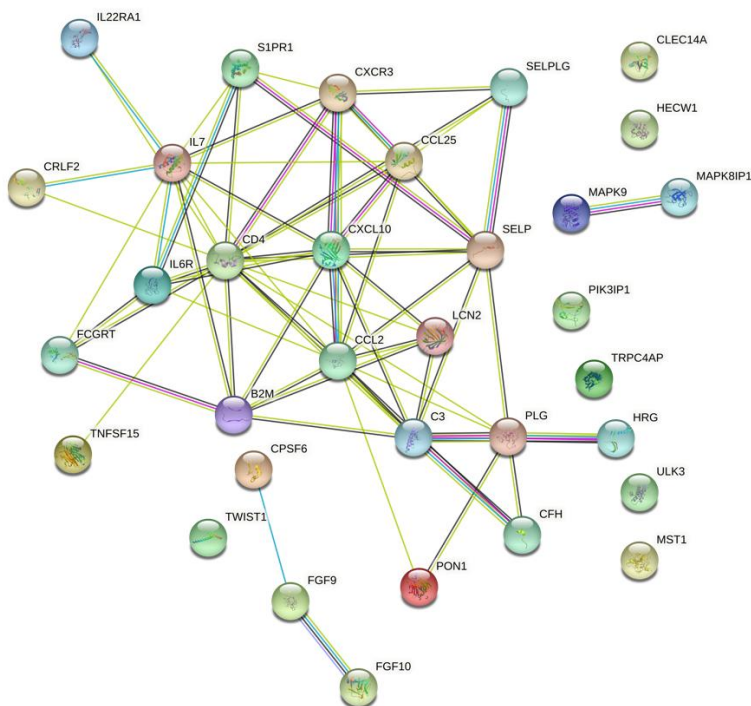
Proteomic delineation of gastrointestinal complications induced by ZIKV has not been reported yet. Among the gastrointestinal diseases and biofunctions predicted to be activated by ZIKV are gastroenteritis, enteritis, colitis, inflammation of gastrointestinal tract and abnormality of large intestine (Figure 17Aii). IPA predicted a significant activation of all gastrointestinal complication based on their p-values of < 0.05 . All these predictions were induced by >20 dysregulated host proteins which were significantly up-regulated at 12 hpi. Host proteins that were commonly linked to all the predicted gastrointestinal complications were cytokines (CCL2, CCL25), chemokines (CXCL10, CXCL8 and CCL2), interleukins (IL24, IL6R and IL7), complement factor H, tumor necrosis factors (TNFRSF1A, TNFSF15), T-cell interacting proteins (CD40LG), and MAP kinase 9 (Figure 17Aiii). Other uniquely expressed proteins included FGF9 and FGF10, EGFR, CFI, POSTN, CTSS, SPHK1 and CLEC7A. Figure 17B displays the protein-protein interactions between all the proteins in Figure 17Aiii as determined by STRING analysis. All proteins except SPHK1 and MST1 interact with each other. We have similarly explored interacting significantly dysregulated host proteins during influenza A virus infection (142).

3.3.v Proteomic Prediction of ZIKV Activation of DNA Damage Response.

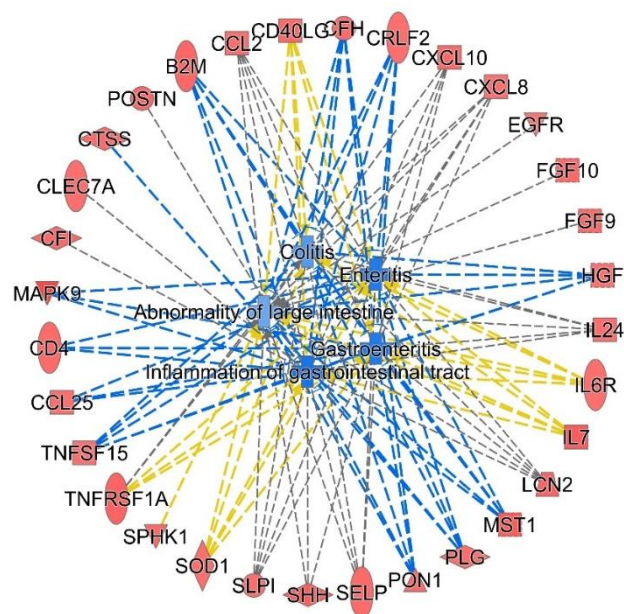
IPA analyses also predicted the induction of G2/M DNA damage checkpoint regulation. Checkpoints are mechanisms that monitor various stages during cell cycle to prevent the transfer of damaged DNA to daughter cells resulting in mutation (143–146). Three main pathways, ATM, ATR, and DNA-PK are activated in response to DNA damage (139). ATM signaling is activated in response to double-stranded breaks and was predicted to be activated by ZIKV at 12 hpi (Figure 18A). G2/M DNA damage checkpoint was also predicted to be induced after ZIKV infection. Induction of this checkpoint ensures that the cell cycle does not proceed to the M-Phase (mitosis) until the damaged DNA is repaired. IPA predicted MAPK9, MAPK12, MAPK13, c-ABL and PLK1 to be involved in the activation of ATM signaling and G2/M DNA damage checkpoint response. Key among these host proteins is c-ABL, which is a tyrosine kinase present in the cytoplasm and nucleus. This protein interacts with ATM which activates several downstream molecules in response to DNA damage (Figure 18B) (147).



B.



C.



D

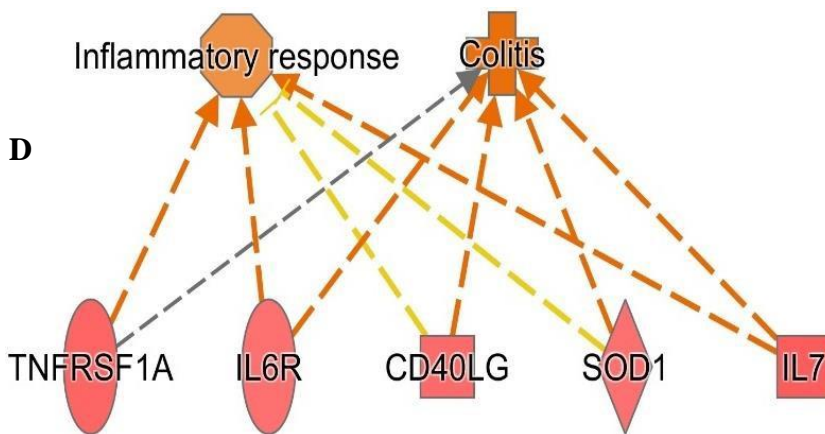
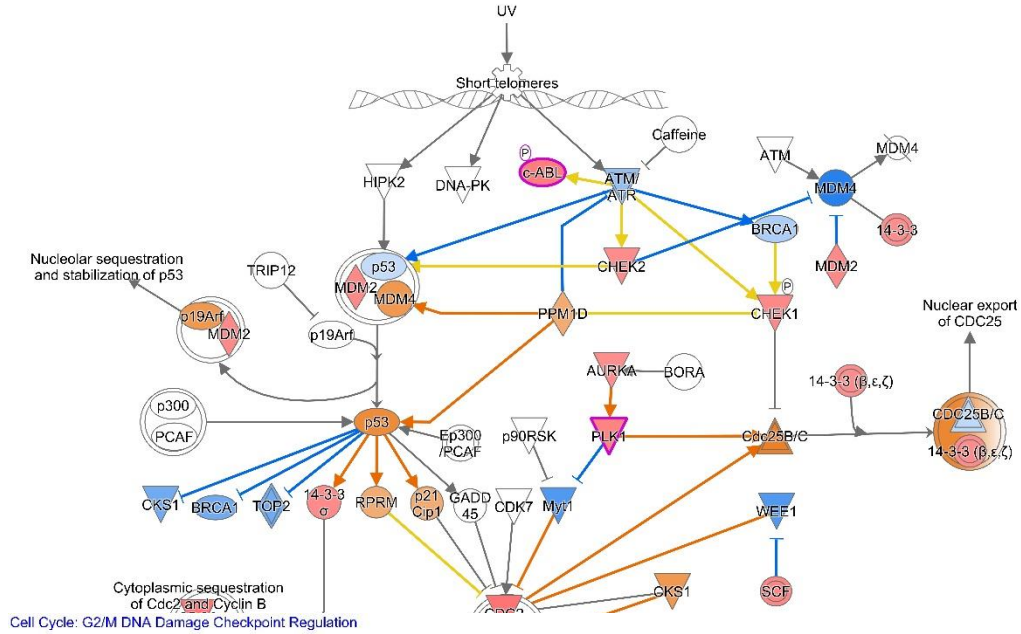


Figure 17: Proteomic prediction by IPA of Disease and function affected by ZIKV infection.

(A) (i) and (ii) Heatmaps of various diseases and functions after 12 h of ZIKV infection. Among various disease and function predicted are various forms of gastrointestinal diseases. Predictions of activation of various disease and function were based on Z scores. Orange color represents activation; blue indicates inhibition. (iii) Tabulation of the various dysregulated host processes which are linked to various gastrointestinal diseases. (B) Protein-protein interaction among proteins in Figure 18iii generated by String software. (C) Networks of dysregulated host proteins linked to the various gastrointestinal diseases predicted by IPA. (D) Network of predicted effect of increased expression of downstream molecules involved in gastroenteritis.

ii.



iii.

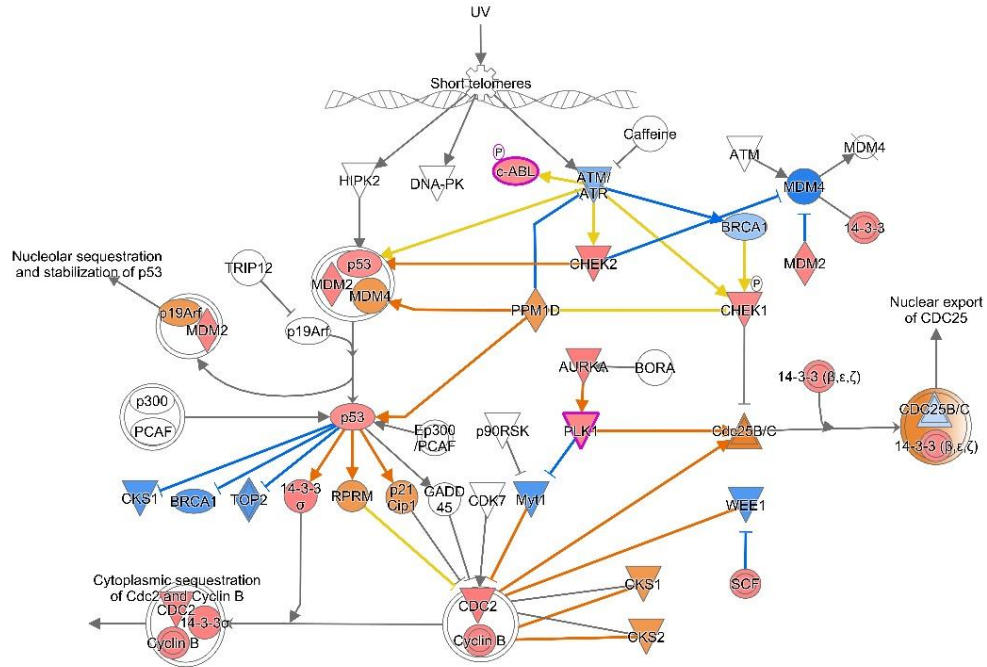


Figure 18: Interactions between network molecules and DNA damage checkpoint pathways

(A) Links between top disease and function networks at 12 hpi and immune checkpoint signaling pathways. (B) Changes in activation of DNA damage checkpoint signaling pathway across all three time points of (i) 12, (ii) 24 and (iii) 48 hpi.

Chapter 4: Discussion and Conclusion.

4.1. Discussion.

Vector-borne viruses like Zika, Chikungunya, West Nile, are a major public threat globally. In the last two centuries, preventative and targeted strategies against emerging viral diseases have been the driving force to overcome pandemic and epidemic outcomes. Global warming, urbanization, air travel movement have tremendously contributed to the survival of these vectors leading to the spread of the infections. The Global vector response 2017-2030 reported by the WHO was implemented with an aim of reducing vector-borne disease by 75%, cases by 65% and prevent possible epidemics in all countries by 2030 (148).

Aside from the vector route of transmission, other modes of transmission are being described, posing a new challenge in terms of controlling and preventing illnesses caused by these viruses. Knowledge of the virus life cycle, disease caused upon infection, at the molecular level, *in vivo* markers expressed upon infection aids toward the development of the therapeutic modalities. The incidence of microcephaly in babies born to ZIKV infected mothers, and neurodevelopmental challenges in ZIKV microcephalic babies, semen persistence of infectious viral particles accounting for sexual transmission of the virus heightens the need to gain more knowledge of ZIKV biology. Learning about ZIKV biology entails understanding the virus's life cycle, as well as the many host-dependent structures it utilizes during its replication cycle, such as pathways and host proteins (117,119,126).

Prior to commencement of my PhD thesis, ZIKV had gained global attention due to reports of high prevalence of microcephaly in babies born to ZIKV infected pregnant mothers in Brazil, the country that was hosting the Olympic games in 2016. Although the African and Asian strains of ZIKV had been found in only a few countries, including Brazil, it had generated concerns in the global network of CDC and WHO agencies at the time due to the unpredictability of facing a potential pandemic state in the near future. Even though ZIKV had been known for more than a decade, there were no therapeutic modalities such as vaccine, antivirals, and rapid diagnostic kits for management of suspected ZIKV infected patients during the 2015-16 microcephaly high incidence reported in Brazil.

Various researchers have utilized a proteomic approach in invitro model system to identify host

proteins as well as pathways dysregulated during ZIKV virus infection. Gaining more basic information about ZIKV biology to identify potential targets in its replicative cycle might help in the development of appropriate interventions and management strategies to control ZIKV driven diseases as well as its spread. Given the inherent mutability of RNA genomes, one approach which is becoming more recognized is the identification of host proteins which viruses like ZIKV use and/or require during their replicative cycles. Some recent studies used mass spectrometry to identify and measure host proteins dysregulated at a single time point post-infection after ZIKV infection. Garcez and colleagues infected human neurospheres derived from neural stem cells with ZIKV and reported 199 downregulated and 259 upregulated host proteins which were reported to be involved in organelle localization, regulation, protein folding translation and cell cycle related processes (80). Among the dysregulated protein namely TLR4 (toll-like receptor 4) and the RNA helicase DDX6, involved in viral recognition, the authors provided evidence that indicates that ZIKV infection arrest cell cycle.

Jiang and colleagues performed a proteomic analysis of human neural progenitor cells infected with ZIKV and found doublecortin (DCX) was downregulated at both the mRNA and protein levels after ZIKV infection (149). ZIKV infection of neural progenitor cells disrupts the formation of the growing fetal brain leading to microcephaly. DCX is involved in both differentiation and migration of neural progenitor cells. Xin and colleagues performed a proteomic analysis of C6/36 mosquito cells and identified 200 host proteins that were significantly dysregulated, including CHCHD2 which promoted ZIKV replication and inhibited IFN- β production cascade pathways (150). Scaturro and colleagues also performed mass spectrometry to identify ZIKV interactome in infected SK-N-BE2 cell line, which are neuroblastoma cell lines originated from the bone marrow after 72hrs of ZIKV infection (127). The researchers discovered 386 ZIKV-interacting proteins, as well as ZIKV-specific and pan-flavivirus activity, and host factors involved in neural development, retinal abnormalities, and infertility (127). Most of the ZIKV proteomic studies however identified cellular targets affected by ZIKV at a single time point in infection (80,149,150). We prioritized to gain further insights to reveal ZIKV impact on host protein topology and relevant functional changes among the cellular network via a proteomic approach using cell line based *in vitro* model utilizing multiple time points of infection. Several validation studies were also carried out to characterize changes and lay out comprehensive profile in the host cellular proteome during infection.

My PhD research work utilized two main proteomic platforms namely the SOMAScan and 6x plex TMT M/S, to examine ZIKV-induced cellular protein dysregulation at multiple time points to assess kinetics of cell proteomic dysregulation. The SOMAScan is a novel multiplexed proteomic technique that allows simultaneous screening of >1300 proteins in each of up to 92 samples. We also decipher the host protein topology during the time course of infections; therefore, cells were infected with ZIKV under conditions in which virtually all cells were simultaneously infected and then time course specific analysis were performed. Although the SOMAScan platform was initially chosen for its unique reactivity to human proteins, the vast majority of its chemically modified aptamer nucleotides also bind non-human primate proteins. (151), allowing meaningful analyses of the monkey Vero cells which are non-human cell line and Caco-2 cells which are human colon derived cells used in research. I also performed a 6x plex Tandem Mass Tagging Mass Spectrometry analysis as a comparative tool to identify more proteomic hits due to broader coverage of Mass Spectrometry (MS). Despite the broad coverage range of mass spectrometry, detection of peptides for proteins is mainly based on its abundance thus the advantage utilizing SOMAScan tool aside its many advantages listed by manufacturers was specifically to recognize and measure dysregulation of low abundance proteins, many of which are not usually detected and measured by mass spectrometry, thus providing complementary information to that already generated in previous generated proteomic screens (108). For instance, only approximately 35% of the proteins detected after SomaLogic analysis were simultaneously detected after Mass Spectrometry analysis. Thus, we can speculate that the 65% of the remaining SomaLogic proteins were low abundant hence were not detected by the Mass Spectrometer as shown in Supplementary Figure S4(152). The IPA tool, which is a licensed web-based software application for the analysis, integration, and interpretation of data acquired from 'omics investigations, such as metabolomics, proteomics, and others, was used for bioinformatic analysis of proteomic data generated from both platforms (153). It is used to decipher the meaning of omics data and find novel targets or candidate biomarkers in biological systems (153).

Vero cells and Caco-2 cells were used in my PhD research to achieve the objective of my thesis. Vero cells, which are African green monkey kidneys, were utilized to provide a baseline data for further comparison to more relevant human cells, Caco-2 cells. (60). Caco-2 cells are human colorectal adenocarcinoma cells derived from the gastrointestinal tract (117). Caco-2 cells were chosen to determine the role of Zika at the proteomic level in relation to gastrointestinal associated

complications reported in infected patients. Both cell lines were chosen because earlier research indicated that they were extremely permissive to ZIKV infection, making them appropriate for our study (154,155).

4.1.i. Vero Cell Proteomic Changes Induced by ZIKV Infection

GO analyses using the PANTHER classification system (PANTHER13.1) and IPA analysis of dysregulated Vero cell proteins after ZIKV infection identified the Janus kinase (JAK)-signal transducer and activator of transcription 3 (STAT3) signaling (JAK/STAT) pathway as one of the biological processes most affected by ZIKV infection by 24 and 48 hpi. The JAK/STAT pathway is one of three major pathways in the innate immune system which is the first line of defense during viral infection. This pathway is activated after infection by other flaviviruses such as Dengue 2 and Japanese encephalitis virus (156,157). During ZIKV infection, pathogen recognition receptor (PRR) immune sensors detect pathogen-associated molecular patterns (PAMPs) which triggers secretion of interferons, proinflammatory cytokines, chemokines, and interferon stimulated genes (ISGs) (158). Both ZIKV single-stranded and double-stranded viral RNA are detected by the PRR toll like receptor 3 (TLR3) which triggers the innate immune response (59). STAT3 was significantly downregulated also by 24 to 48 h post ZIKV infection and was previously shown to be downregulated in C6/36 cells infected with ZIKV both at the protein and mRNA levels (150).

STAT3, when phosphorylated by JAK, translocate into the nucleus, and activates numerous genes involved in cell growth and apoptosis in response to cellular stimuli. The JAK-STAT pathway is activated when IFN α/β bind to their respective receptors (70). This induces the expression of ISGs which promote an antiviral state (159). Some viral proteins also induce activation of the JAK/STAT pathway. ZIKV nonstructural proteins 2B and 3B inhibit JAK-STAT signaling by promoting the degradation of Jak1 (160). Other Flavivirus proteins, such as dengue NS2A, NS4A, and NS4B also inhibit this pathway by reducing the phosphorylation and nuclear translocation of STAT1, the key component of the type 1 IFN signal transduction pathway (161). The lack of a functional interferon system in Vero cells indicates activation of the JAK/STAT pathway to be virus induced pattern. Activation of this pathway induced the expression of ISG15, a cellular protein that inhibits viral replication and regulates host immune response during viral infection (162). ISG15 and STAT1 have been found by many investigators, including other

proteomic findings by our research group, to be significantly up-regulated by many viruses, including influenza virus and reovirus (163,164). While ISG15 was upregulated 1.41-fold in Vero cells by 48 hpi after ZIKV infection, and STAT1 was down-regulated to 0.91-fold compared to mock, these dysregulations were not significant according to p-value or Z-score. By contrast, ISG15 and STAT1 were significantly up-regulated by both influenza virus (to 5.1-fold and 3.9-fold, respectively) and by reovirus strain type 3 Dearing (to 6.7-fold and 3.7-fold, respectively) (165,166). STAT1 plays an important role in the interferon signaling cascade (167). The mild dysregulation of both ISG15 and STAT1, which did not reach significant levels, of these two key innate immunity molecules in ZIKV-infected Vero cells could indicate fundamental differences in how ZIKV induces protein alterations compared to other viruses known to significantly alter these proteins (165,166). Additional study of ZIKV-induced protein alterations in additional cell types are warranted to provide more information about virus–host interactions of this important reemerging pathogen.

ISG15 is an interferon stimulated gene that is highly expressed during viral replication and has been reported to be involved in the Ubiquitin Proteasome System (UPS). The UPS system involves tagging of proteins for enzymatic degradation. Some flaviviruses like Dengue-2 and Japanese encephalitis, as well as ZIKV, have been reported to adapt the UPS in their replicative cycles (150,168,169). ISG15 also colocalizes with histone deacetylase 6 (HDAC6) and p62 in autophagic degradation of ubiquitinated cellular components (170). HDAC6 is an enzyme encoded by the HDAC6 gene and is involved in transcriptional regulation, cell cycle progression, and developmental events (171). P62, also known as sequestosome 1 (SQSTM1), binds to the autophagosome to help traffic it into the lysosome for degradation. MG132, a ubiquitin proteasome inhibitor, enhances colocalization of ISG15, HDAC6 and p62, leading to autophagy (170). ISG15 has been found to modulate the autophagy pathway, which regulates a range of processes including protein degradation, antigen presentation, cytokine signaling, and cell death, according to recent research (172). ISG15 was reported by Xu et al., 2015, to conjugate to Beclin-1, a key activator of the autophagic pathway, inhibiting autophagy activation (173).

Complement system activation has been shown to have a variety of antiviral effects, including direct neutralization of both enveloped and non-enveloped viruses as well as inducing other immune responses (174). As a result, several viruses have evolved distinct mechanisms for

dysregulating the complement system, hence increasing their infectivity (174). With regards to flaviviruses such as Dengue, West Nile, and Yellow Fever complements have been reported to inhibit viral replication level as well as induce inflammatory responses which lead to increases in the severity of disease (175,176). IPA predicted the activation of the complement cascade in our study by 24 hpi. During infection, viral NS1, one of the nonstructural proteins produced after cleavage of the viral polyprotein by host and viral proteases, aids viral pathogenesis by interaction with complement proteins and regulators involved in the complement cascade (175). Complement 4, which plays a role in the alternate and the classical complement pathways, is cleaved by C4-NSI into two subunits, C4a (an anaphylatoxin) and C4b (opsonin) which aid in elimination of viral particles (177). This reduces circulating C4 during an infection. In Vero cells, downregulation of both subunits was detected at 24 and 48 hpi, which might be due to reduced circulating C4 due to increased expression of NS1. However, its expression level declined by more than fourfold from 24 to 48 hpi, which is a result of increased NS1 at 48 h compared to 24 h after ZIKV infection. Complement factor 1, also known as C3b/C4b inactivator, regulates the complement pathway by cleaving C3b and C4b (178). It was upregulated at 24 hpi, which might explain downregulation of C4b at this time point. Downregulation of C4b might be a result of inactivation of complement factor 1; however, further studies need to be done to confirm this finding. Activation of complements induced the secretion of cytokine C-C motif chemokine ligand 5 (CCL5) and C-X-C motif chemokine ligand 11 (CXCL11), which were similarly dysregulated at 24 and 48 hpi. These two chemokines are involved in the NF- κ B pathway (179). The NF- κ B pathway forms part of the innate immunity system and is activated in response to viral infection. The increased expression level of these two chemokines correlates with the increased NS1 expression from 24 to 48 h after ZIKV infection, similar to during DENV infection (179).

IPA analyses of the significantly dysregulated proteins also identified protein synthesis amongst the top diseases and functions induced after ZIKV infection. This finding correlates with the significant up-regulation of eukaryotic translation initiation factor 5A (EIF5A) at 48 hpi in the Vero cells. EIF5A also was upregulated in C6/36 cells infected by Dengue-2, which indicates a potential marker which needs to be validated to determine its efficacy/potential value in development of future interventions (180). We also found EIF4G2, another eukaryotic translation initiation factor, was significantly downregulated by 24 and 48 hpi, and EIF4G2 was similarly downregulated in West Nile virus-infected human glioblastoma (A172) cells at 24 hpi (181).

Predicted activation and inhibition of signaling pathways included IGF signaling, PI3K/Akt signaling, ERK/MAPK signaling, and Tec kinase signaling (Figure 10). Some of these signaling pathways have been previously implicated in ZIKV infection (119,126,127). Scaturro and colleagues used an integrated proteomic approach that identified 386 host proteins that interact with ZIKV proteins and mapped more than 1200 ZIKV-induced phosphoprotein alterations. The PI3K/Akt signaling, ERK/MAPK signaling and ATM-ATR signaling pathways were found to be dramatically modulated (127). Tec kinases are the second largest family of non-receptor tyrosine kinases. They are involved in activation and development of B and T cells (182). The Tec kinase pathway is linked to numerous downstream cellular events, including Ca²⁺ influx, proliferation, differentiation, apoptosis, gene expression, actin reorganization, and adhesion or migration (183). This signaling pathway also is involved in several processes, such as apoptosis of neuroglia and oligodendrocytes, and activation of neuronal and motor neuron cell death, that have been reported in ZIKV pathology (184). One member of the Tec kinase family is Bruton's tyrosine kinase (BTK) which plays an important role in TLR3 signaling. It mediates antiviral responses during ZIKV infection by detection of double-stranded RNA (185). BTK-deficient macrophages were unable to clear intracellular dengue virus infection due to inactivated TLR3 signaling (185), suggesting its essential role as a gate keeper for viral clearance / inactivation (or another way of expression). Activation of TLR3 signaling during ZIKV has already been reported to lead to innate immune response (59). Thus, activation of Tec kinase during ZIKV infection could be caused by increased viral double-stranded RNA which results in activation of TLR3 signaling. However, a transcriptomic analysis of ZIKV-infected monocytes, and of monocyte-derived macrophages, identified inhibition of this pathway, indicating that additional studies are warranted to establish the link (s), if any, between BTK and other kinases within the Tec family that might be involved in ZIKV pathology (186).

Measuring proteins rather than its corresponding mRNA transcripts as was done by Lee et al., 2012 has an advantage because all proteins measured corresponds to the levels of mRNA measured however not all mRNA are translated to their corresponding proteins as they can be enzymatically degraded by miRNAs, the genetic code misread during ribosomal translation resulting in a different amino acid hence protein among other factors. Thus, use of identification of host proteins for future diagnostic purpose against ZIKV infection as well to gain for information about the virus was considered ideal based on the inherent variation between mRNA

and proteins (187–189).

A limitation pointed out by a reviewer during submission is the use of Vero cells due to their lack of a functional interferon response system indicated the proteomic findings reported will not accurately recapitulate a normal *in vivo* infection (190). However, Vero cells though not human originated have been successfully used to generate vaccines for some infectious diseases and proteomic data generated were similarly confirmed in human originated cell line (191–193). Thus, it will be important to perform similar assays in more relevant human cells to compare ZIKV-mediated host protein dysregulation hence similar studies were done on Caco-2 cells.

4.1. ii. ZIKV disrupts proteins involved in the neurosensory system in Vero cells.

Although several groups have used proteomic approaches to elucidate ZIKV-triggered host protein responses, such studies were performed on different types of stem cells, non-neuronal and neuronal progenitors, lineages, and cell lines (194,195). These have been extremely informative in identifying signaling pathways, cellular processes controlled by ZIKV-affected host proteins, post-translational modifications, and protein–protein interactions (195–199). Most of these examined single time points post-infection. The lack of longitudinal data sets that provide profiles of time-specific protein dysregulation hampers our ability to differentiate ZIKV-induced persistent versus transient protein dysregulations (127,200–202). Temporal protein expression monitoring data are critically important in predicting the potential impact specific protein changes within a dynamically changing proteome may have on certain signaling pathways and resulting bio-functions in infected cells. In addition, temporal proteomic patterns aid in the identification of key initiator proteins, protein modifications and proteomic networks that ZIKV uses to establish and maintain a successful infection cycle and, thus, contributes information relevant for clinical intervention. We recently used an aptamer-based targeted proteomic tool, SOMAScan, to examine the expression of >1,300 proteins across three separate time points in ZIKV-infected Vero and human U251 glioma cells. Similar to the current study, we identified a dynamic shift in proteomic changes from transient to persistent protein dysregulations, as ZIKV infection progressed over time (127,128). Here, we complemented our previous targeted studies by measuring about five times as many proteins in an unbiased manner, and, because recent clinical reports suggest a potential link between congenital ZIKV infection and neurosensory abnormalities in children that had suffered in utero ZIKV infection. We also focused our analysis on proteins which showed

significant dysregulation and found to be linked to the development of the neurosensory system.

Although most differentially expressed proteins at the early 12 hpi time point appeared to reflect acute responses to ZIKV infection and had returned to baseline at 48 hpi, it was very intriguing to identify that almost one-third of the proteins identified at later times are linked to modulating neurosensory system functions and development. For example, E3 ubiquitin-protein ligase ZNRF2 is a zinc-finger protein that plays a role in protein polyubiquitination (203). In addition to its possible ubiquitin ligase activity to preserve neurotransmission and neuroplasticity, ZNRF2 is highly expressed during murine neuronal development (204). Some studies have reported ZIKV-mediated dysregulation of other E3 ubiquitin-protein ligases (205), but this is the first study implicating increases (>2-fold) in the amount of ZNRF2 in the early ZIKV-induced protein response at 12 hpi. Numerous other previously unreported zinc-finger proteins also were exclusively increased by ZIKV infection at the early time point, including ZNF830, ZSWIM8, ZPR1; a full list is shown in Figure 11B. ZPR1 may play roles in the development of the sensory nervous system and in embryonic growth. For example, Gangwani and colleagues used *Zpr1*^{-/-} murine blastocysts and showed that ZPR1 deficiency resulted in restricted proliferation of inner cell mass and abnormal trophectoderm formation, and lack of nuclear compartments like germ and Cajal bodies (206), this suggests the possible involvement of ZPR1 in placental development and dysfunction which impact in fetal development. Absence of these sub-nuclear bodies leads to the mis localization of survival motor neuron 1 (SMN1), a protein that interacts with ZPR1. SMN1 deficiency or dysfunction in motor neuron-like cells is associated with loss of growth cones, structural defects in axons that impair pathfinding and innervating abilities of these neurons lacking SMN1 from a mice model of SMA also demonstrated that overexpression of ZPR1 in these neurons corrects the abnormal axonal growth (207). It is tempting to speculate that increases in ZPR1 protein during early stages of ZIKV infection reflects a protective host response, but this requires further studies. Unlike the 12 hpi significantly differentially expressed proteins, all of which were found increased by ZIKV infection, there were significantly higher and lower ZIKV-induced protein levels at 24 hpi.

mRNA of some of these proteins had been identified in previous transcriptomic analyses, but most had not previously been demonstrated at the proteomic level. Several of these proteins play key roles in neurosensory development. COMT (Catechol O-methyltransferase), a kinase

reduced more than 1.5-fold at 24 hpi, is involved in neurosensory responses like nociception, balance, hearing, and catecholamine metabolism (208,209). Du and co-workers documented several severe malformations in a COMT missense murine model, including abnormal auditory startle response, impaired movement behavior, and loss of inner and outer hair cells with degeneration of cochlear neurons and vestibular defects, collectively causing deafness and degeneration of the vestibular sensory/balancing system in mice by 8 weeks of age (210). Here we demonstrate ZIKV-mediated COMT reduction in Vero cells, providing first evidence for a potential molecular link between ZIKV infection and developmental impairment of cells within the auditory and vestibular sensory apparatus of the organ of Corti.

Furthermore, levels of ATP6V1B2, a non-catalytic subunit of the peripheral V1 complex of vacuolar ATPase, were increased by 24 hpi. This protein is involved in the fusion of flavivirus and endosomal membranes (211,212). ATP6V1B2 over-expression in Zebrafish embryos resulted in loss of sensory hair cells, suggesting the critical role of this molecule during early development of the auditory system in vertebrates (213). Moreover, whole-exome sequencing of human clinical samples identified an ATP6V1B2 mutation that contributes to disrupted lysosome acidification and sensorineural hearing loss (214,215). Similar outcomes were observed with some DNA and RNA viruses, but this is the first report with ZIKV.

Proteomic host responses to ZIKV infection also affected proteins linked to the retinal sensory system. Levels of the transporter and ATP-binding protein ABCF1 were significantly reduced by 24 hpi. ABCF1 is an essential early gene in development and homozygous deletion leads to the embryonic lethality of mice at day 3.5 post coitum (216). ABCF1 is involved in visual photo-transduction in the retina. Guo et al. discovered that ABCF1 is released from and binds to photoreceptor outer segments (POSs) to facilitate their phagocytosis by retinal pigment epithelial cells (RPEs) (217). Photoreceptors in the retinal POS convert light into electrical signals, and the resulting photo-oxidative stress requires RPEC-modulated phagocytosis as an essential mechanism for recycling dysfunctional POSs to facilitate retinal regeneration (218). Intriguingly, recent clinical evidence in children who had been exposed to ZIKV in utero demonstrated chorioretinal atrophy as one of several types of eye disorders observed in up to 7% of screened infants (219). No specific proteins or mechanisms have been proposed for ZIKV-associated retinal abnormalities. Our proteomic data implicate ABCF1 as a potential retinal target protein during

ZIKV infection. If ZIKV were to infect retinal cells early during development, this may trigger ABCF1 (and/or related proteins) dysregulation in host cells, which disturbs retinal homeostasis at a critical time during development and contributes to long-term retinal abnormalities.

Levels of PLAUR, a receptor for urokinase plasminogen activator, were significantly reduced at 24 hpi. PLAUR affects the migration, morphology, and quantity of neurons. Reduced levels of PLAUR increase the susceptibility of RPECs to anoikis and cause decreased cellular movement (216,220). Our observed ZIKV-induced decrease in PLAUR protein levels by 24 hpi raises the possibility that ZIKV can delay a developmental neural program that includes altered programmed cell death as shown in retinal cells, presumably resulting in the lack of metabolic support for photoreceptor cells, abnormal photoreceptor excitability, and retinal degeneration. Along the same lines, levels of ABLIM1, an actin-binding protein, were reduced by ZIKV infection by 24 hpi, despite its increase at later time points. Erkman and colleagues reported that ABLIM1 is required for proper pathfinding of retinal ganglion cells and axon guidance because a dominant-negative mutation of this gene causes axons of the optic nerve to form abnormal trajectories to the optic disc and show defective fasciculation and growth (217). Similarly, levels of the GTPase-activating protein ACAP2, which modulates neurite outgrowth (218), also were reduced by 24 hpi. Additional proteins included AAAS, ACSF3, and ADSSL1, which are known to be associated with neurodevelopmental abnormalities that present with intellectual disability and impaired learning and memory. Collectively, our results identify a ZIKV-induced complex protein signature associated with neural development and cognitive deficits that is supported by clinical *in vivo* data linking congenital ZIKV infection with cognitive deficits in neonates (219,220).

IPA predicted numerous elevated activity and inhibitory functions (Figure 12C). As indicated earlier, approximately one-third of the affected upstream molecules were transcription regulators, of which one-third are predicted to be activated and two-thirds are predicted to be inhibited by ZIKV. Many upstream regulators can be fit into an interconnecting network (Figure 12D) and most are predicted to interact with at least one other regulator molecule. The IPA “Grow” feature enabled us to link this interaction network to various bio-functions and diseases. In addition to activating apoptosis and inhibitory effects on transcription, transactivation, cell movement, and interphase, ZIKV infection was predicted to negatively impact upstream regulators associated with

embryonic development. This included vasculogenesis, epithelial-mesenchymal transition, T cell development, development of connective tissue, and limb development (Figure 12D, lower panel). To the best of our knowledge, the present proteomic study is the first to relate ZIKV-mediated temporal proteomic changes at a/the cellular level to mirror clinical manifestations of neurosensory impairments which were identified in children with congenital exposure to ZIKV infection. We cannot dismiss the value of further studies in such more prominent *ex vivo* and *in vivo* models to reflect spatio-temporal responses in cell type manner. We opted for proteomic profiling of temporal changes in protein expression in infected host cells as a promising way to discover early changes in protein networks and corresponding pathways that may initiate and promote downstream neurosensory defects. Monitoring the topology/landscape of temporal protein expression will also help determine cell-specific protein alterations in physiologically relevant developmental lineage-specific cell and tissue using animal models as they relate to neurosensory transduction. Additional *in vitro* and *in vivo* proteomic investigations in related models are warranted to better understand the impact ZIKV infection has on molecular mechanisms that initiate abnormalities in the development and function of the neurosensory system after ZIKV infection.

4.1.iii ZIKV Induces DNA Damage Response (DDR) and Alters the Proteome of Gastrointestinal Cells.

We have been examining proteomic alterations induced by ZIKV infection in various cell types, including monkey kidney Vero (60), human U-251 astrocytoma (119), and human Sertoli cell lines (126). Most protein dysregulation occurred at 48 hpi or later in these other cells. However, the pattern of protein dysregulation in ZIKV-infected gastrointestinal-derived human colorectal adenocarcinoma cells appears to be much more rapid, with most significantly dysregulated proteins being detected as early as 12 hpi. Another difference between these cell types is that ZIKV normally grows to a substantially higher titer in Caco-2 cells than in many other cells, as previously observed (154). It is presently unclear whether the differences in absolute virus titer produced and more rapid kinetics of host protein dysregulation, are related.

Bioinformatic analyses by IPA identified several ZIKV-induced pathways which are predicted to be activated or inhibited by 12 hpi. One of the pathways was DNA damage checkpoint regulation. The genome of a single cell is constantly destroyed by endogenous (genetic

abnormalities) and external agents (such as ultra-violet (UV) radiation, ionizing radiation (IR), as well as infection with a range of microorganisms) throughout its life (221,222). Cells use a global signaling network called the DDR to detect and repair DNA damage to ensure genomic stability (222). The ability to repair DNA damages quickly and accurately is critical for cellular survival and genomic integrity. DNA damage, if not repaired properly, can result in erroneous alterations in the genetic code, resulting in higher a mutational load and an increased risk of cancer (223). DNA damage checkpoints are regulatory mechanisms that exist at various stages of the cycle cell involved to inhibit the progression of the cell cycle against DNA damage. This inhibition activates signaling pathways that initiate DNA damage repair or programs the cells towards apoptosis in case the damage cannot be repaired. Some viruses, such as polyomaviruses and herpesviruses, exploit the DDR to enable them to complete their replicative cycles (224–228). The DDR is primarily mediated by members of the PI3K kinase family, which includes ataxia telangiectasia mutated (ATM), ATM and Rad3-related (ATR), and DNA-dependent protein kinase (DNA-PK), as well as members of the poly (ADP-ribose) polymerase (PARP) (222). Double-strand breaks (DSBs) activate ATM and DNA-PK, whereas ATR is triggered by single-stranded DNA (ssDNA) formed by DSBs or stalled replication forks. PARP1 is responsible for detecting and repairing single-strand breaks (SSBs) (229,230). The identification of the break by the DSB sensor complex, MRE11-RAD50-NBS1 (MRN), is an early event following the development of a DSB (222). At the site of the break, the MRN complex binds and activates ATM (231,232). Active ATM subsequently phosphorylates DDR downstream effector proteins including histone H2AX and cell cycle checkpoint proteins like p53 and CHK2, causing cell cycle arrest to repair the damaged DNA (233). IPA predicted Ataxia telangiectasia mutated (ATM) signaling to be activated after 12 hpi of ZIKV infection in Caco-2 cells. Hammack and colleagues reported that ZIKV infection activates the ATM/Chk2 signaling pathway in human neural progenitor cells and inhibits the progression of cells through the S phase, leading to an increase in viral replication (234).

Cyclin-dependent kinase (CDK) signaling, linked to DDR, was predicted to be inhibited by 12 hpi. During DDR, CDK5 phosphorylates ATM thereby inhibiting its kinase activity and regulating its response to double-stranded breaks that occur during the cell cycle (235,236). CDK5 signaling plays a significant role in neuronal function, namely the control of cytoskeletal architecture and dynamics, axonal guidance, neuronal migration, and cell adhesion, and participates in the pathological changes in neurodegenerative diseases (237). The CDK5 signaling

pathway was predicted to be inhibited in the presence of the activation of ATM after ZIKV infection. Inhibition of this pathway might indicate that ZIKV hijacks ATM signaling, as was reported in human neural progenitor cells to enhance its replication (234).

IPA also predicted several diseases and biofunctions that were altered by ZIKV infection. Among the diseases predicted after ZIKV infection was gastrointestinal diseases. ZIKV clinical symptoms are nonspecific; thus, ZIKV infection was often misdiagnosed in patients. ZIKV gastrointestinal involvement has not been investigated in detail yet, despite the fact patients experience gastrointestinal complications (238). Identification of host proteins that induce gastrointestinal complications during ZIKV infection will highlight other strategies the virus adapts at the proteomic level in addition to areas that have been mainly studied. The various predicted gastrointestinal diseases were colitis, enteritis, gastroenteritis, inflammation of the gastrointestinal tract, and abnormality of the large intestine. All these gastrointestinal complications are predicted to be induced by most of the same dysregulated host proteins, all of which were upregulated. These included proinflammatory cytokines and cathepsins, which have been reported to be expressed in response to viral infections (239–241). Some proteins that were linked to the various gastrointestinal conditions have also been reported to be involved in embryonic development. The Sonic Hedgehog (SHH) protein is critically essential for neural development (242). This protein is important for the development of the brain and spinal cord (central nervous system), eyes, limbs, and many other parts of the body (242). Lipid metabolism has been reported to be exploited by Flaviviruses during infection as an ATP source (154,243–245). Sphingosine kinase 1 (SphK1) is a lipid kinase that is involved in various cellular functions, including proliferation, survival, tumorigenesis, development, inflammation, and immunity (246–248). Some of these dysregulated host proteins have been reported in other studies that utilized proteomics to identify biomarkers for the management of inflammatory bowel diseases. Periostin (POSTN) is known to bind to integrins to support the adhesion and migration of epithelial cells. POSTN was significantly upregulated by ZIKV by 12 hpi as well, as reported by Chan et al., who performed a proteomic study and detected biomarkers during inflammatory bowel disease (249). These host proteins also may serve as potential targets for the development of therapeutic intervention against ZIKV and need future validation.

The primary focus of this research project has been to identify global changes within host

protein profile from Vero and Caco-2 cells responding to ZIKV infection, and then explore disease phenotype associated tissue and cell type specified regulatory proteins. These findings allowed me to identify promising protein candidates as summarized in Supplementary Table 2 (the comparative table). The captivating question came not only to validate protein fold changes for significance but also which of these proteins could be speculated as an effective drug target(s) to determine their role during the life cycle of the virus, to uncover molecular mechanisms of ZIKV biology. To achieve this, proteomic data generated from both cell lines were compared to identify proteins that were commonly and differentially dysregulated following ZIKV infection, and a comparison was made with several research groups. In addition, our proteomic data were also compared with our findings by Sher et al., 2019 of ZIKV infected human astrocytes because ZIKV was shown targeting neural progenitor cells which are the brain stems cells that differentiate into defined glial cells of the brain. The outcome of this analysis speculated relative evidence of ZIKV contribution at the proteomic level regarding its contribution in the induction of microcephaly (119). The cumulative results also prompted us to design futuristic human disease replica assays to identify several protein targets in response to viral infection using *in vivo* disease model system which will be discussed further in future directions.

A total of 38 significantly dysregulated host proteins were identified across all 3 cell lines with a fold change cut-off of ≥ 1.25 or ≤ 0.80 , with a p-value < 0.05 . Supplementary Table 2 in the Appendix section shows the comparative list of commonly and differentially dysregulated host proteins after ZIKV infection identified in Vero, Caco-2, and U251 cells. Across all 3-cell lines, eIF5A, MDK, and CXCL11 were commonly significantly dysregulated.

eIF5A is a multifunctional nucleocytoplasmic shuttle protein that is involved in a variety of biological activities such as cell proliferation, apoptosis regulation and has been linked to cancer and skeletal stem cell differentiation (250–253). Following the post-translational modification of eIF5A by deoxyhypusine synthase (DHS) and deoxyhypusine hydroxylase (DOHH), hypusinated eIF5A triggers the replication of diverse viruses, including RNA viruses such as EBOV and ZIKV, DNA viruses, such as herpes simplex virus 1 and vaccinia virus, and retroviruses, such as HIV, among others (254). Conditional knockout eIF5A mice were reported to exhibit gross defects in forebrain development, reduced growth, and premature death, validating the biological significance of this target potentially demonstrated in our data (255). Although it will be interesting

to clarify brain-specific loss of function to rescue the phenotype, it will be intriguing to know how the congenital ZIKV defects could be rescued with regards to eIF5A expression during viral infection. Most interestingly, the contribution of hijacked eIF5A and mediated function during ZIKV infection other than brain tissue and cell type may open a new window to pinpoint the cellular tribulations observed in various gastrointestinal complications following ZIKV infected patients.

Several viral infections trigger excessive expression of proinflammatory cytokines a phenomenon called a cytokine storm, which tends to exacerbate the disease condition in the process, however, the/a profile of markers is significantly associated with viral load (256). There is currently strong evidence showing that in severe COVID-19 conditions, an overactive immune system and a pro-inflammatory cytokine storm are reported in infected patients, which leads to acute respiratory distress syndrome and multi-organ failure (257). IL-6 receptor antagonists, α -1 adrenergic receptor inhibitors, and the glucocorticoid dexamethasone are among the treatments now being studied in clinical trials to help reduce this cytokine storm (257). In recent years, there have been highlighted reports of cytokine/chemokine signatures associated with the ZIKV such as CXCL10, CCL2, CCL5 among others, that were specifically identified in the acute phase of viral infection (256). Overexpression of these immune signatures, for instance CXCL10, have been associated with the induction of microcephaly and Guillain-Barre syndrome. In my proteomic study, CXCL11 a closely related chemokine of CXCL10 was commonly upregulated at 48hrs of ZIKV infection in all cell lines (Supplementary Table 2). Lima et al., 2019 also demonstrated that IFN- α , CXCL10, and CXCL9 levels were significantly higher in CSF samples obtained from ZIKV-induced microcephaly cases, compared to healthy control subjects (258). The respective cytokine storm may be a potential indicator and/or possible therapeutic target for managing ZIKV infected patients after further validations.

The third highlighted candidate, MDK, is known as neurite growth-promoting factor 2 (NEGF2) which is a neurotrophic factor involved in the structural and functional development of the brain (259). MDK also has cytokine properties as it was reported to inhibit HIV infection in cell cultures in an autocrine and paracrine manner by blocking the attachment of HIV particles to permissive cells (260). MDK was simultaneously downregulated in all cell lines after 48 hrs. of ZIKV infection when viral titers are produced, allowing us to speculate whether this protein may

have an antiviral impact during the ZIKV cycle as well as heightening its therapeutic potential for future validation studies. We have also noticed three promising candidate proteins namely, NCAM1, ISG15, and HMGN1 which several studies have provided compelling evidence suggesting being utilized by ZIKV during its replicative cycle. For instance, depletion of NCAM1 by sgRNA1 in U-251 MG cells has been reported to remarkably attenuate ZIKV infection (191). Overexpression of NCAM1 in HEK 293T cells was reported to increase viral binding and entry.

ISG15 (interferon-stimulated gene 15) is one of the inflammatory mediators and is essential for antiviral defense against ZIKV infection (261). Singh et al., 2019 demonstrated how ISG15 restricts ZIKV replication in human corneal epithelial cells. Further, ISG15 knockout mice exhibited vulnerability to ZIKV infection upon infection (261). We observed a drastic response with ISG15 levels raising the question to explore how ISG15 is modulated during ZIKV specific host response. The possibility of post-translational modification resulting from ZIKV infection and changes in the modulation of ISG15 by ISGylation during intra- and extra-cellular function should be investigated. There are cumulative data that shows that viruses manipulate the ubiquitination and ISGylation of ISG15 (262). Although ISGylation is shown to inhibit viruses like ZIKV, HIV, and influenza A, there is more to explore on the modulation of ISG15 at intracellular activity and secretion (263). We suggest that either ZIKV specific structural proteins may also contribute to conjugation of ISG15 and then regulate intracellular function and secretion of ISG15 or viral-specific proteins can be modified by conjugation enzymes to regulate ISG15 signaling, or viral-specific de-ISGylases (DIGs) may regulate the intracellular activity and secretion of ISG15 following ZIKV infection. It is important to note that several viruses manipulate the ubiquitination and ISGylation to escape from RIG-like receptors and high jacking posttranscriptional modification to suppress innate immune response for their replication cycle.

HMGN1 (High-mobility group nucleosome-binding protein) functions as a non-histone chromatin-binding protein in the cell nucleus and regulates chromosome architecture and gene transcription (264). This protein has also been shown to trigger endogenous inflammatory signals. HMGN1 functions not only as an endogenous TLR4 ligand, mediating directly immune tolerance, but also stimulates acute cytokine production (264). HMGN1 as well other isoforms were reported by Nagao et al., 2014 to promote astrocyte differentiation from neural progenitor cells during brain development (265). Across all the 3-cell lines, HMGN1 was differential and significantly

dysregulated after 48 hrs. of ZIKV infection where high viral titers are produced across all cell lines. HMGN1 astrocytic function, indicate this protein maybe potentially relevant in ZIKV disease pathology during brain development hence a promising protein target in the virus biology. Other proteins were differentially dysregulated indicating cell-specific response to ZIKV infection and Figure S4 in the Supplementary section shows the interaction between these proteins generated using String software. For instance, FER, SNX4, STAT3, C4A, C4B, TNFRSF21, RTN4R, PDPK1, L1CAM, and GRN were all commonly downregulated in both Vero cells and U251 cells but differentially dysregulated in Caco-2 cells. This differential protein still however provides information on the cell-dependent infectivity approach of ZIKV. Another reason could be the varied differential expression of certain proteins depending on the cell type.

4.2 Conclusion.

Host antiviral responses to ZIKV infection comprise several cellular pathways which have been cumulatively shown over the last decade. To understand how the protein-specific platform plays a role in monitoring the outcome of infection and protection, we can speculate that blocking or altering critical host factors could highlight as well as uncover other useful information of the ZIKV replicative cycle. Since host innate response is crucial for anti-viral activity, we aimed to identify viral-induced dynamic topological changes at a proteomic level during time course in specifically using aptamer-based SomaLogic technology and TMT M/S in a well-established *in vitro* cell-specific system. For instance, using both tools identified HIST1H1C, HMGN1, GRN, LGALS3BP, SPINT2, AK1 to be similarly dysregulated across all 3-time points. Among host proteins as well as pathways that were induced, activated as well as inhibited by ZIKV infection were cytokines, translation initiation factors, and activation of the complement cascade, JAK/STAT, and Tec kinase pathways. At the neurosensory level, ZIKV dysregulated host proteins (GJA1, CTSD, GRN, PLAUR, NCAM, CST3, among others) were identified to be involved in auditory development, development of the optic nerves' macular development, etc. Intriguingly, lipid metabolism was also predicted to be induced during neurosensory alternations as well as in the induction of gastrointestinal complication, suggesting probing further as several research groups provided very compelling evidence of Zika utilizing lipid metabolism during its replicative cycle (266). L1CAM, NCAM1, MDK, MICA, and ISG15 as well as CSTD, CTSH, and GRN which are related to brain development and immune response were also exploited with significant

changes mirroring an important proteomic link within the antiviral signaling.

While our understanding of ZIKV-host interactions has increased intensely using these two proteomic tools, to identify as well as predict the involvement of ZIKV at the proteomic level in neurosensory alterations as well as gastrointestinal involvement was novel which has indeed added into existing ZIKV proteomic literature. The identified targets should be further investigated to determine their role in the virus replicative cycle. The functional validation of these targets will lead to exposing more information of how the virus survives in its host and ultimately will be used to design novel antiviral agents and better vaccination strategies.

4.3 Future Direction.

Emerging viral infections are an undisputable health concern worldwide and are still the driving force threatening the health of individuals. Here, we explore a few future assays that can be used to demonstrate functional interactions among the identified protein targets:

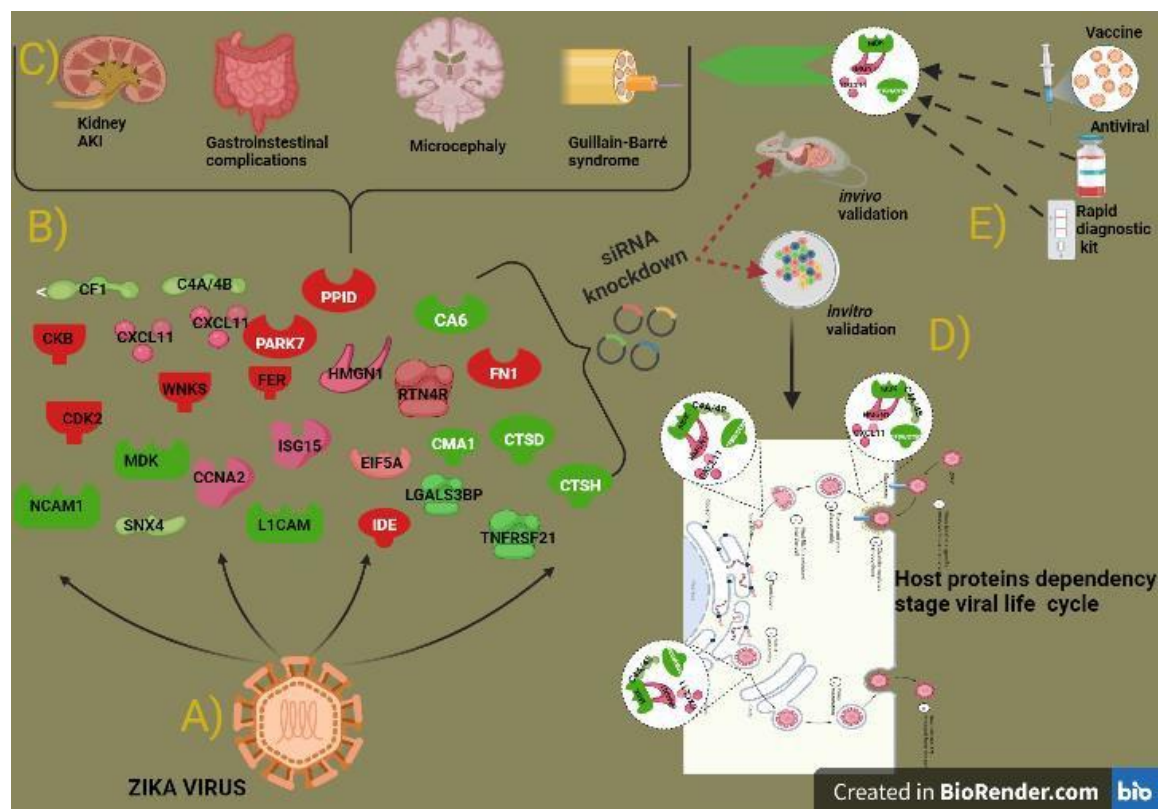
1) In order to address the third objective, and to gain better insights into the molecular mechanisms of Zika infection as well as confirm their use as biomarkers we will perform *in vitro* functional assays of proteins that are most profoundly associated with ZIKV . siRNA screening of candidates hosts proteins shown in Supplementary section Table S2 which existing literature indicates their brain related functions like eIF5A, NCAM1, MDK, SHH and HMGN1 will be validated to gain more understanding and if possible speculate their relevance in the induction of ZIKV induced microcephaly. Preliminary validation CLIC1, one of the dysregulated host proteins in Table S2 based on the availability of siRNAs and antibodies showed enhanced viral replication with the knockdown of this protein. Further validation of this promising proteomic candidate is still ongoing to gain more understanding of CLIC1's role during ZIKV replicative cycle.

2) Upregulated and downregulated candidates that were identified in the signaling pathway as versus activated or inhibited proteins will be validated first; utilizing known inhibitors of those pathways to establish its relevance with regards to virus replication; these are ISG15, CXCL11 and NCAM1, L1CAM, HMGN1, HDAC6, and PLAUR, ABLIM1 and others, second; validating expression profile of host proteins predicated by IPA to be in these pathways through Western blotting to confirm their correlated trend.

3) To address the functional significance of identified candidate host proteins in relation to the

complications reported in ZIKV infected patients, we will generate a loss of function assays to validate ZIKV-specific commonly dysregulated host protein using a knockdown/knockout approach and rescue assays. Once we validate the target candidates, we will assess top protein targets reported in neurosensory alternations and gastrointestinal disturbances in transgenic and/or knock-out mouse models.

Figure 19: Summary of future directions: A and B shows ZIKV, and the commonly dysregulated host protein displayed in Table S2 in the appendix section. C) reported disease complications reported in ZIKV infected we are speculating could be due to dysregulation of host proteins in B) during ZIKV infection. D) *Invitro* and *in vivo* validation of protein target and investigating stage of virus Lifecycle proteins are utilized. E) Future diagnostic usefulness of promising protein targets.



References

1. Pierson TC DM. Flaviviruses. 6th ed Lip. In Knipe DM HP (ed), editor. Philadelphia, PA.: Fields virology; 2013. p 747–794.
2. Faye O, Freire CCM, Iamarino A, Faye O, de Oliveira JVC, Diallo M, et al. Molecular Evolution of Zika Virus during Its Emergence in the 20th Century. PLoS Negl Trop Dis. 2014;8(1):36.
3. Glover KKM, Coombs KM. Zika virus infection: a review of available techniques toward early detection. J Mol Biochem. 2017;6(Victoria 2016):26–32.
4. Kindhauser MK, Allen T, Frank V, Santhana RS, Dye C. Zika: Origine et propagation d'un virus transmis par des moustiques. Bull World Health Organ. 2016;94(9):675-686C.
5. Dick G. Zika isolation and serological specificity. Trans R Soc Trop Med Hyg. 1952;46(5):509–20.
6. Olson JG, Ksiazek TG, Suhandiman G, Triwibowo V. Zika virus, a cause of fever in central Java, Indonesia. Trans R Soc Trop Med Hyg. 1981;75(3):389–93.
7. Moore DL, Causey OR, Carey DE, Reddy S, Cooke AR, Akinkugbe FM, et al. Arthropod-borne viral infections of man in Nigeria, 1964-1970. Ann Trop Med Parasitol. 1975;69(1):49–64.
8. Haddow AD, Schuh AJ, Yasuda CY, Kasper MR, Heang V, Huy R, et al. Genetic characterization of Zika virus strains: Geographic expansion of the Asian lineage. PLoS Negl Trop Dis. 2012;6(2).
9. Fagbami AH. Zika virus infections in Nigeria: virological and sero-epidemiological investigations in Oyo State. J Hyg (Lond). 1979;83:213–9.
10. Duffy MR, Chen T-H, Hancock WT, Powers AM, Kool JL, Lanciotti RS, et al. Zika Virus Outbreak on Yap Island, Federated States of Micronesia. N Engl J Med. 2009;360(24):2536–43.
11. Oehler E, Watrin L, Larre P, Leparc-Goffart I, Lastere S, Valour F, et al. Zika virus infection complicated by Guillain-Barre syndrome--case report, French Polynesia, December 2013. Euro

- Surveill [Internet]. 2014;19(9):79. Available from: <http://www.ncbi.nlm.nih.gov/pubmed/24626205>
12. Zanoluca C, De Melo VCA, Mosimann ALP, Dos Santos GIV, dos Santos CND, Luz K. First report of autochthonous transmission of Zika virus in Brazil. *Mem Inst Oswaldo Cruz*. 2015;110(4):569–72.
 13. Victora CG, Schuler-Faccini L, Matijasevich A, Ribeiro E, Pessoa A, Barros FC. Microcephaly in Brazil: How to interpret reported numbers? *Lancet*. 2016;387(10019):621–4.
 14. Heymann DL, Hodgson A, Sall AA, Freedman DO, Staples JE, Althabe F, et al. Zikavirus and microcephaly: Why is this situation a PHEIC? *Lancet* [Internet]. 2016;387(10020):719–21. Available from: [http://dx.doi.org/10.1016/S0140-6736\(16\)00320-2](http://dx.doi.org/10.1016/S0140-6736(16)00320-2)
 15. Mittal R, Nguyen D, Debs LH, Patel AP, Liu G, Jhaveri VM, et al. Zika virus: An emerging global health threat. *Front Cell Infect Microbiol*. 2017;7(486).
 16. Veronica Sikka, Vijay Kumar Chattu, Raaj K Popli, Sagar C Galwankar, Dhanashree Kelkar, Stanley G Sawicki, Stanislaw P Stawicki and TJP. The Emergence of Zika Virus as a Global Health Security Threat: A Review and a Consensus Statement of the INDUSEM Joint working Group (JWG). *J Glob Infect Dis*. 8(1):3–15.
 17. Vest KG. Zika Virus: A Basic Overview of an Emerging Arboviral Infection in the Western Hemisphere. *Disaster Med Public Heal Prep*. 2016;10(5):707–712.
 18. Wang A, Thurmond S, Islas L, Hui K, Hai R. Zika virus genome biology and molecular pathogenesis. *Emerg Microbes Infect* [Internet]. 2017;6(3). Available from: <http://dx.doi.org/10.1038/emi.2016.141>
 19. Siddiqui AH, Negi C, Singh S, Parveen S. Zika Virus: A Review. *Int J Life-Sciences SciRes*. 2017;3(6):1509–15.
 20. Kuno G, Chang GJJ. Full-length sequencing and genomic characterization of Bagaza, Kedougou, and Zika viruses. *Arch Virol*. 2007;152(4):687–96.

21. Chambers TJ, Hahn CS, Galler R, Rice CM. Flavivirus genome organization, expression, and replication. *Annu Rev Microbiol.* 1990;44:649–88.
22. Tan TY, Fibriansah G, Kostyuchenko VA, Ng TS, Lim XX, Zhang S, et al. Capsid protein structure in Zika virus reveals the flavivirus assembly process. *Nat Commun* [Internet]. 2020;11(1):1–13. Available from: <http://dx.doi.org/10.1038/s41467-020-14647-9>
23. Lin HH, Huang LM, Wu SC. Zika virus molecular biology and perspectives for vaccine development: A review. *J Nurs Res.* 2017;25(1):3–6.
24. Didier Musso et. al. City of New Orleans Zika Virus Plan. *Nature.* 2016;11(1):10–20.
25. Li T, Zhao Q, Yang X, Chen C, Yang K, Wu C, et al. Structural insight into the Zika virus capsid encapsulating the viral genome. *Cell Res.* 2018;28(4):497–9.
26. Oliveira ERA, Mohana-Borges R, de Alencastro RB, Horta BAC. The flavivirus capsid protein: Structure, function and perspectives towards drug design. *Virus Res* [Internet]. 2017;227:115–23. Available from: <http://dx.doi.org/10.1016/j.virusres.2016.10.005>
27. Yu IM, Zhang W, Holdaway HA, Li L, Kostyuchenko VA, Chipman PR, et al. Structure of the immature dengue virus at low pH primes proteolytic maturation. *Science* (80-). 2008;319(5871):1834–7.
28. Shang Z, Song H, Shi Y, Qi J, Gao GF. Crystal Structure of the Capsid Protein from Zika Virus. *J Mol Biol* [Internet]. 2018;430(7):948–62. Available from: <https://doi.org/10.1016/j.jmb.2018.02.006>
29. zika virus protein [Internet]. [cited 2021 Mar 6]. Available from: <https://www.sinobiological.com/research/virus/zika-virus-protein>
30. Mondotte JA, Lozach P-Y, Amara A, Gamarnik A V. Essential Role of Dengue Virus Envelope Protein N Glycosylation at Asparagine-67 during Viral Propagation. *J Virol.* 2007;81(13):7136–48.
31. Sirohi D, Chen Z, Sun L, Klose T, Pierson TC, Rossmann MG, et al. The 3.8Å cryo-EM structure of Zika Virus. *Science* (80-) [Internet]. 2016;1848(6284):3047–54. Available from:

<http://www.ncbi.nlm.nih.gov/pubmed/27033547>0A<http://www.pubmedcentral.nih.gov/articlerender.fcgi?artid=PMC4845755>

32. Fontes-Garfias CR, Shan C, Luo H, Muruato AE, Medeiros DBA, Mays E, et al. Functional Analysis of Glycosylation of Zika Virus Envelope Protein. *Cell Rep* [Internet]. 2017;21(5):1180–90. Available from: <https://doi.org/10.1016/j.celrep.2017.10.016>
33. Carbaugh DL, Baric RS, Lazear HM. Envelope Protein Glycosylation Mediates ZikaVirus Pathogenesis. *J Virol*. 2019;93(12):1–16.
34. Akhras S, Herrlein ML, Elgner F, Holzhauser T, Hildt E. Zikv envelope domain-specific antibodies: Production, purification and characterization. *Viruses*. 2019;11(8):748.
35. Dai L, Song J, Lu X, Deng YQ, Musyoki AM, Cheng H, et al. Structures of the Zika Virus Envelope Protein and Its Complex with a Flavivirus Broadly Protective Antibody. *Cell Host Microbe* [Internet]. 2016;19(5):696–704. Available from: <http://dx.doi.org/10.1016/j.chom.2016.04.013>
36. Shi Y, Gao GF. Structural Biology of the Zika Virus. *Trends Biochem Sci* [Internet]. 2017;42(6):443–56. Available from: <http://dx.doi.org/10.1016/j.tibs.2017.02.009>
37. Lindenbach BD, Rice CM, Shi Y, Gao GF. Genetic Interaction of Flavivirus Nonstructural Proteins NS1 and NS4A as a Determinant of Replicase Function. *J Virol* [Internet]. 2017;42(6):443–56. Available from: <http://dx.doi.org/10.1016/j.tibs.2017.02.009>
38. Javed F, Manzoor KN, Ali M, Haq IU, Khan AA, Zaib A, et al. Zika virus: what we need to know? *J Basic Microbiol*. 2018;58(1):3–16.
39. Shiryaev SA, Chernov A V., Aleshin AE, Shiryaeva TN, Strongin AY. NS4A regulates the ATPase activity of the NS3 helicase: A novel cofactor role of the non-structural protein NS4A from West Nile virus. *J Gen Virol*. 2009;90(9):2081–5.
40. Wang B, Thurmond S, Hai R, Song J. Structure and function of Zika virus NS5 protein: perspectives for drug design. *Cell Mol Life Sci*. 2018;75(10):1723–36.

41. Wang B, Tan XF, Thurmond S, Zhang ZM, Lin A, Hai R, et al. The structure of Zika virus NS5 reveals a conserved domain conformation. *Nat Commun* [Internet]. 2017;8:1–6. Available from: <http://dx.doi.org/10.1038/ncomms14763>
42. Zhao B, Yi G, Du F, Chuang YC, Vaughan RC, Sankaran B, et al. Structure and function of the Zika virus full-length NS5 protein. *Nat Commun* [Internet]. 2017;8:1–9. Available from: <http://dx.doi.org/10.1038/ncomms14762>
43. Upadhyay AK, Cyr M, Longenecker K, Tripathi R, Sun C, Kempf DJ. Crystal structure of full-length Zika virus NS5 protein reveals a conformation similar to Japanese encephalitis virus NS5. *Acta Crystallogr Sect Struct Biol Commun*. 2017;73:116–22.
44. Best SM. The Many Faces of the Flavivirus NS5 Protein in Antagonism of Type II Interferon Signaling. *J Virol*. 2017;91(3):1–14.
45. Dick GW, Kitchen SF HA. Zika virus Isolations and serological specificity Isolations and serological specificity. *Trans R Soc Trop Med Hyg*. 1952;46(5):509–20.
46. Kraemer MUG, Sinka ME, Duda KA, Mylne A, Shearer FM, Brady OJ, et al. The global compendium of *Aedes aegypti* and *Ae. albopictus* occurrence. *Sci Data*. 2015;2:1–8.
47. Ledermann JP, Guillaumot L, Yug L, Saweyog SC, Tided M, Machieng P, et al. *Aedes hensilli* as a Potential Vector of Chikungunya and Zika Viruses. *PLoS Negl Trop Dis*. 2014;8(10).
48. Ioos S, Mallet HP, Leparç Goffart I, Gauthier V, Cardoso T, Herida M. Current Zika virus epidemiology and recent epidemics. *Med Mal Infect* [Internet]. 2014;44(7):302–7. Available from: <http://dx.doi.org/10.1016/j.medmal.2014.04.008>
49. Grard G, Caron M, Mombo IM, Nkoghe D, Mboui Ondo S, Jiolle D, et al. Zika Virus in Gabon (Central Africa) - 2007: A New Threat from *Aedes albopictus*? *PLoS Negl Trop Dis*. 2014;8(2):1–6.
50. Schuler-Faccini L, Ribeiro EM, Feitosa IML, Horovitz DDG, Cavalcanti DP, Pessoa A, et al. Possible Association Between Zika Virus Infection and Microcephaly — Brazil, 2015. *MMWR Morb Mortal Wkly Rep*. 2016;65(3):59–62.

51. Didier Musso, Claudine Roche, Emilie Robin, Tuxuan Nhan, Anita Teissier V-MC-L. Potential Sexual Transmission of Zika Virus. *Emerg Infect Dis.* 2015;21(2):359–61.
52. Kurscheidt FA, Mesquita CSS, Damke GMZF, Damke E, Carvalho ARB d. A, Suehiro TT, et al. Persistence and clinical relevance of Zika virus in the male genital tract. *Nat Rev Urol* [Internet]. 2019;16(4):211–30. Available from: <http://dx.doi.org/10.1038/s41585-019-0149-7>
53. Harrower J, Kiedrzyński T, Baker S, Upton A, Rahnama F, Sherwood J, et al. Sexual transmission of Zika Virus and persistence in Semen, New Zealand, 2016. *Emerg Infect Dis.* 2016;22(10):1855–7.
54. D’Ortenzio E, Matheron S, Yazdanpanah Y, de Lamballerie X, Hubert B, Piorkowski G, Maquart M, Descamps D, Damond F L-GI. Evidence of Sexual Transmission of Zika Virus. *N Engl J Med.* 2016;374(22):2195–8.
55. Arsuaga M, Bujalance SG, Díaz-Menéndez M, Vázquez A, Arribas JR. Probable sexual transmission of Zika virus from a vasectomised man. *Lancet Infect Dis* [Internet]. 2016;16(10):1107. Available from: [http://dx.doi.org/10.1016/S1473-3099\(16\)30320-6](http://dx.doi.org/10.1016/S1473-3099(16)30320-6)
56. Barzon L, Percivalle E, Pacenti M, Rovida F, Zavattoni M, Del Bravo P, et al. Virus and Antibody Dynamics in Travelers with Acute Zika Virus Infection. *Clin Infect Dis.* 2018;66(8):1173–80.
57. Besnard M, Lastère S, Teissier A, Cao-Lormeau VM, Musso D. Evidence of perinatal transmission of zika virus, French Polynesia, December 2013 and February 2014. *Eurosurveillance* [Internet]. 2014;19(13):20751. Available from: <http://dx.doi.org/10.2807/1560-7917.ES2014.19.13.20751>
58. Musso D, Nhan T, Robin E, Roche C, Bierlaire D, Zisou K, et al. Potential for Zika virus transmission through blood transfusion demonstrated during an outbreak in French Polynesia, November 2013 to February 2014. *Eurosurveillance* [Internet]. 2014;19(14):20761. Available from: <http://dx.doi.org/10.2807/1560-7917.ES2014.19.14.20761>
59. Hamel R, Dejarnac O, Wichit S, Ekchariyawat P, Neyret A, Luplertlop N, et al. Biology of Zika Virus Infection in Human Skin Cells. *J Virol.* 2015;89(17):8880–96.

60. Glover KKM, Gao A, Zahedi-Amiri A, Coombs KM. Vero Cell Proteomic Changes Induced by Zika Virus Infection. *Proteomics*. 2019;19(4).
61. Lozach PY, Burleigh L, Staropoli I, Navarro-Sanchez E, Harriague J, Virelizier JL, et al. Dendritic cell-specific intercellular adhesion molecule 3-grabbing non-integrin (DC-SIGN)-mediated enhancement of dengue virus infection is independent of DC-SIGN internalization signals. *J Biol Chem*. 2005;280(25):23698–708.
62. Krishnan MN, Sukumaran B, Pal U, Agaisse H, Murray JL, Hodge TW, et al. Rab 5 Is Required for the Cellular Entry of Dengue and West Nile Viruses. *J Virol*. 2007;81(9):4881–5.
63. Barba-Spaeth G, Longman RS, Albert ML, Rice CM. Live attenuated yellow fever 17D infects human DCs and allows for presentation of endogenous and recombinant T cell epitopes. *J Exp Med*. 2005;202(9):1179–84.
64. Tassaneetrithep B, Burgess TH, Granelli-Piperno A, Trumpfheller C, Finke J, Sun W, et al. DC-SIGN (CD209) mediates dengue virus infection of human dendritic cells. *J Exp Med*. 2003;197(7):823–9.
65. Foo S, Chen W, Chan Y, Bowman JW, Chang L, Choi Y, et al. induce M2-skewed immunosuppression during pregnancy. *Nat Microbiol*. 2018;2(11):1558–70.
66. Michlmayr D, Andrade P, Gonzalez K, Balmaseda A. study in Nicaragua. 2018;2(11):1462–70.
67. Lum FM, Lin C, Susova OY, Teo TH, Fong SW, Mak TM, et al. A sensitive method for detecting Zika virus antigen in patients' whole-blood specimens as an alternative diagnostic approach. *J Infect Dis*. 2017;216(2):182–90.
68. Lum FM, Low DKS, Fan Y, Tan JKL, Lee B, Chan JKY, et al. Zika virus infects human fetal brain microglia and induces inflammation. *Clin Infect Dis*. 2017;64(7):914–20.
69. B. D. Lindenbach, C. L. Murray, H.-J. Thiel CMR. *Fields Virology*. Lippincott Williams & Wilkins, editor. Philadelphia, PA.; 2013. 712–746 p.
70. Ye J, Zhu B, Fu ZF, Chen H, Cao S. Immune evasion strategies of flaviviruses. *Vaccine* [Internet]. 2013;31(3):461. Available from: <http://dx.doi.org/10.1016/j.vaccine.2012.11.015>.

71. Iranpour M, Moghadam AR, Yazdi M, Ande SR, Alizadeh J, Wiechec E, et al. Apoptosis, autophagy and unfolded protein response pathways in arbovirus replication and pathogenesis. *Expert Rev Mol Med*. 2016;18:1–21.
72. Sharma V, Sharma M, Dhull D, Sharma Y, Kaushik S, Kaushik S. Zika virus: An emerging challenge to public health worldwide. *Can J Microbiol*. 2020;66(2):87–98.
73. Anna R. Plourde EMB. A Literature Review of Zika Virus. *Emerg Infect Dis*. 2016;22(7):1185–92.
74. Dupont-Rouzeyrol M, O'Connor O, Calvez E, Daures M, John M, Grangeon J-P, et al. Co-infection with Zika and dengue viruses in 2 patients, New Caledonia, 2014. *Emerg Infect Dis*. 2015;21(2):381.
75. Musso D GD. Zika virus. *Clin Microbiol Rev*. 2016;29:487–524.
76. Lyle R. Petersen DJJ, Ann M. Powers and Margaret A. Honein. Zika Virus, Review Article. *N Engl J Med*. 2016;374(16).
77. Murray JS. Understanding Zika virus. *J Spec Pediatr Nurs*. 2017;22(1):1–9.
78. Alcendor DJ. Zika virus infection and implications for kidney disease. *J Mol Med*. 2018;96(11):1145–51.
79. Liu T, Tang L, Tang H, Pu J, Gong S, Fang D, et al. Zika virus infection induces acute kidney injury through activating NLRP3 inflammasome via suppressing Bcl-2. *Front Immunol*. 2019;10(1925):1–17.
80. Garcez PP, Loiola EC, Da Costa RM, Higa LM, Trindade P, Delvecchio R, et al. Zika virus: Zika virus impairs growth in human neurospheres and brain organoids. *Science*. 2016;352(6287):816–8.
81. Brasil P, Pereira JP, Moreira ME, Ribeiro Nogueira RM, Damasceno L, Wakimoto M, et al. Zika Virus Infection in Pregnant Women in Rio de Janeiro. *N Engl J Med*. 2016;375(24):2321–34.

82. Caroline Marrs, Gayle Olson, George Saade, Gary Hankins, Tony Wen, Janak Patel and SW. Zika Virus and Pregnancy: A Review of the Literature and Clinical Considerations. *Am J Perinatol*. 2016;33(7):625–639.
83. Delvecchio R, Higa L, Pezzuto P, Valadão A, Garcez P, Monteiro F, et al. Chloroquine, an Endocytosis Blocking Agent, Inhibits Zika Virus Infection in Different Cell Models. *Viruses* [Internet]. 2016;8(12):322. Available from: <http://www.mdpi.com/1999-4915/8/12/322>
84. Driggers RW, Ho C-Y, Korhonen EM, Kuivanen S, Jääskeläinen AJ, Smura T, et al. Zika Virus Infection with Prolonged Maternal Viremia and Fetal Brain Abnormalities. *N Engl J Med*. 2016;374(22):2142–51.
85. Zhang N, Zhang N, Qin CF, Liu X, Shi L, Xu Z. Zika Virus Disrupts Neural Progenitor Development and Leads to Microcephaly in Mice. *Cell Stem Cell* [Internet]. 2016;19(1):120–6. Available from: <http://dx.doi.org/10.1016/j.stem.2016.04.017>
86. Cugola FR, Fernandes IR, Russo FB, Freitas BC, Dias JLM, Guimarães KP, et al. The Brazilian Zika virus strain causes birth defects in experimental models. *Nature* [Internet]. 2016;534(7606):267–71. Available from: <http://dx.doi.org/10.1038/nature18296>.
87. Jonathan J. Miner, Bin Cao, Jennifer Govero, Amber M. Smith, Estefania Fernandez, Omar H. Cabrera, Charise Garber, Michelle Noll, Robyn S. Klein, Kevin K. Noguchi IUM and MSD. Zika virus infection during pregnancy in mice causes placental damage and fetal demise. *Cell*. 2016;165(5):1081–1091.
88. Leonhard SE, Mandarakas MR, Gondim FAA, Bateman K, Ferreira MLB, Cornblath DR, et al. Diagnosis and management of Guillain–Barré syndrome in ten steps. *Nat Rev Neurol* [Internet]. 2019;15(11):671–83. Available from: <http://dx.doi.org/10.1038/s41582-019-0250-9>
89. Cao-Lormeau VM, Blake A, Mons S, Lastère S, Roche C, Vanhomwegen J, et al. Guillain-Barré Syndrome outbreak associated with Zika virus infection in French Polynesia: A case-control study. *Lancet*. 2016;387(10027):1531–9.

90. Parra B, Lizarazo J, Jiménez-Arango JA, Zea-Vera AF, González-Manrique G, Vargas J, et al. Guillain–Barré Syndrome Associated with Zika Virus Infection in Colombia. *N Engl J Med*. 2016;375(16):1513–23.
91. Gorchakov R, Berry RM, Patel SM, El Sahly HM, Ronca SE, Murray KO. Optimizing PCR detection of Zika virus from various body fluids. *Am J Trop Med Hyg*. 2019;100(2):427–33.
92. Gourinat AC, O’Connor O, Calvez E, Goarant C, Dupont-Rouzeyrol M. Detection of Zika virus in urine. *Emerg Infect Dis*. 2015;21(1):84–6.
93. Lanciotti RS, Kosoy OL, Laven JJ, Velez JO, Lambert AJ, Johnson AJ, et al. Genetic and serologic properties of Zika virus associated with an epidemic, Yap State, Micronesia, 2007. *Emerg Infect Dis*. 2008;14(8):1232–9.
94. Hayes EB. Zika virus outside Africa. *Emerg Infect Dis*. 2009;15(9):1347–50.
95. de Araújo TVB, Ximenes RA de A, Miranda-Filho D de B, Souza WV, Montarroyos UR, de Melo APL, et al. Association between microcephaly, Zika virus infection, and other risk factors in Brazil: Final report of a case-control study. *Lancet Infect Dis*. 2018;18(3):328–36.
96. WHO. Countries and Territories with Current or Previous Zika Virus Transmission. [Internet]. 2019 [cited 2020 May 6]. Available from: <https://www.who.int/emergencies/diseases/zika/countries-with-zika-and-vectors-table.pdf>
97. Vetter P, Dayer JA, Schibler M, Allegranzi B, Brown D, Calmy A, et al. The 2014–2015 Ebola outbreak in West Africa: Hands On. *Antimicrob Resist Infect Control* [Internet]. 2016;5(1):1–17. Available from: <http://dx.doi.org/10.1186/s13756-016-0112-9>
98. Ollmann Saphire E. A Vaccine against Ebola Virus. *Cell* [Internet]. 2020;181(1):6. Available from: <http://dx.doi.org/10.1016/j.cell.2020.03.011>.
99. WHO. Region of the Americas/Pan American Health Organization. PLISA Health Information Platform for the Americas: Cases of Zika Virus Disease, by Country or Territory [Internet]. 2019. Available from: <http://www.paho.org/%0Adata/index.php/en/mnu-topics/zika/524-zika-weekly-en.htm>.

100. Mlacker S, Shafa G, Aldahan AS, Shah V., Samarkandy S, Nouri K. Origin of the Zikavirus revealed: a historical journey across the world. *Int J Dermatol*. 2016;55(12):1369– 72.
101. Barrows Nicholas J., Campos Rafael K., Powell Steven, Prasanth Reddisiva K., Schott- Lerner Geraldine, Soto-Acosta Ruben, Galarza-Muñoz Gaddiel, McGrath Erica L., Urrabaz-Garza Rheanna, Gao Junling, Wu Ping, Menon Ramkumar, Saade George, Fernandez-Salas Il BSS and G-BMA. A screen of FDA-approved drugs for inhibitors of Zika virus infection. *Cell Host Microbe* August 10; 2016;20(2):259–270.
102. Masmajan Sophie, Musso Didier, Vouga Manon, Pomar Leo DP, Stojanov Milos PA and DB. Review. Zika Virus. *Pathogens*. 2020;9(898).
103. Baz M, Boivin G. Antiviral agents in development for zika virus infections. *Pharmaceuticals*. 2019;12(3).
104. Castanha PMS, Marques ETA. A Glimmer of Hope: Recent Updates and Future Challenges in Zika Vaccine Development. *Viruses*. 2020;12(12):25–31.
105. Ramanathan K, Antognini D, Combes A, Paden M, Zakhary B, Ogino M, et al. Safety, tolerability, and immunogenicity of two Zika virus DNA vaccine candidates in healthy adults: randomised, open-label, phase 1 clinical trials. *Lancet*. 2018;391(January):552–62.
106. Rodriguez-Barraquer I, Costa F, Nascimento EJM, Júnior NN, Castanha PMS, Sacramento GA, et al. Impact of preexisting dengue immunity on Zika virus emergence in a dengue endemic region. *Science* (80). 2019;363(6427):607–10.
107. Katzelnick LC, Gresh L, Halloran ME, Mercado JC, Kuan G, Gordon A, et al. Antibody-dependent enhancement of severe dengue disease in humans. *Science* (80-). 2017;358(6365):929–32.
108. SomaLogic I. SOMAScan Proteomic Assay Technical White Paper. SomaLogic. 2015.
109. Gold L, Ayers D, Bertino J, Bock C, Bock A, Brody EN, et al. Aptamer-based multiplexed proteomic technology for biomarker discovery. *PLoS One*. 2010;5(12).

110. SomaLogic. (2020). Proteomics can help address the COVID-19 pandemic. Retrieved from <http://www.somallogic.com/COVID-19-response>. 2020.
111. Technical White Paper SOMAScan™ Proteomic Assay. 2013;1–24.
112. Jiang J, Opanubi KJ, Coombs KM. Non-biased enrichment does not improve quantitative proteomic delineation of reovirus T3D-infected HeLa cell protein alterations. *Front Microbiol.* 2012;3(310):1–16.
113. Yates JR, Ruse CI, Nakorchevsky A. Proteomics by mass spectrometry: Approaches, advances, and applications. *Annu Rev Biomed Eng.* 2009;11:49–79.
114. Chandor SB. Chapter 14 - Mass Spectrometry. *JAMA J Am Med Assoc.* 2006;295:2417–8.
115. TMT pro Label Reagents — higher multiplex quantitation for up to 16 samples TMT pro16plex Label Reagents.
116. Glover KKM, Zahedi-Amiri A, Lao Y, Spicer V, Klonisch T, Coombs KM. Zika Infection Disrupts Proteins Involved in the Neurosensory System. *Front Cell Dev Biol.* 2020;8(July).
117. Glover K, Coombs KM. ZIKV infection induces DNA damage response and alters the proteome of gastrointestinal cells. *Viruses.* 2020;12(7):771.
118. Sielaff M, Kuharev J, Bohn T, Hahlbrock J, Bopp T, Tenzer S, et al. Evaluation of FASP, SP3, and iST protocols for proteomic sample preparation in the low microgram range. *J Proteome Res.* 2017;16(11):4060–72.
119. Sher AA, Glover KKM, Coombs KM. Zika virus infection disrupts astrocytic proteins involved in synapse control and axon guidance. *Front Microbiol.* 2019;10:596.
120. Honein MA, Dawson AL, Petersen EE, Jones AM, Lee EH, Yazdy MM, et al. Birth Defects Among Fetuses and Infants of US Women With Evidence of Possible Zika Virus Infection During Pregnancy. 2021;30333(1):59–68.
121. Scherer DC, Brockman JA, Chent Z, Maniatis TOM, Ballard DW. Signal-induced degradation of I kappa B alpha requires site-specific ubiquitination. *Proc Natl Acad Sci U S A.* 1995;92(24):11259–63.

122. Ziebuhr J, Snijder EJ, Gorbalenya AE. Virus-encoded proteinases and proteolytic processing in the Nidovirales. *J Gen Virol.* 2000;81(Pt 4):853–79.
123. Jiang X, Dong X, Li SH, Zhou YP, Rayner S, Xia HM, et al. Proteomic analysis of Zika virus infected primary human fetal neural progenitors suggests a role for doublecortin in the pathological consequences of infection in the cortex. *Front Microbiol.* 2018;9:1067.
124. Devhare P, Meyer K, Steele R, Ray RB, Ray R. Zika virus infection dysregulates human neural stem cell growth and inhibits differentiation into neuroprogenitor cells. *Cell Death Dis.* 2017;8(10):1–8.
125. Park T, Kang MG, Baek SH, Lee CH, Park D. Zika virus infection differentially affects genome-wide transcription in neuronal cells and myeloid dendritic cells. *PLoS One* [Internet]. 2020;15(4):1–14. Available from: <http://dx.doi.org/10.1371/journal.pone.0231049>.
126. Rashid MU, Zahedi-Amiri A, Glover KKM, Gao A, Nickol ME, Kindrachuk J, Wilkins JA CK. Zika virus dysregulates human Sertoli cell proteins involved in spermatogenesis with little effect on tight junctions. *PLoS Negl Trop Dis.* 2020;14(6):e0008335.
127. Scaturro P, Stukalov A, Haas DA, Cortese M, Draganova K, Płaszczyc A, et al. An orthogonal proteomic survey uncovers novel Zika virus host factors. *Nature* [Internet]. 2018;561(7722):253–7. Available from: <http://dx.doi.org/10.1038/s41586-018-0484-5>.
128. Scaturro P, Kastner AL, Pichlmair A. Chasing intracellular Zika virus using proteomics. *Viruses.* 2019;11(9):878
129. Nielsen-saines K, Angeles L, Janeiro R De, Kerin T, Angeles L, Vasconcelos Z, et al. Delayed childhood neurodevelopment and neurosensory alterations in the second year of life in a prospective cohort of ZIKV-exposed children. *Nat Med.* 2019;25(8):1213–7.
130. Cynthia A. Moore, MD, J. Erin Staples, William B. Dobyns A, Pessoa, Camila V. Ventura, Eduardo Borges da Fonseca E, Marques Ribeiro, Liana O. Ventura, Norberto Nogueira Neto J, Fernando Arena and SAR. Congenital Zika Syndrome: Characterizing the Pattern of Anomalies for Pediatric Healthcare Providers. *JAMA Pediatr.* 2017;171(3):288–295.

131. Elgueta R, Benson MJ, Vries VC De, Wasiuk A, Guo Y, Noelle RJ. Molecular mechanism and function of CD40/CD40L engagement in the immune system. *Immunol Rev.* 2009;229(1):152–72.
132. Cuadrado A, Nebreda AR. Mechanisms and functions of p38 MAPK signaling. *Biochem J.* 2010;429(3):403–17.
133. Wang J, Knaut H. Chemokine signaling in development and disease. *Development.* 2014;141(22):4199–205.
134. Dalod M, Chelbi R, Malissen B, Lawrence T. Dendritic cell maturation : functional specialization through signaling specificity and transcriptional programming. *EMBO J.* 2014;33(10):1104–16.
135. Hillmer EJ, Zhang H, Li HS WS. STAT3 signaling in immunity. *Cytokine Growth Factor Rev.* 2016;31(713):1–15.
136. Chen J, He W, Hu X, Shen Y, Cao J, Wei Z, et al. A role for ErbB signaling in the induction of reactive astrogliosis. *Cell Discov.* 2017;3:17044.
137. Liu W, Li J, Song Y, Li Y, Jia Y, Zhao H. Cdk5 links with DNA damage response and cancer. *Mol Cancer.* 2017;16(1):60.
138. Hammack C, Ogden SC, Madden JC, Medina A, Xu C, Phillips E, et al. Zika Virus Infection Induces DNA Damage Response in Human Neural Progenitors That Enhances Viral Replication. *J Virol.* 2019;93(20):1–20.
139. Weitzman MSC and MD. Viral manipulation of DNA repair and cell cycle checkpoints. *DNA Repair.* 2009;8(9):1166–1176.
140. Gaspar M, Shenk T. Human cytomegalovirus inhibits a DNA damage response by mislocalizing checkpoint proteins. *Proc Natl.* 2006;103(8):2821–6.
141. Shabab T, Khanabdali R, Moghadamtousi SZ, Kadir A, Mohan G, Shabab T, et al. Neuroinflammation pathways : a general review Neuroinflammation pathways : a general review. *Int J Neurosci.* 2017;127(7):624-633.

142. Mccorrister S, Hu P, Chong P, Silaghi A, Westmacott G, Coombs KM, et al. Highly Pathogenic H5N1 and Novel H7N9 Influenza A Viruses Induce More Profound Proteomic Host Responses than Seasonal and Pandemic H1N1 Strains. *J Proteome Res.* 2015;14(11):4511–23.
143. Ciccia A, Elledge SJ. Review The DNA Damage Response : Making It Safe to Play withKnives. *Mol Cell.* 2010;40(2):179–204.
144. Zhou BS, Elledge SJ. checkpoints in perspective. *Nature.* 2000;408:433–9.
145. Kastan MB, Bartek J. Cell-cycle checkpoints and cancer. *Nature.* 2004;432(7015):316–23.
146. Abraham RT. Cell cycle checkpoint signaling through the ATM and ATR kinases. *GenesDev.* 2001;15(17):2177–96.
147. Lindholm D, Pham DD, Cascone A, Eriksson O, Wennerberg K, Saarma M. c-Abl Inhibitors Enable Insights into the Pathophysiology and Neuroprotection in Parkinson ’ sDisease. *Front Aging Neurosci.* 2016;8:254.
148. World Health Organization (WHO). Global Vector Control Response 2017-2030[Internet]. ISBN: 978 92 4 151297 8; 2017 [cited 2021 Jun 5]. Available from: <https://www.who.int/vector-control/publications/global-control-response/en>
149. Jiang X, Dong X, Li SH, Zhou YP, Rayner S, Xia HM, et al. Proteomic analysis of Zika virus infected primary human fetal neural progenitors suggests a role for doublecortin in the pathological consequences of infection in the cortex. *Front Microbiol.* 2018;9:1–15
150. Xin Q-L, Deng C-L, Chen X WJ, Wang S-B, Wang W, Deng F, Zhang B XG, L-K. Z. Quantitative Proteomic Analysis of Mosquito C6/36 Cells Reveals Host Proteins Involvedin Zika Virus Infection. *J Virol.* 2017;91:e00554-17.
151. SomaLogic I. SOMAScan Proteomic Assay Technical White Paper. SomaLogic. 2015;1–14
152. No Title [Internet]. [cited 2021 Jul 12]. Available from: <https://gtexportal.org/home/multiGeneQueryPage>
153. http://pages.ingenuity.com/rs/ingenuity/images/IPA_data_sheet.pdf.

154. Chan JFW, Yip CCY, Tsang JOL, Tee KM, Cai JP, Chik KKH, et al. Differential cell line susceptibility to the emerging Zika virus: implications for disease pathogenesis, non- vector-borne human transmission and animal reservoirs. *Emerg Microbes Infect.* 2016;5(1):1–12.
155. Neural H, Cells P, Anfasa F, Siegers J, van der Kroeg M, Mumtaz N, et al. Phenotypic Differences between Asian and African Lineage Zika Viruses in. *mSphere.* 2017;2(4):1–10.
156. Souza-Neto JA, Sim S, Dimopoulos G. An evolutionary conserved function of the JAK- STAT pathway in anti-dengue defense. *Proc Natl Acad Sci U S A.* 2009;106(42):17841–6.
157. Lin CC, Chou CM, Hsu YL, Lien JC, Wang YM, Chen ST, et al. Characterization of two mosquito STATs, AaSTAT and CtSTAT: Differential regulation of tyrosine phosphorylation and DNA binding activity by lipopolysaccharide treatment and by Japanese encephalitis virus infection. *J Biol Chem.* 2004;279(5):3308–17.
158. Lester SN LK. Toll-like receptors in antiviral innate immunity. *J Mol Biol.* 2014;426(6):1246–64.
159. Takaoka A, Yanai H. Interferon signaling network in innate defense. *Cell Microbiol.* 2006;8(6):907–22
160. Wu Y, Liu Q, Zhou J, Xie W, Chen C, Wang Z, et al. Zika virus evades interferon- mediated antiviral response through the co-operation of multiple nonstructural proteins invitro. *Cell Discov [Internet].* 2017;3:1–14. Available from: <http://dx.doi.org/10.1038/celldisc.2017.6>
161. Muñoz-Jordán JL, Sánchez-Burgos GG, Laurent-Rolle M, García-Sastre A. Inhibition of interferon signaling by dengue virus. *Proc Natl Acad Sci U S A.* 2003;100(SUPPL. 2):14333–8.
162. Lenschow, D. J., Lai, C., Frias-Staheli, N., Giannakopoulos, N. V., Lutz, A., Wolff, T., Osiak, A., Levine, B., Schmidt, R. E., García-Sastre, A., Leib, D. A., Pekosz, A., Knobeloch, K. P., Horak, I., & Virgin, H. W. 4th. IFN-stimulated gene 15 functions as acritical antiviral molecule against influenza, herpes, and Sindbis viruses. *Proc Natl AcadSci U S A.* 2007;104(4):1371–1376.

163. Berard AR, Cortens JP, Krokhin O, Wilkins JA, Severini A, Coombs KM. Quantification of the Host Response Proteome after Mammalian Reovirus T1L Infection. *PLoS One*. 2012;7(12).
164. Coombs KM, Berard A, Xu W, Krokhin O, Meng X, Cortens JP, et al. Quantitative Proteomic Analyses of Influenza Virus-Infected. *J Virol*. 2010;84(20):10888–906.
165. Kroeker AL, Ezzati P, Halayko AJ, Coombs KM. Response of primary human airway epithelial cells to influenza infection: A quantitative proteomic study. *J Proteome Res*. 2012;11(8):4132–46.
166. Ezzati P, Komher K, Severini G, Coombs KM. Comparative proteomic analyses demonstrate enhanced interferon and STAT-1 activation in reovirus T3D-infected HeLa cells. *Front Cell Infect Microbiol*. 2015;5:30.
167. Kiu H NS. Biology and significance of the JAK/STAT signaling pathways. *Growth Factors*. Epub. 2012;30(2):88–106.
168. Byk LA, Iglesias NG, De Maio FA, Gebhard LG, Rossi M, Gamarnik A V. Dengue virus genome uncoating requires ubiquitination. *MBio*. 2016;7(3):e00804-16.
169. Zhang LK, Chai F, Li HY, Xiao G, Guo L. Identification of host proteins involved in Japanese encephalitis virus infection by quantitative proteomics analysis. *J Proteome Res*. 2013;12(6):2666–78
170. Nakashima H, Nguyen T, Goins WF, Chiocca EA. Interferon-stimulated gene 15 (ISG15) and ISG15-linked proteins can associate with members of the selective autophagic process, histone deacetylase 6 (HDAC6) and SQSTM1/p62. *J Biol Chem*. 2015;290(3):1485–95.
171. Zheng Y, Zhu G, Tang Y, Yan J, Han S, Yin J, et al. HDAC6, A Novel Cargo for Autophagic Clearance of Stress Granules, Mediates the Repression of the Type I Interferon Response During Coxsackievirus A16 Infection. *Front Microbiol*. 2020;11:78.
172. Perng YC, Lenschow DJ. ISG15 in antiviral immunity and beyond. *Nat Rev Microbiol* [Internet]. 2018;16(7):423–39. Available from: <http://dx.doi.org/10.1038/s41579-018-0020-5>

173. Xu D, Zhang T, Xiao J, Zhu K, Wei R, Wu Z, et al. Modification of BECN1 by ISG15 plays a crucial role in autophagy regulation by type I IFN/ interferon. *Autophagy*. 2015;11(4):617–28.
174. Mellors J, Tipton T, Longet S, Carroll M. Viral Evasion of the Complement System and Its Importance for Vaccines and Therapeutics. *Front Immunol*. 2020;11:1450.
175. Shresta S. Role of complement in dengue virus infection: Protection or pathogenesis? *MBio*. 2012;3(1):1–2.
176. Conde JN, Silva EM, Barbosa AS, Mohana-Borges R. The complement system in flavivirus infections. *Front Microbiol*. 2017;8:213.
177. Avirutnan P, Fuchs A, Hauhart RE, Somnuk P, Youn S, Diamond MS, et al. Antagonism of the complement component C4 by flavivirus nonstructural protein NS1. *J Exp Med*. 2010;207(4):793–806.
178. Nilsson SC, Sim RB, Lea SM, Fremeaux-Bacchi V, Blom AM. Complement factor I in health and disease. *Mol Immunol*. 2011;48(14):1611–20.
179. Fink J, Gu F, Ling L, Tolfvenstam T, Olfat F, Chin KC, et al. Host gene expression profiling of dengue virus infection in cell lines and patients. *PLoS Negl Trop Dis*. 2007;1(2).
180. Shih YT, Yang CF, Chen WJ. Upregulation of a novel eukaryotic translation initiation factor 5A (eIF5A) in dengue 2 virus-infected mosquito cells. *Virol J*. 2010;7:1–9.
181. Koh WL, Ng ML. Molecular mechanisms of West Nile virus pathogenesis in brain cells. *Emerg Infect Dis*. 2005;11(4):629–32.
182. Bunnell SC, Diehn M, Yaffe MB, Findell PR, Cantley LC, Berg LJ. Biochemical interactions integrating Itk with the T cell receptor- initiated signaling cascade. *J Biol Chem* [Internet]. 2000;275(3):2219–30. Available from: <http://dx.doi.org/10.1074/jbc.275.3.2219>
183. Chau CH, Chen KY, Deng HT, Kim KJ, Hosoya KI, Terasaki T, et al. Coordinating Etk/Bmx activation and VEGF upregulation to promote cell survival and proliferation. *Oncogene*. 2002;21(57):8817–29.

184. Souza BSF, Sampaio GLA, Pereira CS, Campos GS, Sardi SI, Freitas LAR, et al. Zikavirus infection induces mitosis abnormalities and apoptotic cell death of human neural progenitor cells. *Sci Rep*. 2016;6(December):1–13.
185. Lee KG, Xu S, Kang ZH, Huo J, Huang M, Liu D, et al. Bruton's tyrosine kinase phosphorylates Toll-like receptor 3 to initiate antiviral response. *Proc Natl Acad Sci U S A*. 2012;109(15):5791–6.
186. Lum F, Lee D, Chua T, Tan JLL, Lee CYP, Liu X, et al. Zika Virus Infection Preferentially Counterbalances Human. *mSphere*. 2018;3(2):1–18.
187. Shebl FM, Pinto LA, García-Piñeres A, Lempicki R, Williams M, Harro C, et al. Comparison of mRNA and protein measures of cytokines following vaccination with human papillomavirus-16 L1 virus-like particles. *Cancer Epidemiol Biomarkers Prev*. 2010;19(4):978–81.
188. Anderson L, Seilhamer J. A comparison of selected mRNA and protein abundances in human liver. *Electrophoresis*. 1997;18(3–4):533–7.
189. Gygi SP, Rochon Y, Franza BR, Aebersold R. Correlation between Protein and mRNA Abundance in Yeast. *Mol Cell Biol*. 1999;19(3):1720–30.
190. Emeny JM, Morgan MJ. Regulation of the interferon system: Evidence that Vero cells have a genetic defect in interferon production. *J Gen Virol*. 1979;43(1):247–52.
191. Srivastava M, Zhang Y, Chen J, Sirohi D, Miller A, Zhang Y, et al. Chemical proteomic tracks virus entry and uncovers NCAM1 as Zika virus receptor. *Nat Commun* [Internet]. 2020;11(1):1–10. Available from: <http://dx.doi.org/10.1038/s41467-020-17638-y>
192. Nicolson C, Major D, Wood JM, Robertson JS. Generation of influenza vaccine viruses on Vero cells by reverse genetics: An H5N1 candidate vaccine strain produced under a quality system. *Vaccine*. 2005;23(22):2943–52.
193. Barrett, P Noel; Terpening, Sara J; Snow, Doris; Cobb, Ronald R; Kistner O. Vero cell technology for rapid development of inactivated whole virus vaccines for emerging viral diseases. *Epub*. 2017;16(9):883–94.

194. Rosa-Fernandes L, Cugola FR, Russo FB, Kawahara R, de Melo Freire CC, Leite PEC, et al. Zika virus impairs neurogenesis and synaptogenesis pathways in human neural stem cells and neurons. *Front Cell Neurosci.* 2019;13:64.
195. Beys-da-Silva WO, Rosa RL, Santi L, Berger M, Park SK, Campos AR, Terraciano P, Varela APM, Teixeira TF, Roehe PM, Quincozes-Santos A, Yates JR 3rd, Souza DO, Cirne-Lima EO GJ. Zika Virus Infection of Human Mesenchymal Stem Cells Promotes Differential Expression of Proteins Linked to Several Neurological Diseases. *Mol Neurobiol.* 2019;56(7):4708–17.
196. Berard AR, Coombs KM, Severini A. Quantification of the host response proteome after herpes simplex virus type 1 infection. *J Proteome Res.* 2015;14(5):2121–42.
197. Hoxhaj G, Najafov A, Toth R, Campbell DG, Prescott AR MC. ZNRF2 is released from membranes by growth factors and, together with ZNRF1, regulates the Na⁺/K⁺ATPase. *J Cell Sci.* 2012;125(19):4662–75.
198. Simon PF, McCorrister S, Hu P, Chong P, Silaghi A, Westmacott G, Coombs KM KD. Highly Pathogenic H5N1 and Novel H7N9 Influenza A Viruses Induce More Profound Proteomic Host Responses than Seasonal and Pandemic H1N1 Strains. *J Proteome Res.* 2015;14(11):4511–23.
199. Zahedi-Amiri A, Sequiera GL, Dhingra S, Coombs KM. Influenza a virus-triggered autophagy decreases the pluripotency of human-induced pluripotent stem cells. *Cell Death Dis [Internet].* 2019;10(5):337. Available from: <http://dx.doi.org/10.1038/s41419-019-1567-4>
200. Araki T, Milbrandt J. ZNRF Proteins Constitute a Family of Presynaptic E3 Ubiquitin Ligases. *J Neurosci.* 2003;23(28):9385–94.
201. Gangwani L, Flavell RA, Davis RJ. ZPR1 Is Essential for Survival and Is Required for Localization of the Survival Motor Neurons (SMN) Protein to Cajal Bodies. *Mol Cell Biol.* 2005;25(7):2744–56.
202. Wen F, Armstrong N, Hou W, Cruz-Cosme R, Obwolo LA, Ishizuka K, et al. Zika virus increases mind bomb 1 levels, causing degradation of pericentriolar material 1 (PCM1) and dispersion of PCM1-containing granules from the centrosome. *J Biol Chem.* 2019;294(49):18742–55.

203. McWhorter ML, Monani UR, Burghes AHM, Beattie CE. Knockdown of the survival motor neuron (Smn) protein in zebrafish causes defects in motor axon outgrowth and pathfinding. *J Cell Biol.* 2003;162(5):919–31.
204. Rossoll W, Jablonka S, Andreassi C, Kröning AK, Karle K, Monani UR, et al. Smn, the spinal muscular atrophy-determining gene product, modulates axon growth and localization of β -actin mRNA in growth cones of motoneurons. *J Cell Biol.* 2003;163(4):801–12.
205. Ahmad S, Wang Y, Shaik GM, Burghes AH, Gangwani L. The zinc finger protein ZPR1 is a potential modifier of spinal muscular atrophy. *Hum Mol Genet.* 2012;21(12):2745–58.
206. Tunbridge EM, Harrison PJ, Weinberger DR. Catechol-o-Methyltransferase, Cognition, and Psychosis: Val158Met and Beyond. *Biol Psychiatry.* 2006;60(2):141–51.
207. Petrova E, Gracias S, Beauclair G, Tangy F, Jouvenet N. Uncovering flavivirus host dependency factors through a genome-wide gain-of-function screen. *Viruses.* 2019;11(1).
208. Fernandez-Garcia MD, Meertens L, Chazal M, Hafirassou ML, Dejarnac O, Zamborlini A, et al. Vaccine and wild-type strains of yellow fever virus engage distinct entry mechanisms and differentially stimulate antiviral immune responses. *MBio.* 2016;7(1):1–15.
209. Yongyi Yuan, Xue Gao, Feng Xin PD. Atp6v1b2 Plays Important Roles in the Early Development of Hearing, the Pectoral Fin, the Cardiovascular System, and the Swim Bladder of the Zebrafish, Supporting a Role for the Gene in Syndromic Hearing Loss. *bioRxiv.*
210. Menendez I, Carranza C, Herrera M, Marroquin N, Foster J, Cengiz FB, et al. Dominant deafness-onychodystrophy syndrome caused by an ATP6V1B2 mutation. *Clin Case Reports.* 2017;5(4):376–9.
211. Wilcox SM, Arora H, Munro L, Xin J, Fenninger F, Johnson LA, et al. The role of the innate immune response regulatory gene ABCF1 in mammalian embryogenesis and development. *PLoS One.* 2017;12(5):1–16.
212. Yuan Y, Zhang J, Chang Q, Zeng J, Xin F, Wang J, et al. De novo mutation in ATP6V1B2 impairs lysosome acidification and causes dominant deafness- onychodystrophy syndrome. *Cell Res.* 2014;24(11):1370–3.

213. Guo F, Ding Y, Caberoy N, Alvarado G, Wang F, Chen R, et al. ABCF1 extrinsically regulates retinal pigment epithelial cell phagocytosis. *Mol Biol Cell*. 2015;26(12):2311–20.
214. Alfano D, Iaccarino I, Stoppelli MP. Urokinase signaling through its receptor protects against anoikis by increasing BCL-xL expression levels. *J Biol Chem* [Internet]. 2006;281(26):17758–67. Available from: <http://dx.doi.org/10.1074/jbc.M601812200>
215. Kevany BM, Palczewski K. Phagocytosis of retinal rod and cone photoreceptors. *Physiology*. 2010;25(1):8–15.
216. Powell EM, Mars WM, Levitt P. Hepatocyte Growth Factor/Scatter Factor Is a Motogen for Interneurons Migrating from the Ventral to Dorsal Telencephalon and hippocampal interneurons (Anderson et al., 1997; Pleasure et al., 2000). Additionally, the analysis of chimeric, X-gal-expressing. *Neuron*. 2001;30:79–89.
217. Erkman L, Yates PA, McLaughlin T, McEvilly RJ, Whisenhunt T, O’Connell SM, et al. APOU domain transcription factor-dependent program regulates axon pathfinding in the vertebrate visual system. *Neuron*. 2000;28(3):779–92.
218. Etoh K, Fukuda M. Structure-function analyses of the small GTPase Rab35 and its effector protein centaurin- β 2/ACAP2 during neurite outgrowth of PC12 cells. *J Biol Chem*. 2015;290(14):9064–74.
219. Nielsen-Saines K, Brasil P, Kerin T, Vasconcelos Z, Gabaglia CR, Damasceno L, Pone M, Abreu de Carvalho LM, Pone SM, Zin AA, Tsui I, Salles TRS, da Cunha DC, Costa RP, Malacarne J, Reis AB, Hasue RH, Aizawa CYP, Genovesi FF, Einspieler C, Marschik PB, Per MM. Delayed childhood neurodevelopment and neurosensory alterations in the second year of life in a prospective cohort of ZIKV-exposed children. *Nat Med*. 2019;25(8):1213–7.
220. Ziqi Zhao, Ziwei Shang, Zilton Vasconcelos, Chunfeng Li YJ, Shulong Zu, Jingyi Zhang, Fengchao Wang, Li Yao JJJ, , Patricia Brasil M, Elisabeth Moreira, Cheng-Feng Qin, Tara Kerin, Karin Nielsen-Saines, Genhong Cheng XZ and ZX. Of Mice and Children: Zika Virus Infection Leads to Variable Defects in Multiple Neurological Functions and Behaviors. *SSRN Electr J* doi 102139/ssrn3335070. 2019.

221. Ghosal G CJ. DNA damage tolerance: a double-edged sword guarding the genome. *Transl Cancer Res.* 2013;2(3):107–29.
222. Ryan EL, Hollingworth R, Grand RJ. Activation of the DNA damage response by RNAviruses. *Biomolecules.* 2016;6(1):2–24.
223. Jackson SP, Bartek J. The DNA-damage response in human biology and disease. *Nature.* 2009;461(7267):1071–8.
224. Dahl J, You J, Benjamin TL. Induction and Utilization of an ATM Signaling Pathway by Polyomavirus. *J Virol.* 2005;79(20):13007–17.
225. Lilley CE, Carson CT, Muotri AR, Gage FH, Weitzman MD. DNA repair proteins affect the lifecycle of herpes simplex virus 1. *Proc Natl Acad Sci U S A.* 2005;102(16):5844–9.
226. Kudoh A, Fujita M, Zhang L, Shirata N, Daikoku T, Sugaya Y, et al. Epstein-Barr virus lytic replication elicits ATM checkpoint signal transduction while providing an S-phase-like cellular environment. *J Biol Chem* [Internet]. 2005;280(9):8156–63. Available from: <http://dx.doi.org/10.1074/jbc.M411405200>
227. Shirata N, Kudoh A, Daikoku T, Tatsumi Y, Fujita M, Kiyono T, et al. Activation of ataxia telangiectasia-mutated DNA damage checkpoint signal transduction elicited by herpes simplex virus infection. *J Biol Chem* [Internet]. 2005;280(34):30336–41. Available from: <http://dx.doi.org/10.1074/jbc.M500976200>
228. Zhao X, Madden-Fuentes RJ, Lou BX, Pipas JM, Gerhardt J, Rigell CJ, et al. Ataxia Telangiectasia-Mutated Damage-Signaling Kinase- and Proteasome-Dependent Destruction of Mre11-Rad50-Nbs1 Subunits in Simian Virus 40-Infected Primate Cells. *J Virol.* 2008;82(11):5316–28.
229. Yang J, Yu Y, Hamrick HE, Duerksen-Hughes PJ. ATM, ATR and DNA-PK: Initiators of the cellular genotoxic stress responses. *Carcinogenesis.* 2003;24(10):1571–80.
230. Ciccia A ES. The DNA damage response: making it safe to play with knives. *Mol Cell.* 2010;40(2):179-204.

231. Lee JH, Paull TT. ATM activation by DNA double-strand breaks through the Mre11-Rad50-Nbs1 complex. *Science* (80-). 2005;308(5721):551–4.
232. Falck J, Coates J, Jackson SP. Conserved modes of recruitment of ATM, ATR and DNA-PKcs to sites of DNA damage. *Nature*. 2005;434(7033):605–11.
233. Cimprich KA, Cortez D. ATR: an essential regulator of genome integrity.1. Cimprich KA, Cortez D: ATR: an essential regulator of genome integrity. *Nat Rev Mol Cell Biol* 2008, 9:616–27. *Nat Rev Mol Cell Biol* [Internet]. 2008;9(8):616-27.Available from:<http://www.ncbi.nlm.nih.gov/pubmed/18594563>%0A<http://www.pubmedcentral.nih.gov/articlerender.fcgi?artid=PMC2663384>
234. Hammack C, Ogden SC, Madden JC Jr, Medina A, Xu C, Phillips E, Son Y, Cone A, Giovinazzi S, Didier RA, Gilbert DM, Song H, Ming G, Wen Z, Brinton MA, Gunjan ATH. Zika Virus Infection Induces DNA Damage Response in Human Neural Progenitors That Enhances Viral Replication. *J Virol*. 2019;93(20):e00638-19.
235. Tian B, Yang Q, Mao Z. Phosphorylation of ATM by Cdk5 mediates DNA damage signaling and regulates neuronal death. *Nat Cell Biol*. 2009;11(2):211–8.
236. Huang E, Qu D, Zhang Y, Venderova K, Haque ME, Rousseaux MWC, et al. The role of Cdk5-mediated apurinic/apyrimidinic endonuclease 1 phosphorylation in neuronal death. *Nat Cell Biol*. 2010;12(6):563–71.
237. Dhavan R TL. A decade of CDK5. *Nat Rev Mol Cell Biol*. 2001;2(10):749-59.
238. Slavov S, Matsuno A, Yamamoto A, Otaguiri K, Cervi M, Covas D, et al. Zika virus infection in a pediatric patient with acute gastrointestinal involvement. *Pediatr Rep*. 2017;9(4):1–3.
239. Johnson EM, Doyle JD, Wetzel JD, McClung RP, Katunuma N, Chappell JD, et al. Genetic and Pharmacologic Alteration of Cathepsin Expression Influences Reovirus Pathogenesis. *J Virol*. 2009;83(19):9630–40.

240. Khaiboullina S, Uppal T, Kletenkov K, Jeor SCS, Garanina E, Rizvanov A, et al. Transcriptome profiling reveals pro-inflammatory cytokines and matrix metalloproteinase activation in Zika virus infected human umbilical vein endothelial cells. *Front Pharmacol*. 2019;10:642.
241. Kim H, Mazumdar B, Bose SK, Meyer K, Di Bisceglie AM, Hoft DF, et al. Hepatitis C Virus-Mediated Inhibition of Cathepsin S Increases Invariant-Chain Expression on Hepatocyte Surface. *J Virol*. 2012;86(18):9919–28.
242. Sims JR, Lee SW, Topalkara K, Qiu J, Xu J, Zhou Z, et al. Sonic hedgehog regulates ischemia/hypoxia-induced neural progenitor proliferation. *Stroke*. 2009;40(11):3618–26.
243. Heaton NS, Randall G. Dengue virus-induced autophagy regulates lipid metabolism. *Cell Host Microbe* [Internet]. 2010;8(5):422–32. Available from: <http://dx.doi.org/10.1016/j.chom.2010.10.006>
244. Singh R, Cuervo AM. Lipophagy: Connecting autophagy and lipid metabolism. *Int J Cell Biol*. 2012;2012.
245. Zhang J, Lan Y, Li MY, Lamers MM, Fusade-Boyer M, Klemm E, et al. Flaviviruses Exploit the Lipid Droplet Protein AUP1 to Trigger Lipophagy and Drive Virus Production. *Cell Host Microbe* [Internet]. 2018;23(6):819–831.e5. Available from: <https://doi.org/10.1016/j.chom.2018.05.005>
246. Yamane D, Zahoor MA, Mohamed YM, Azab W, Kato K, Tohya Y, et al. Inhibition of sphingosine kinase by bovine viral diarrhea virus NS3 is crucial for efficient viral replication and cytopathogenesis. *J Biol Chem*. 2009;284(20):13648–59.
247. Seo YJ, Pritzl CJ, Vijayan M, Bomb K, McClain ME, Alexander S, et al. Sphingosine Kinase 1 Serves as a Pro-Viral Factor by Regulating Viral RNA Synthesis and Nuclear Export of Viral Ribonucleoprotein Complex upon Influenza Virus Infection. *PLoS One*. 2013;8(8):1–13.
248. Vijayan M, Seo YJ, Pritzl CJ, Squires SA, Alexander S, Hahm B. Sphingosine kinase 1 regulates measles virus replication. *Virology* [Internet]. 2014;450–451:55–63. Available from: <http://dx.doi.org/10.1016/j.virol.2013.11.039>

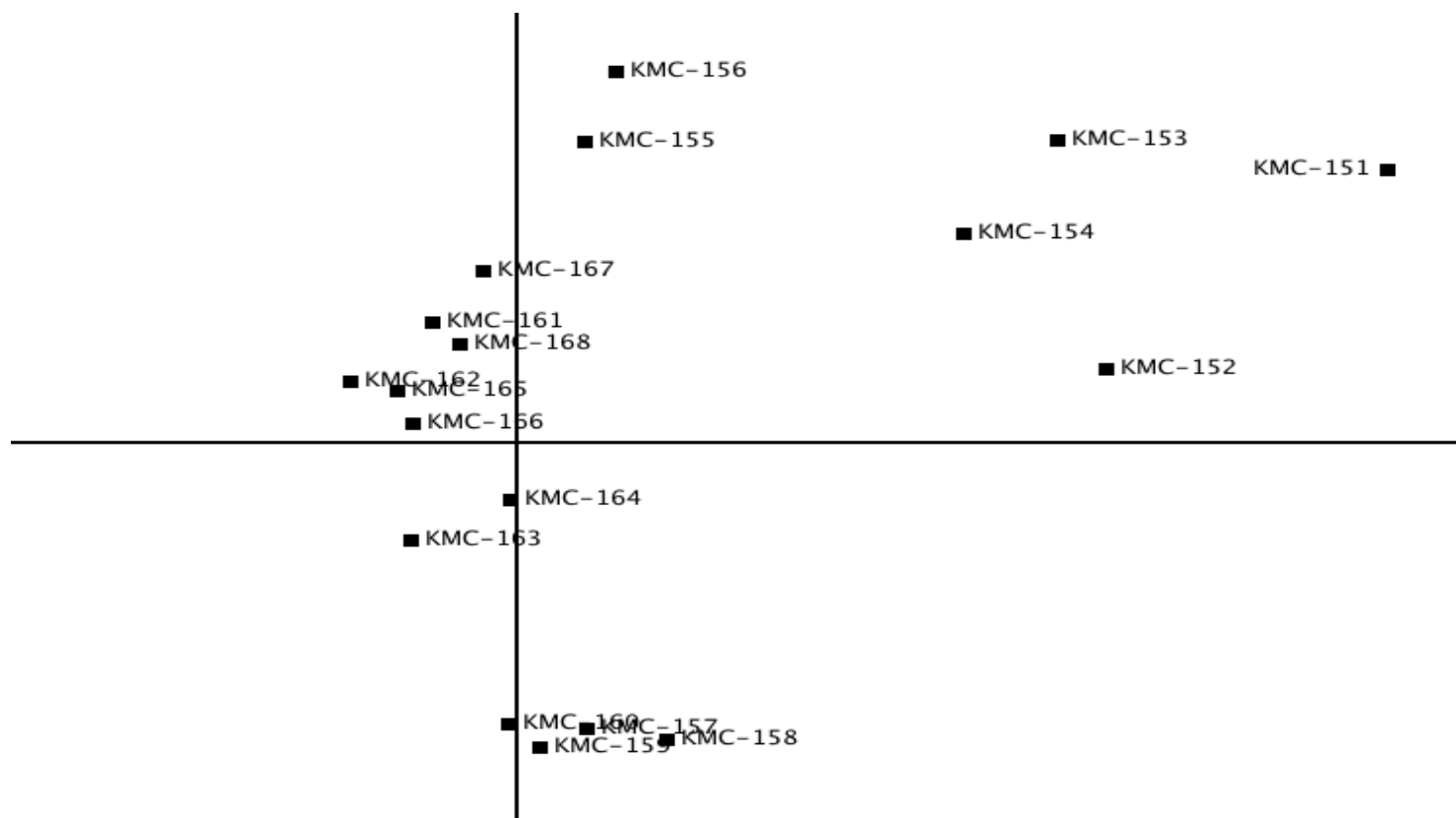
249. Chan PP. Current application of proteomics in biomarker discovery for inflammatory bowel disease. *World J Gastrointest Pathophysiol.* 2016;7(1):27.
250. Ding L, Gao LJ, Gu PQ, Guo SY, Cai YQ, Zhou XT. The role of eIF5A in epidermal growth factor-induced proliferation of corneal epithelial cell association with PI3-k/Akt activation. *Mol Vis.* 2011;17(January):16–22.
251. Taylor CA, Sun Z, Cliche DO, Ming H, Eshaque B, Jin S, et al. Eukaryotic translation initiation factor 5A induces apoptosis in colon cancer cells and associates with the nucleus in response to tumour necrosis factor α signalling. *Exp Cell Res.* 2007;313(3):437–49.
252. Tang DJ, Dong SS, Ma NF, Xie D, Chen L, Fu L, et al. Overexpression of eukaryotic initiation factor 5A2 enhances cell motility and promotes tumor metastasis in hepatocellular carcinoma. *Hepatology.* 2010;51(4):1255–63.
253. Luchessi AD, Cambiaghi TD, Hirabara SM, Lambertucci RH, Silveira LR, Baptista IL, et al. Involvement of eukaryotic translation initiation factor 5A (eIF5A) in skeletal muscle stem cell differentiation. *J Cell Physiol.* 2009;218(3):480–9.
254. Olsen ME, Cressey TN, Mühlberger E, Connor JH. Differential Mechanisms for the Involvement of Polyamines and Hypusinated eIF5A in Ebola Virus Gene Expression. *J Virol.* 2018;92(20):1–15.
255. Kar RK, Hanner AS, Starost MF, Springer D, Mastracci TL, Mirmira RG PM. Neuron specific ablation of eIF5A or deoxyhypusine synthase leads to impairment in development and cognitive functions in mice. *bioRxiv.* 2021.
256. Maucourant C, Queiroz GAN, Samri A, Grassi MFR, Yssel H, Vieillard V. Zika virus in the eye of the cytokine storm. *Eur Cytokine Netw.* 2019;30(3):74–81.
257. Gamage AM, Sen K, Chan WOY, Liu J, Tan CW, Ong YK, et al. Infection of human Nasal Epithelial Cells with SARS-CoV-2 and a 382-nt deletion isolate lacking ORF8 reveals similar viral kinetics and host transcriptional profiles. *PLoS Pathog* [Internet]. 2020;16(12):1–21. Available from: <http://dx.doi.org/10.1371/journal.ppat.1009130>
258. Lima MC, de Mendonça LR, Rezende AM, Carrera RM, Aníbal-Silva CE, Demers M, et al. The transcriptional and protein profile from human infected neuroprogenitor cells is strongly

- correlated to zika virus microcephaly cytokines phenotype evidencing a persistent inflammation in the CNS. *Front Immunol.* 2019;10:1928.
259. Ross-Munro E, Kwa F, Kreiner J, Khore M, Miller SL, Tolcos M, et al. Midkine: The Who, What, Where, and When of a Promising Neurotrophic Therapy for Perinatal Brain Injury. *Front Neurol.* 2020;11:568814.
 260. Hovanessian AG. Midkine, a cytokine that inhibits HIV infection by binding to the cell surface expressed nucleolin. *Cell Res.* 2006;16(2):174–81.
 261. Singh PK, Singh S, Farr D KA. Interferon-stimulated gene 15 (ISG15) restricts Zika virus replication in primary human corneal epithelial cells. *Ocul Surf.* 2019;17(3):551-559.
 262. Chiang C, Liu G, Gack MU. Viral evasion of rig-i-like receptor-mediated immunity through dysregulation of ubiquitination and isgylation. *Viruses.* 2021;13(2).
 263. Swaim CD, Canadeo LA, Monte KJ, Khanna S, Lenschow DJ, Huibregtse JM. Modulation of Extracellular ISG15 Signaling by Pathogens and Viral Effector Proteins. *Cell Rep [Internet].* 2020;31(11):107772. Available from: <https://doi.org/10.1016/j.celrep.2020.107772>
 264. Arts RJW, Huang PK, Yang D, Joosten LAB, van der Meer JWM, Oppenheim JJ, et al. High-mobility group nucleosome-binding protein 1 as endogenous ligand induces innate immune tolerance in a TLR4-Sirtuin-1 dependent manner in human blood peripheral mononuclear cells. *Front Immunol.* 2018;9:526.
 265. Functions M. T ISSUE -SPECIFIC TEM CELLS High Mobility Group Nucleosome-Binding Family Proteins Promote Astrocyte Differentiation of Neural Precursor Cells. 2014;2983–97.
 266. Leier HC, Weinstein JB, Kyle JE, Lee JY, Bramer LM, Stratton KG, et al. A global lipid map defines a network essential for Zika virus replication. *Nat Commun [Internet].* 2020;11(1):1–15. Available from: <http://dx.doi.org/10.1038/s41467-020-17433-9>
 267. Rombo F, Bayliss R, Tuplin A, Yeoh S. The journey of Zika to the developing brain. *Mol Biol Rep [Internet].* 2020;47(4):3097–115. Available from: <https://doi.org/10.1007/s11033-020-05349-0>

268. Coombs KM., Simon P F, McLeish N J, Zahedi-Amiri A. Kobasa D. Aptamer Profiling of A549 Cells Infected with Low-Pathogenicity and High-Pathogenicity Influenza Viruses. *Viruses* 2019;11(1028).
269. Marion T, Elbahesh H, Thomas PG, DeVincenzo JP, Webby R, Schughart K. Respiratory Mucosal Proteome Quantification in Human Influenza Infections. *PLoS ONE*. 2016; 11(4): e0153674.

Appendix: Supporting Information.

Figure S1A: PCA of > 1300 SOMAScan protein for 3 biological replicates after 12, 24 and 48hr ZIKV of infection.



Replicate 1	Sample ID		Replicate 2	Sample ID		Replicate 3	Sample ID
12 Mock 1	KMC-151		12 Mock 2	KMC-157		12 Mock 3	KMC-163
12 infected 1	KMC-152		12 infected 2	KMC-158		12 infected 3	KMC-164
24 Mock 1	KMC-153		24 Mock 2	KMC-159		24 Mock 3	KMC-165
24 infected 1	KMC-154		24 infected 2	KMC-160		24 infected 3	KMC-166
48 Mock 1	KMC-155		48 Mock 2	KMC-161		48 Mock 3	KMC-167
48 infected 1	KMC-156		48 infected 2	KMC-162		48 infected 3	KMC-168

Figure S1B: Heatmap of fold-changes

showing the most dysregulated of host proteins across all 3 time points after ZIKV infection. Blue indicates downregulated while red indicated up regulated.

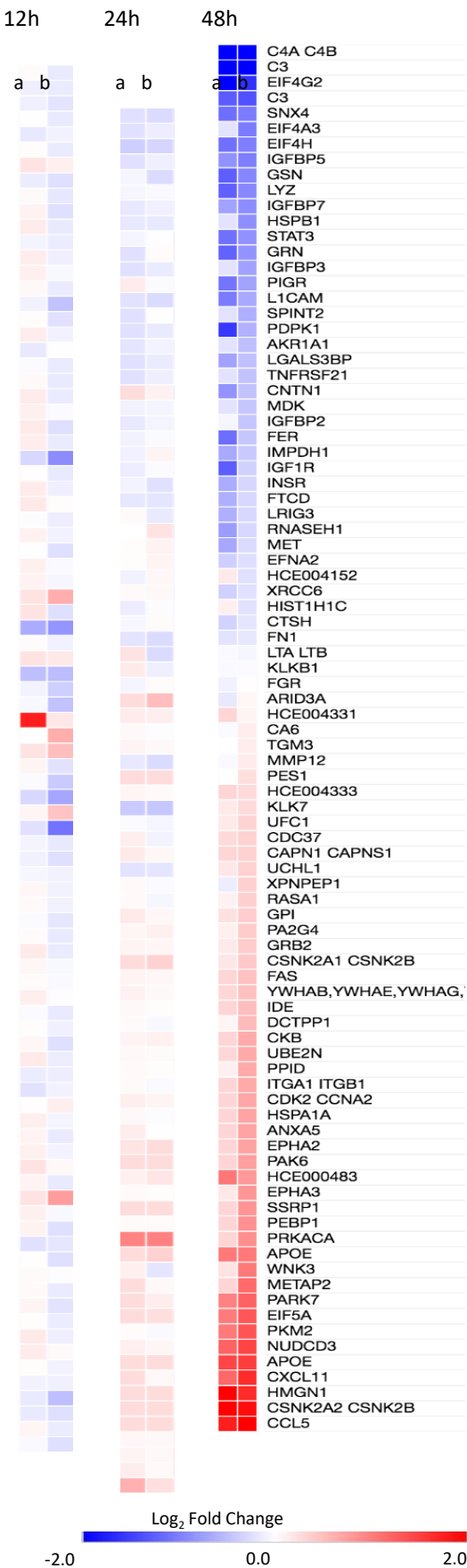
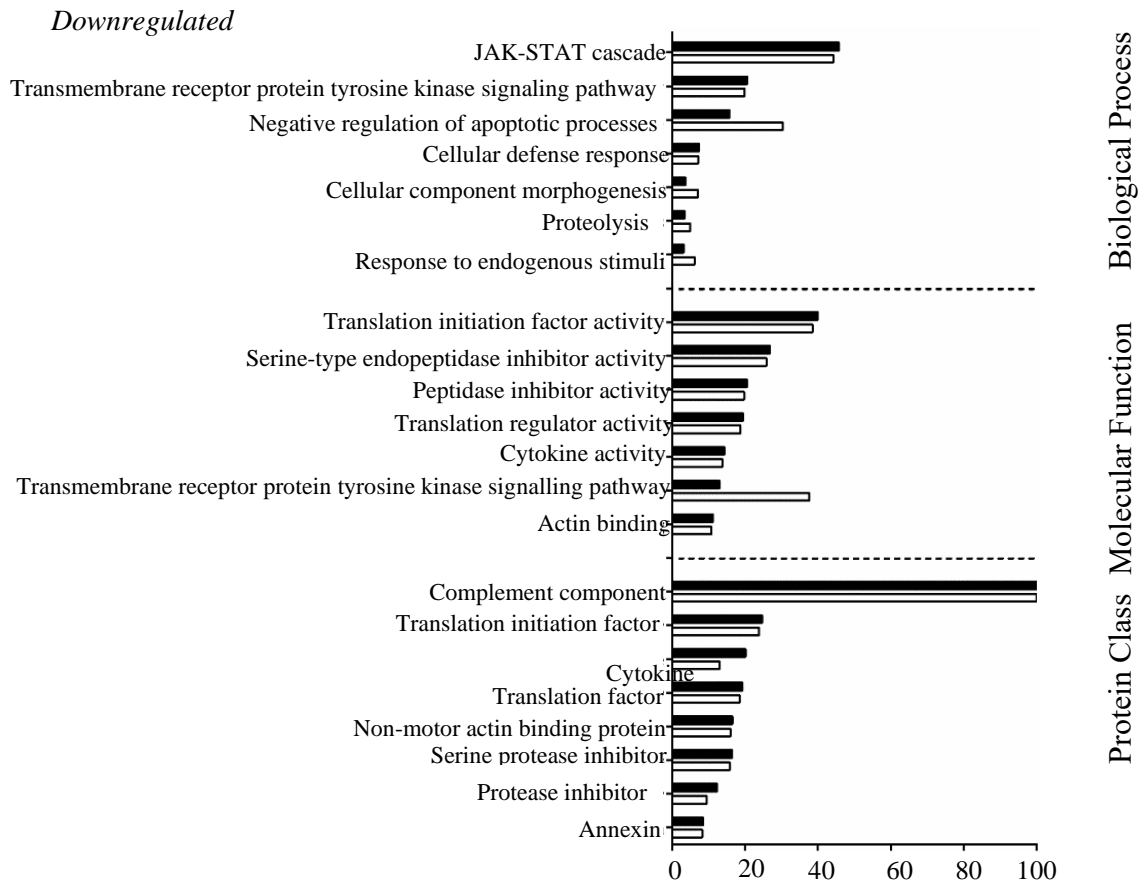


Figure S1C: GO analysis of using fold changes dysregulated host proteins.



Upregulated

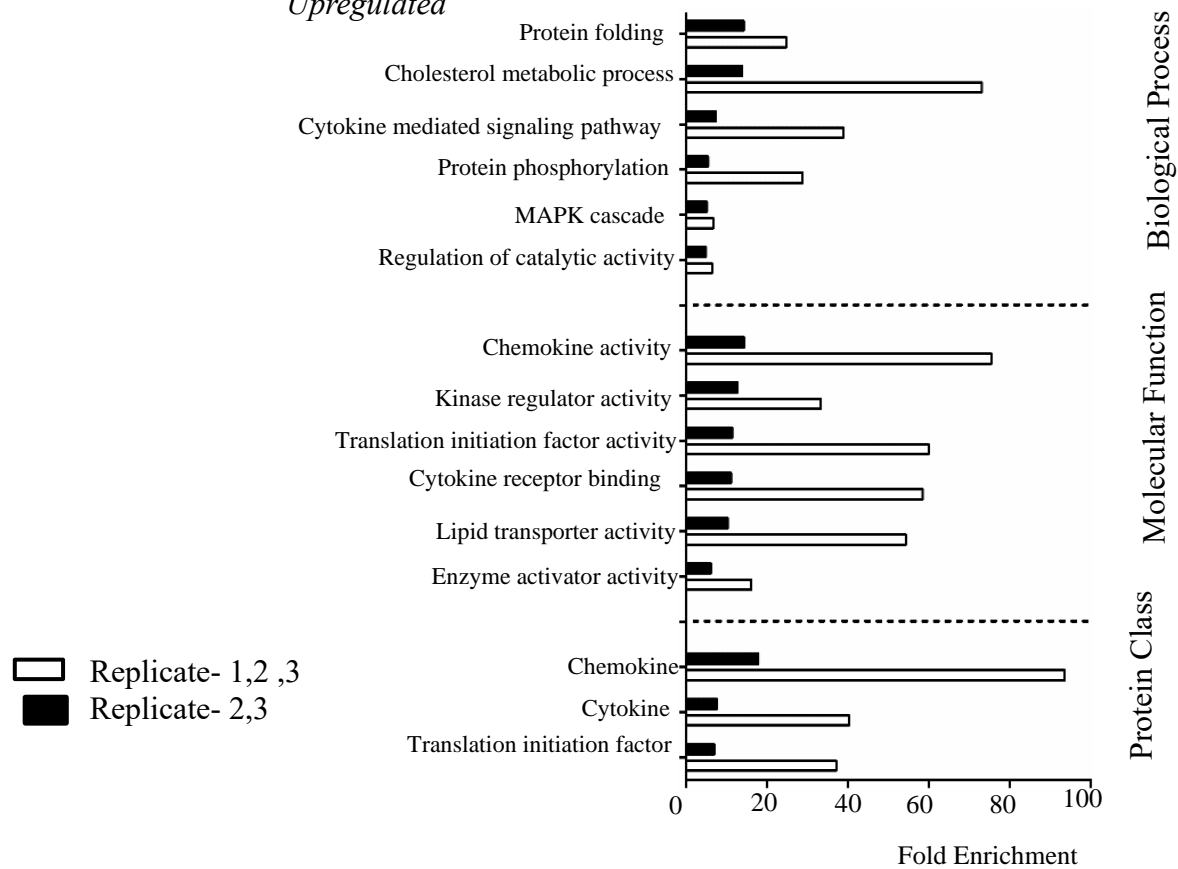


Table S1. IPA-predicted dysregulated bio-functions, activation state and specific molecules associated with each biofunction.

Categories	Diseases or Functions Annotation	p-value	Predicted Activation State	Activation Z-score	# Molecules
Neurological Disease	Degeneration of nervous system	4.52E-04	Increased	3.647	16
Neurological Disease	Movement Disorders	6.51E-05	Increased	3.416	46
Neurological Disease	Ataxia	0.001	Increased	3.402	14
Neurological Disease	Neurodegeneration	4.73E-04	Increased	3.192	17
Neurological Disease, Organismal Injury and Abnormalities	Astrocytosis	3.58E-06	Increased	2.941	10
Neurological Disease, Organismal Injury and Abnormalities	Neurodegeneration of brain	4.53E-05	Increased	2.94	10
Neurological Disease, Organismal Injury and Abnormalities	Neurodegeneration of cerebellum	1.98E-06	Increased	2.791	8
Organismal Injury and Abnormalities	Organ Degeneration	1.49E-06	Increased	2.783	31
Developmental Disorder, Hereditary Disease, Metabolic Disease, Organismal Injury and Abnormalities	Lysosomal storage disease	3.46E-14	Increased	2.778	18
Lipid Metabolism, Molecular Transport, Small Molecule Biochemistry	Accumulation of sphingolipid	3.48E-07	Increased	2.768	8
Cellular Compromise	Degeneration of cells	1.63E-04	Increased	2.714	19

Cell Death and Survival, Cellular Compromise, Neurological Disease, Organismal Injury and Abnormalities, Tissue Morphology	Neurodegeneration of Purkinje cells	7.62E-06	Increased	2.608	7
Lipid Metabolism, Molecular Transport, Small Molecule Biochemistry	Accumulation of glycosphingolipid	2.48E-08	Increased	2.584	7
Lipid Metabolism, Molecular Transport, Small Molecule Biochemistry	Accumulation of cholesterol	4.99E-04	Increased	2.433	6
Carbohydrate Metabolism, Uptake of D-	glucose	4.55E-04	Increased	2.359	13
Molecular Transport, Small Molecule Biochemistry	Accumulation of cerebroside	3.38E-07	Increased	2.219	5
Lipid Metabolism, Molecular Transport, Small Molecule Biochemistry	Concentration of lipid	1.32E-08	Increased	2.208	46
Lipid Metabolism, Molecular Transport, Small Molecule Biochemistry	Accumulation of ganglioside	1.01E-08	Increased	1.993	6
Lipid Metabolism, Molecular Transport, Small Molecule Biochemistry	Accumulation of glucosylceramide	1.77E-06	Increased	1.982	4
Lipid Metabolism, Molecular Transport, Small Molecule Biochemistry	Accumulation of ganglioside GM2	4.26E-08	Increased	1.964	5
Lipid Metabolism, Molecular Transport, Small Molecule Biochemistry	Accumulation of lipid	1.97E-07	Increased	1.964	23

Lipid Metabolism, Small Molecule Biochemistry	Hydrolysis of glycosphingolipid	3.99E-05	Decreased	-1.982	5
Carbohydrate Metabolism	Metabolism of polysaccharide	0.001	Decreased	-2	14
Protein Degradation, Protein Synthesis	Catabolism of protein	3.50E-04	Decreased	-2.048	28
Lipid Metabolism, Small Molecule Biochemistry	Catabolism of glycosphingolipid	2.72E-07	Decreased	-2.183	6
Lipid Metabolism, Small Molecule Biochemistry	Hydrolysis of sphingolipid	7.68E-06	Decreased	-2.19	6
Lipid Metabolism, Small Molecule Biochemistry	Metabolism of glycosphingolipid	7.48E-05	Decreased	-2.211	8
Lipid Metabolism, Small Molecule Biochemistry	Metabolism of glycolipid	1.82E-04	Decreased	-2.23	9
Lipid Metabolism, Small Molecule Biochemistry	Metabolism of sphingolipid	3.46E-05	Decreased	-2.249	12
Lipid Metabolism, Small Molecule Biochemistry	Catabolism of sphingolipid	4.54E-09	Decreased	-2.392	8
			Decreased	-2.429	85
Cellular Movement	Cell movement	2.26E-05	Decreased	-2.669	76
Cellular Movement	Migration of cells	6.46E-05	Decreased	-2.744	13
Lipid Metabolism, Small Molecule Biochemistry	Catabolism of lipid	1.09E-06	Decreased	-2.778	34
Organismal Development	Size of body	7.01E-04	Decreased	-2.915	10
Lipid Metabolism, Small Molecule Biochemistry	Hydrolysis of lipid	0.001	Decreased	-2.966	27
Lipid Metabolism, Small Molecule Biochemistry	Fatty acid metabolism	2.21E-04			

Table S2: Differentially dysregulated host proteins after ZIKV infection in Caco-2, U251 cells and Vero cells

	CACO-2 cells	U251 cells	VERO cells	CACO-2 cells	U251 cells	VERO cells	CACO-2 cells	U251 cells	VERO cells
	12 hpi	12hpi	12hpi	24 hpi	24hpi	24hpi	48 hpi	48hpi	48hpi
Gene name	FC	FC	FC	FC	FC	FC	FC	FC	FC
CA6	1.43	0.98	1.38	1.02	0.93	1.03	1.03	0.83	1.10
FN1	1.04	1.01	0.88	0.95	0.85	1.39	0.65	0.46	0.87
PARK7	1.29	1.03	0.90	1.12	1.22	1.31	1.04	1.66	1.92
CDK2	1.67	1.03	0.94	1.49	0.79	1.23	1.14	1.06	1.52
CCNA2	1.67	1.03	0.94	1.49	0.79	1.23	1.14	1.06	1.52
EIF5A	1.43	1.04	0.91	1.38	1.14	1.04	1.49	1.51	1.99
WNK3	1.80	0.92	0.90	1.58	0.95	0.97	1.25	0.72	1.79
PAK6	1.45	1.01	0.89	1.10	1.21	1.02	1.33	1.10	1.57
PPID	1.63	1.00	0.93	2.28	1.06	0.99	1.63	0.74	1.51
CKB	0.96	0.99	0.90	0.79	0.99	1.06	1.07	3.85	1.50
IDE	1.72	1.02	0.92	1.06	1.18	1.02	1.11	1.23	1.39
CFI	1.38	0.91	0.86	1.03	0.65	1.44	1.07	0.17	1.01
FER	1.51	0.98	0.60	1.09	1.23	0.86	1.25	0.45	0.75
SNX4	1.46	1.02	0.92	1.43	1.15	0.82	1.24	0.65	0.56
STAT3	1.42	1.02	0.91	1.29	0.90	0.81	1.34	0.51	0.61
C4A	1.58	0.92	0.89	1.19	1.12	0.81	1.07	0.35	0.27
C4B	1.58	0.96	0.89	1.19	1.04	0.81	1.07	0.25	0.27
TNFRSF21	1.49	1.02	0.90	1.25	0.97	0.97	0.83	0.66	0.73
RTN4R	1.30	0.99	0.88	1.20	0.91	0.91	0.90	0.39	0.79
MDK	1.58	1.02	0.84	1.19	0.59	0.98	0.72	0.20	0.75
PDPK1	1.67	0.97	0.99	1.56	1.03	1.08	1.42	0.64	0.68
L1CAM	1.44	0.90	0.85	1.06	0.88	0.90	1.16	0.34	0.66
HIST1H1C	1.42	0.92	0.62	0.80	0.82	0.92	0.74	1.32	0.86
MICA	1.72	0.86	0.74	1.06	1.10	1.07	1.11	1.32	1.08
CMA1	1.32	0.99	0.78	1.04	1.13	0.97	1.19	0.42	0.92
HMGN1	1.59	1.02	0.78	0.93	1.17	1.05	0.80	2.31	2.25
CXCL11	1.10	0.87	0.73	1.06	2.76	1.04	1.39	8.61	2.25
CDH5	1.28	1.01	0.90	1.15	1.33	1.19	1.28	1.18	1.26
ISG15	1.31	1.00	0.88	1.18	1.26	1.02	1.29	2.75	1.41
PSMD7	1.13	1.04	0.93	1.10	1.32	0.98	0.70	1.22	1.36
NCAM1	1.36	0.94	0.91	1.20	1.03	1.11	1.13	0.68	0.84
GRN	1.41	0.96	0.96	1.04	0.66	1.00	1.00	0.20	0.61
LGALS3BP	1.30	0.98	0.89	1.05	0.83	0.94	0.89	0.59	0.73
CTSD	1.08	1.05	0.95	1.06	0.97	0.99	1.05	0.74	0.80
CTSH	1.41	1.00	0.93	1.13	1.07	1.02	1.24	0.59	0.87
CLIC 1	1.54	0.72	0.87	1.26	1.08	0.98	1.25	1.47	1.21

Fold change cut-offs used were ≥ 1.25 or ≤ 0.80 , with p-value < 0.05 . Values based on three biologic replicates. **Bolded red** represents significantly up-regulated protein. **Bolded blue** represents significantly downregulated protein.

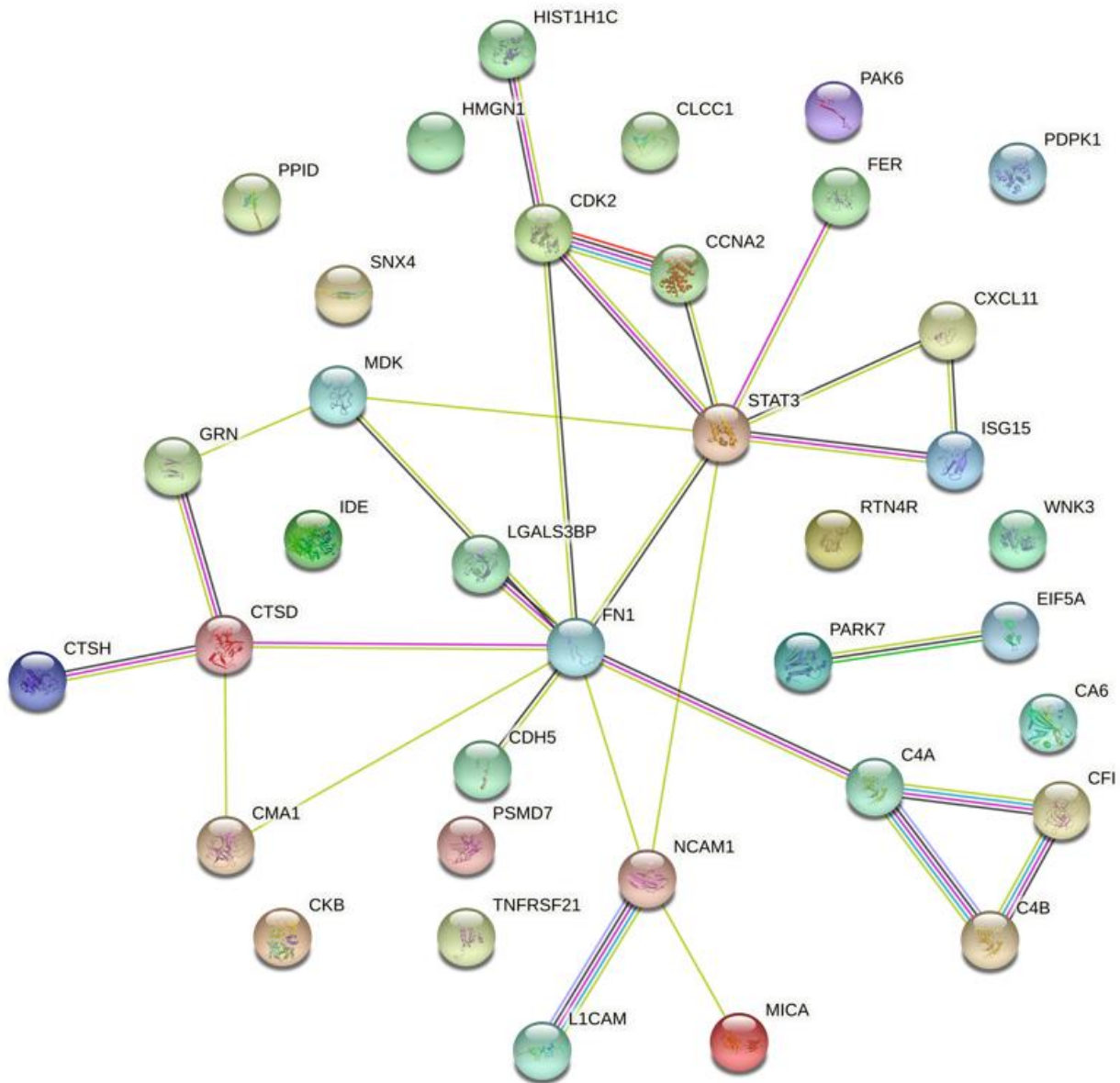


Figure S3: Protein-protein interaction network of commonly and differentially dysregulated host proteins after ZIKV infection identified in Vero, Caco-2 and U251 cells.

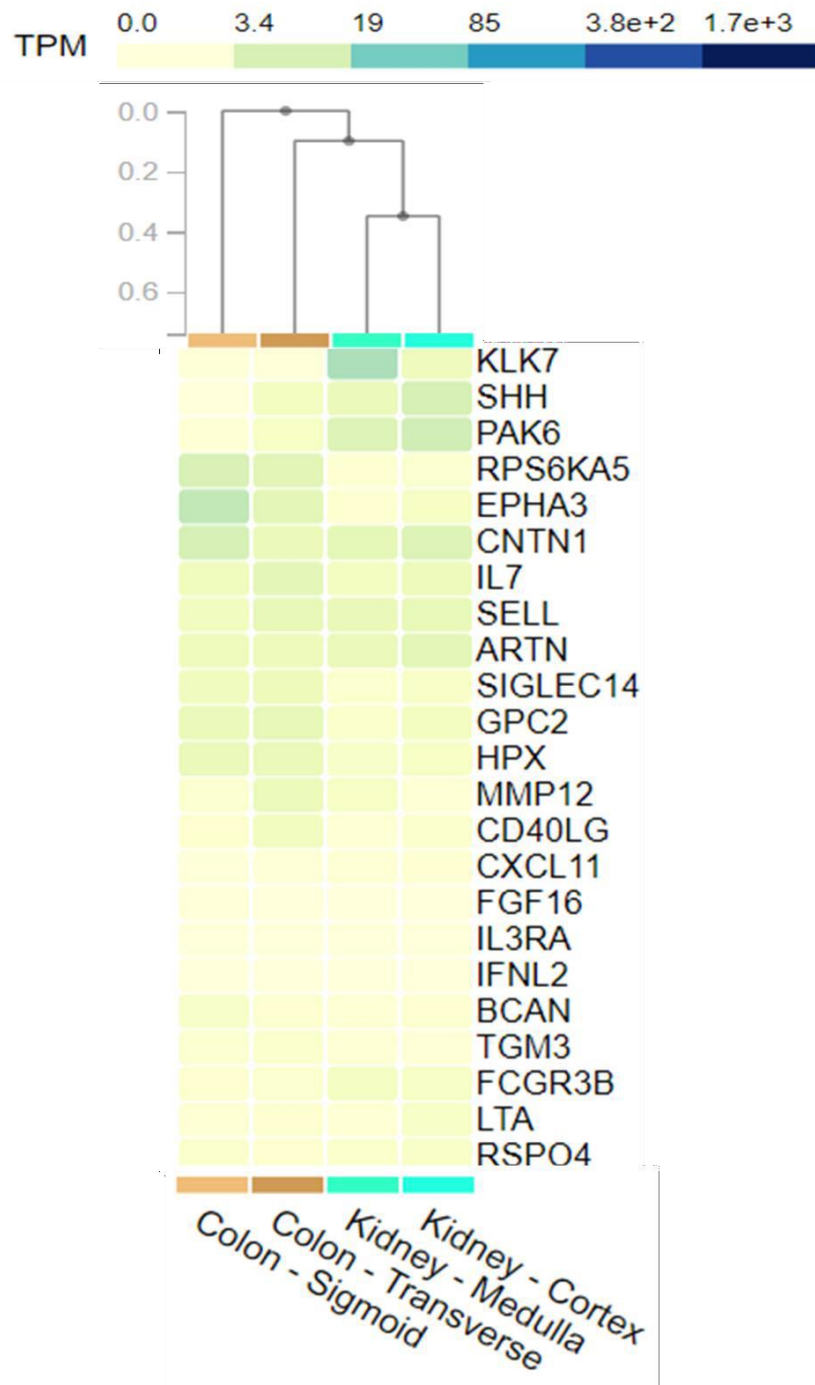


Figure S4: Expression profile of low abundant SOMAScan proteins undetected by Mass spectrometry.